CAPITAL UNIVERSITY OF SCIENCE AND TECHNOLOGY, ISLAMABAD

Strengthening of Strength Deficient Corroded RCC Beams using Carbon-fiber-reinforced-polymer and Basalt-fiber-reinforced-polymer

by

Shaikh Aqeeb ur Rehman

A thesis submitted in partial fulfillment for the degree of Master of Science

in the

Faculty of Engineering

Department of Civil Engineering

2024

I want to dedicate this achievement my parents, teachers and friends who always encourage and support me in every crucial time

CERTIFICATE OF APPROVAL

Strengthening of Strength Deficient Corroded RCC Beams using Carbon-fiber-reinforced-polymer and Basalt-fiber-reinforced-polymer

by

Shaikh Aqeeb ur Rehman

Registration No: (MCE223009)

THESIS EXAMINING COMMITTEE

S. No.	Examiner	Name	Organization
(a)	External Examiner	Dr. Muhammad Noman	IIU, Islamabad
(b)	Internal Examiner	Dr. M. Usman Farooqi	CUST, Islamabad
(c)	Supervisor	Dr. Muazzam Ghous Sohail	CUST, Islamabad

Dr. Muazzam Ghous Sohail
Thesis Supervisor
September, 2024

Dr. Ishtiaq Hassan
Head
Dept. of Civil Engineering
September, 2024

Dr. Imtiaz Ahmad Taj
Dean
Faculty of Engineering
September, 2024

Author's Declaration

I, **Shaikh Aqeeb ur Rehman,** hereby state that my MS thesis titled **Strengthening of Strength Deficient Corroded RCC Beams using Carbon-fiber-reinforced-polymer and Basalt-fiber-reinforced-polymer** is my own work and has not been submitted previously by me for taking any degree from Capital University of Science and Technology, Islamabad or anywhere else in the country/abroad.

At any time if my statement is found to be incorrect even after my graduation, the University has the right to withdraw my MS Degree.

(Shaikh Aqeeb ur Rehman)

Registration No: (MCE223009)

Plagiarism Undertaking

I solemnly declare that research work presented in this thesis titled **Strengthening of Strength Deficient Corroded RCC Beams using Carbon-fiber-reinforced-polymer and Basalt-fiber-reinforced-polymer** is exclusively my research work with no remarkable contribution from any other individual. Small contribution/help wherever taken has been acknowledged and that complete thesis has been written by me.

I understand the zero tolerance policy of the Higher Education Commission and CUST towards plagiarism. Therefore, I as an author of the above titled thesis declare that no part of my thesis has been plagiarized and any material used as reference is properly cited.

I undertake that if I am found guilty of any formal plagiarism in the above titled thesis even after award of MS Degree, the University reserves the right to withdraw/revoke my MS degree and that HEC and the University have the right to publish my name on the HEC/University website on which names of students are placed who submitted plagiarized work.

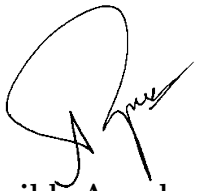

(Shaikh Aqeeb ur Rehman)
Registration No: (MCE223009)

Acknowledgement

In the Name of Allah, The Most Gracious, The Most Merciful. Praise be to God, the Cherisher and Sustainer of the worlds. All thanks to Almighty Allah, The Lord of all that exist, who bestowed me with His greatest blessing i.e. knowledge and Wisdom to accomplish my task successfully.

Thousands of salutations and benedictions to the Holy prophet **Hazrat Muhammad (PBUH)** the chosen-through by whom grace the sacred Quran was descended from the Most High.

I am very thankful to **Engr. Dr. Muazzam Ghous Sohail**, a great teacher, mentor and supervisor who made a difference in all aspect of my life.

I want to express my heartiest regards to my parents who always supported me morally, spiritually & prayed for my success.

Shaikh Aqeeb ur Rehman

Abstract

This study compares the performance of carbon fiber reinforced polymers (CFRP) and Basalt fiber reinforced polymers (BFRP) as flexural strengthening on corroded and strength-deficient concrete beams. Concrete is the most commonly used construction material however its inherent brittleness and low tensile strength lead to several undesirable issues, like cracking and deterioration which necessitates regular structural repairs. Another critical challenge in reinforced concrete (RC) members is the Corrosion of its reinforcement. Corrosion significantly reduces the strength of structural members, ultimately leading to their failure. Common causes of Corrosion include chloride ingress, sulfate attack, carbonation, permeability of concrete, inadequate cover depth, and cracks. Since Corrosion takes several years to manifest itself, it becomes very difficult for researchers to study the behavior and loss in strength after Corrosion has initiated.

In this study, Corrosion was accelerated by artificially applied electrical current in the RC beams, so that a certain level of Corrosion could be achieved in short time. Up to 10% of weight loss on steel bars were selected and current was applied to reinforcement of beams. These specimens were tested undergo flexural testing in the laboratory to compare the performance of controlled, corroded, and CFRP/BFRP-strengthen members. The CFRP and BFRP laminates increased the beam strength by 20- 22% and 15 to 17 %, respectively as compared to the control sound beams. In case of corroded beams, the strength regain was 15-17% and 8-10%, respectively for CFPR and BFRP compared to the corroded beams. The preloaded beams up to 70% of ultimate capacity and then strengthened, not just achieved the strength to virgin control beam but had up 7% and 5% higher strength compared to the control beams. The findings will provide insights into the suitability of these materials for long-term member strengthening, potentially reducing the need for new construction and lowering carbon emissions associated with manufacturing processes, thereby promoting sustainable and eco-friendly development.

Contents

List of Figures

List of Tables

Chapter 1

Introduction

1.1 Background

Primary problem of concrete is that it is fragile, which causes damage, deterioration, cracking and demands routine structural component repairs, but there is another issue that arises in RCC members that is corrosion. Due to corrosion member losses its strength and leads to the failure of the member or the structure ultimately. Reasons of corrosions are: Chloride, Sulphate, Carbonation, Alkalinity, Permeability, cover and cracks [1] Reinforcement corrosion in RC beams reduces impact resistance and favors a brittle failure mode. Under quasistatic and falling-weight impact load testing, the impact resistance of reinforced concrete (RC) beams with varied degrees of reinforcement corrosion was examined. The results demonstrated that reinforcement corrosion has a bigger impact on impact resistance than on quasistatic load capacity, and that brittleness can be attributable to interactions between preexisting corrosion damage and flexural cracking generated by loading. [2].

When the member is corroded it loses its strength. It can be regained by different methods named as Concrete jacketing, FRP sheeting, NSM, EBROG, embedded bars, PTMS, UHPC etc [3]. Each method has its own advantages and disadvantages. Keeping in mind the better qualities of FRP sheets and leafs. We are going to select FRP as our prime material for strengthening. FRPs can be used in the concrete structures in following forms. 1) Plates are used at the face to increase

tension capacity. 2) Leafs are placed below beams and slabs to increase their capacity to support loads. 3) In place of steel bars, use FRP bars as reinforcement in beams and slabs. 4) In suspension and bridge girders, FRP cables can be employed as tendons and post-tension members. 5) For containment, wraps around structural concrete components like columns, beams, slabs, etc [4]. Because of its exceptional properties, such as their light weight, better load-bearing strength, low density, high modulus, and excellent chemical resistance, carbon fibre reinforced polymers (CFRP) and basalt fibre reinforced polymer (BFRP) sheets have drawn increased interest from researchers. CFRP is a unique material with additional characteristics including a high strength-to-weight ratio, low toxicity, recyclable qualities, non-corrosive qualities, and great wear resistance. The method for transferring stress at the CFRP-concrete contact is one of the primary factors affecting the effectiveness of reinforcement. [5] According to the findings, mortar-based strengthening systems are less resilient than epoxy-based strengthening systems in difficult climates.

Reinforced concrete (RC) structures are significantly challenged by steel corrosion, particularly in harsh climates with high temperatures, carbonation, moistness, chloride-ingress, and humidity of the cover of concrete [6,7]. In the US, the cost of repairing corroded-damaged infrastructure amounts to 3.5% of the uncultured domestic produce, while the Middle Eastern countries, this figure can rise to 5% [8,9]. The corrosion initiation process is slow, taking years before rust goods seem on the surface. This delay complicates early damage assessment and the evaluation of remedial methods. Once a deteriorated structural member is strengthening or rehabilitated, measuring the regained strength during service is virtually impossible. Structural-behavior of rusted basics and predict their remaining strength, corrosion is exaggeratedly brought in workroom settings by means of the impressed-current-method. This method rapidly achieves a specified degree of corrosion in RC members [11-14]. Faradays law is used to calculate the current intensity and duration required to reach the targeted corrosion level.

Different experimental and analytical investigations are conducted in the past to deduce most efficient and reliable strengthening system using CFRP & BFRP sheets and leafs e.g . EBROG, EB, NSM, hybrid anchors, patch anchors, splay

anchors, bi-directional fiber wrapping, Side wrapping, full wrapping etc. Moreover, various types of adhesives, epoxy resins, Cement-based adhesives (CBAs) played a role in this strengthening system. The objective of this study is to provide experimental investigation that whether CFRP U- shape interval wrapping or BFRP U-shaped interval wrapping are better to enhance members ultimate tensile strength and flexural capacity. Method adopted is, beam members of 4000 psi will be casted then they will be artificially given a certain amount of current to induce corrosion in the reinforcement. Then these specimens will be strengthen with CFRP or BFRP leafs. Finally, these specimens will be tested against flexure in the laboratory to make comparison between controlled, corroded and CFRP/BFRP corroded members. Consequently, the results will be compared and a suggestion will be concluded that this member can be re-strengthen for long time using which suitable material. Hence demand for new members will be reduced and less CO_2 emission will be emitted during manufacturing process. This will rejuvenate sustainable and eco-friendly development.

1.2 Research Motivation and Problem Statement

Sustainability in construction is the requirement of this modern time. Studies are needed to focus on those composites that are eco-friendly and increase the lifespan of the structure because it can reduce the demand of new concrete, ultimately reducing CO2 emission during cement production. CFRPs are extensively used repair laminates, however, since they are expensive for several countries, it important explore cost effective and readily available retrofitting materials. In this regards, BFRP are evaluated in comparison with CFRP as flexure strengthening systems.

Moreover, when it comes to repair those brittle materials after the development of crack or any un-accessible issue, "Replace or Retrofit" is a constant source of worry. More exploration is required to introduce economical and structurally strong material to overcome retrofitting issue. Because every time concrete jacketing is not favorable due to space restriction, weathering conditions, materials transportation issue e.g. sea underwater Piers etc. Afterwards, Sustainable and environmentally friendly development need to be revived by this.

Reinforced concrete (RCC) members are susceptible to various failures, one of the most significant being corrosion attacks. Corrosion reduces the strength of these members, potentially leading to their collapse, which poses a serious risk to the safety of the inhabitants of the building or structure. To address this issue, researchers have extensively studied various retrofitting methods. After a comprehensive literature review, it has been concluded that CFRP (Carbon Fiber Reinforced Polymer) and BFRP (Basalt Fiber Reinforced Polymer) wrapping are effective methods for enhancing the flexural strength and ultimate load capacity of existing RCC beams. These methods support the construction industry in promoting eco-friendly development by focusing on repair and retrofitting rather than replacement.

Fig a): Strength Deficiency due to poor workmanship

Fig b): Strength Deficiency due to earthquake cracks

Fig c): Strength Deficiency due to Corrosion

Fig d): Strengthening using CFRP & BFRP laminates

1.2.1 Research Questions

The following inquiries are addressed in the research study:

1. How much structural performance of corroded RCC beam can be increased using CFRP or BRP?

2. Can strengthen element achieves, same flexural bearing capacity as of uncorroded section?

3. How much 10% in loss of weight of reinforcement can reduce the efficiency of strengthen members?

4. Does CFRP/BFRP strengthen element fails in premature debonding or concrete rupture?

5. How much strength can be regained if control beams are pre-loaded 70% of ultimate laod of CB?

1.3 Overall Goal of the Research Program and Specific Aim of this MS Thesis

The overall goal of the research program is to evaluate and support a structural members strengthening/retrofitting method that can regain the original strength of the member that was damaged due to corrosion, earthquake or mishandling of materials during construction. It will help to draw attention of researchers and industrialists to apply these materials and methodologies to overcome strength deficiency issues.

The Specific aim of this MS research thesis is to investigate the structural performance of corroded and strength deficient beams and its strength regain activity by using CFRP and BFRP wrapping at the soffit of beam using epoxy and adhesives.

1.4 Scope of Work and Study Limitations

Sixteen RCC concrete beams were poured with 4000 psi concrete. 6x of them were corroded for 15 days using impressed current method. 4x beams were re-cracked by applying 70% of ultimate load of control beams. 12x beams were strengthened

with CFRP & BFRP respectively and then investigated in flexure and analyzed. In Table 1.1 is showing the scope of work details.

Two control beams were casted as per the mix design for 4000 psi strength. Two controlled beams were strengthened with BFRP and two were strengthen with CFRP. Two control beams were corroded. Four control beams were cracked 70% and then two were strengthen with BFRP and two were strengthen with CFRP. Four beams were corroded and then two were strengthend with BFRP and two were strengthend with CFRP.

This study is limited to investigate the flexural behavior of corroded, controlled and strength deficient beams when they are strengthened with CFRP and BFRP laminates. No XRD or SEM analysis is conducted due to non-availability of apparatus and time constraints. For Corrosion impressed current methodology is adopted due to possibility of materials availability for electric circuit assembly. This study was self funded by student. If any of the sample gets damaged so we have extra sample to be tested. Thats why 2 beams samples for each category were prepared. For 3 beams sample for each category finances were also a constraint.

1.4.1 Rationale Behind Variable Selection

Carbon fiber reinforced polymer (CFRP) sheet and Basalt fiber reinforced polymer (BFRP) having superior tensile strength (MPa), youngs modulus (GPa), Elongation %, coefficient of thermal expansion is selected, based on availability. For adhesives and fillers; Epoxy resins having good bond strength and resistance against fracture are chosen. Combination of these elements will give a composite that will be more resilient & have improved mechanical properties.

1.5 Brief Methodology

In this experimental study, RCC beams approximately 16x specimens are casted, dimensions are given in Table 1.2, longitudinal and shear reinforcement are provided in all the specimens either controlled or corroded as per ACI 318 design criteria. The beams were flexure control. Members were cured for 28 days. Then

Table 1.1: Scope of Work

Test	Control Beam (CB)	Corroded Beam (C)	Corroded Beam Strengthened with BFRP	Control Beam Strengthened with BFRP	Corroded Beam Strengthened with CFRP	Control Beam Strengthened with CFRP	70% Cracked Control Beam Strengthen with BFRP	70% Cracked Control Beam Strengthen with CFRP
Flexure								

after 28 days impressed current method was used to induce artificial corrosion in the members and loss of weight of reinforcement was also calculated after exposing complete steel from cracked beam. The corroded and sound beams strengthened by CFRP and BFRP using epoxy adhesives for providing proper bondage/anchorage. Samples prepared were then tested for mechanical properties (flexure). The strength regaining was analyzed and compared with previous studies.

1.6 Experimental Setup

The ASTM C78 test method uses a straightforward flexure element with three-point load application to assess the flexural strength of composite Findings are given as modulus of rupture (MOR), a measure of a concrete sample's flexural strength immediately before it crosses yielding point. To calculate the MOR, a testing equipment that can apply and monitor loads at a constant rate without interruption with three-point flex assembly in accordance with the ASTM C78 standard is employed. Experimental setup figure is shown as figure 1.1 below. The specimen in figure 1.1 is supported on the ends in the apparatus assembly and the load is applied through single mid-point. This setup is referred to as three-point flexure strength test of concrete specimen. In figure 1.1, the three point flexure loading setup is explained while in figure 1.2, the schematic diagram of battery assembly for Impressed current method is mentioned. The three-point flexure test is a method used to determine the flexural strength and behavior of materials. The setup for this test typically involves the specimen, support span, loading nose, test machine, load and deflection measurement, preparation, positioning, loading, data collection, analysis, result and interpretations. This setup provides a reliable method to assess the flexural properties of materials, commonly used for testing metals, polymers, ceramics, and composite materials. The specimen is usually a rectangular or cylindrical beam made of the material to be tested. The dimensions of the specimen should be precisely measured, including length, width, and thickness.

In this experimental study, RCC beams approximately 12x specimens shall be casted dimensions are given in Table 1.2. longitudinal and shear reinforcement shall be provided in all the specimens either controlled or corroded. Members will

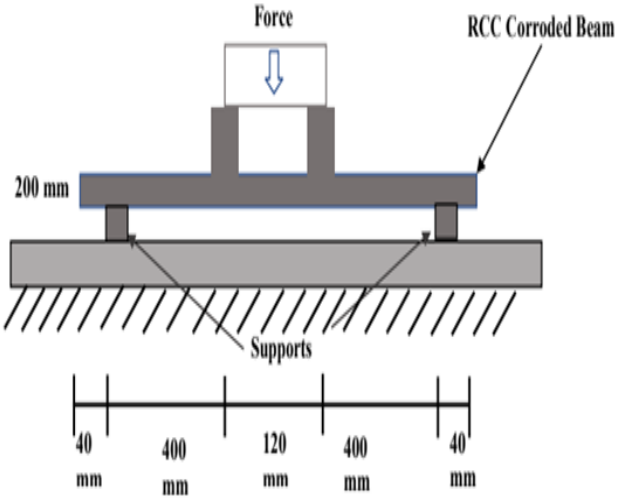

FIGURE 1.1: Four-point flexure test setup sketch

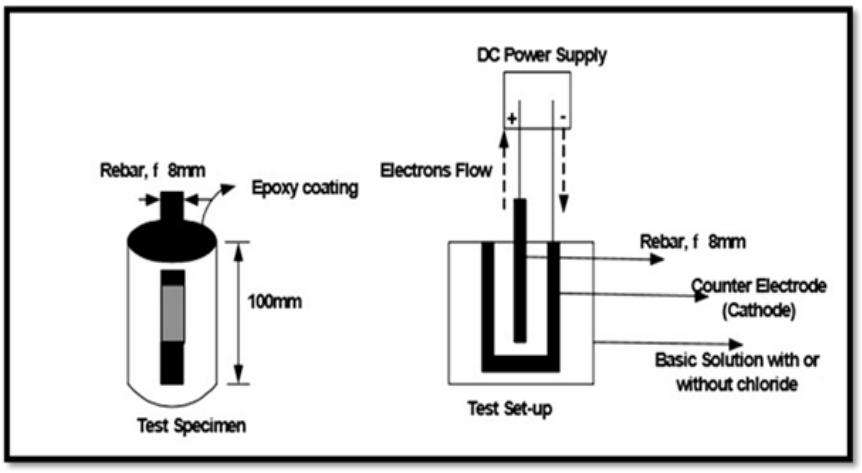

FIGURE 1.2: Battery assembly for Impressed current method (Sohail et.al, 2022)

be cured for 28 days. Moreover, their cylinders will also be cured for compressive strength of concrete. Then after 28 days Impressed current method will be used to induce artificial corrosion in the members. Members will lose its strength; it will be derived by flexure testing. And loss of weight of reinforcement will also be calculated after exposing complete steel from cracked beam. Now corroded members will be strengthen by CFRP and BFRP using epoxy adhesives for providing proper bondage/anchorage. Samples prepared; will then be tested for mechanical properties (flexure). Now, strength regaining results will be analyzed and compared with previous study. Strength regains success will be evaluated from the results and its compatibility with previously adopted methods of strengthening.

1.7 Novelty of the Work, Research Significance and Practical Implementation

To the best of scholars knowledge, since few years, working on use of BFRP in the strengthening of corroded RC beams have been started. Stretching this study avenue we are working on the strengthening of Corroded, controlled and strength deficient RC beams using BFRP and CFRP at the soffit of beam keeping 25mm cover at the sides and 50mm at the ends of beam. To check flexural strength capacity and economical suitability of this technique for retrofitting of strength deficient beams.

Use of BFRP and CFRP laminates on strength regaining of corroded and especially strength deficient pre-loaded beams are not much discussed in literature. BFRP is newly introduced material for flexural strengthening of structural members. But significance of this study is use of BFRP for strengthening of corroded RC members. Current study is aimed to investigate the mechanical properties and failure modes of controlled, corroded and strength deficient beams strengthened with single layer of CFRP/ BFRP at the soffit of beam using locally available epoxy and adhesives.

Externally bonded laminates at soffits are applied keeping 25-50mm cover from sides and ends, keeping shear and tension zone of the beam in consideration. Material saving, strength regaining and less cracks propagation is expectation from this experimental study. It will help structures to withstand against loads for longer periods. Hence demand for new members will be reduced and less carbon emission will be emitted during manufacturing process. This will rejuvenate sustainable and eco-friendly development.

Chapter 2

Literature Review

2.1 Background

Reinforced Concrete (RCC) structures are widely used in civil engineering due to their strength and durability. However, over time, these structures can suffer from demean, particularly due to corrosion of steel reinforcements. This corrosion reduces the strength and lifespan of RCC members, leading to potential safety hazards and high repair costs. To address these challenges, advanced materials like Carbon Fiber Reinforced Polymer (CFRP) and Basalt Fiber Reinforced Polymer (BFRP) have been increasingly researched and utilized for strengthening and retrofitting RCC structures.

CFRP is a composite material consisting of carbon fibers embedded in a polymer matrix. It is known for its exceptional strength-to-weight ratio, high stiffness, and resistance to corrosion and fatigue. These properties make CFRP an ideal candidate for reinforcing and retrofitting RCC structures. Research has shown that CFRP can significantly enhance the flexural strength, bending resistance, and overall durability of concrete beams and other structural elements.

Key advantages of CFRP include:

- CFRP provides significant increases in flexural and tensile strength.
- Its low weight reduces the additional load on structures.
- Unlike steel, CFRP does not corrode, making it suitable for harsh environments.

- CFRP sheets can be easily bonded to existing structures with minimal disruption.
- Studies have demonstrated that CFRP reinforcement can improve bending resistance by up to 58% and bending stiffness by up to 43%, depending on the reinforcement configuration.

BFRP is another composite material, consisting of basalt fibers embedded in a polymer matrix. Basalt fibers are derived from volcanic rock and offer several benefits, such as high thermal stability, good resistance to chemical attack, and excellent mechanical properties. BFRP is emerging as a cost-effective and environmentally friendly alternative to CFRP, particularly in applications where sustainability is a priority.

Key advantages of BFRP include:

- BFRP enhances the structural performance of RCC members.
- Basalt fibers are natural and environmentally friendly, with a lower carbon footprint than carbon fibers.
- BFRP is generally less expensive than CFRP, making it an attractive option for large-scale applications.
- BFRP maintains its properties at advanced temperatures compared to CFRP.

Research has shown that BFRP can improve the flexural performance and damage resistance of concrete beams. When combined with other reinforcement materials like PVA fibers, BFRP sheets can further enhance the load-carrying capacity and extend the service life of RCC structures.

The use of CFRP and BFRP for reinforcing and retrofitting RCC structures offers promising solutions to address the issues of corrosion and structural demean.

These advanced materials not only enhance the strength and durability of existing structures but also contribute to more sustainable and cost-effective construction practices. Ongoing research aims to further understand and optimize their application, ensuring safer and longer-lasting infrastructure.

2.2 Causes of Corrosion and %age Weight Loss of Steel

In reinforced concrete, the high alkalinity of the concrete pore solution forms a passive film on the steel rebar surface, which protects the steel from active electrochemical corrosion. However, in natural environments, particularly marine or Salt Lake areas, aggressive species such as chloride and sulfate ions can penetrate the concrete and compromise this passive film, thereby reducing its protective effect on the steel rebar [1]. The corrosion products that form are typically three to four times larger in volume than the original steel, generating expansive internal forces within the confined concrete. This can lead to cracking, spalling, or delamination of the concrete cover [2], [3], [4].

In cases of localized chloride-induced corrosion, significant cracking might not occur for an extended period [5], [6], [7]. Nevertheless, once the concrete cover cracks, the steel rebar becomes directly exposed to the corrosive environment, which accelerates the corrosion process [8]. This ongoing degradation reduces the load-bearing capacity of the reinforced concrete elements, threatening the long-term durability and safety of the concrete infrastructure [9], [10], [11], [12], [13], [14].

Over the past few decades, the premature failure of concrete structures due to steel corrosion has garnered significant attention worldwide. In 1975, the U.S. National Bureau of Standards conducted a field survey revealing that corrosion-related costs for steel in concrete comprised approximately 40% of the total corrosion losses associated with infrastructure in the United States [15]. A recent study in Switzerland corroborated these findings, indicating that the corrosion costs for road infrastructure identified in the U.S. study over two decades ago remain relevant and are also applicable to Europe [16]. Additionally, within the first ten years of service for the Shinkansen (Japanese Bullet Train), severe rebar corrosion led to cracking and spalling of concrete covers [17]. In 1980, the Highway Science Research Institute of the Ministry of Transport conducted a field survey on 18 wharves in Southern China. The results showed that over 80% of reinforced concrete structures experienced steel corrosion, with some structures showing signs of corrosion within just

5 to 10 years after completion [18], [19]. These findings caused significant concern within the engineering community. Table 2.1 is showing the loss of steel weight due to corrosion reported by the various researchers.

TABLE 2.1: Steel Weight Loss

S. N.	Paper Title	Finding	Reference
1	A Comparative Study on Corrosion Rate of Carbon Steel in NaCl Solution with Continuous and Discontinuous Weight Loss Methods	The research revealed that there was a variation in the amount of weight reduction attributed to corrosion, falling within the range of 2.67% to 5.46%, and with a mean value of 4.17% for specimens of carbon steel submerged in various solutions over a duration of 10 to 50 days.	Ali et al. (2022) [152]
2	Comparison of Percentage Weight Loss and Corrosion Rate Trends in Different Metal Coupons from two Soil Environments	The extent of weight reduction attributable to corrosion in mild steel varied between 2.8% and 5.4%, in carbon steel between 3.6% and 4.5%, and in stainless steel between 0.08% and 0.12%.	Oparaodu et al. (2014) [153]
3	Cathodic Current of Steel Structures with Seawater Resistant Stainless Steel and Estimation of Weight Loss of Sacrificial Anode	The estimation of steel weight reduction can be conducted through the analysis of cathodic current. In the experimental setting, it was observed that seawater-resistant stainless steel exhibited a weight loss approximately 60% lower than that of carbon steel plates.	Kitagawa et al. (2010) [154]
4	Technical note Weight loss investigation of alternating voltage corrosion of 301, 304, and 316 stainless steels in boiling NaCI solution	The weight decrease of stainless steels as a result of cyclic voltage-induced corrosion in a boiling NaCl solution reached levels of 30%, 21%, and 16% correspondingly following a duration of 1500 hours.	Souza et al. (1995) [155]
5	Weight Optimization of Steel Monopile Foundations for Offshore Windfarms	The study examined the potential weight reductions of steel monopiles in offshore wind farms, finding that savings of 10-20% are achievable in comparison to prevailing design methodologies.	Gjersϕe et al. (2015) [156]

Steel corrosion typically results in weight loss due to material degradation caused by chemical reactions with the surrounding environment. Various research studies support this observation, demonstrating that as steel corrodes, there is a concurrent decrease in weight alongside declining corrosion rates [178] [180]. This inverse

relationship between weight loss and corrosion rates holds across different environmental conditions and exposure durations, indicating that higher weight loss correlates with proportionally lower corrosion rates [178]. Advanced monitoring techniques like X-ray imaging and digital processing have been utilized to track the spatial progression of corrosion in steel, further validating the weight reduction resulting from corrosion [179]. Moreover, studies comparing different methods of measuring continuous and discontinuous weight loss have consistently shown that regardless of the measurement approach, corrosion leads to a decrease in steel weight over time [181].

Electrical current-based corrosion methods, such as impressed current techniques, have been observed to reduce both the weight and strength of steel. Research indicates that accelerated corrosion due to these methods can lead to increased corrosion rates, resulting in detrimental effects on the ductility, ultimate load capacity, and mass loss of steel reinforcement [182] [183] [184]. Moreover, the effectiveness of impressed current systems can vary across different corrosion periods, influenced by factors like water electrolysis, which impacts current efficiency and consequently affects the corrosion process and steel mass loss [184]. Additionally, at high alternating current (AC) densities, pitting corrosion can extensively damage steel surfaces, further contributing to weight loss and potentially compromising structural integrity [185]. Therefore, findings from studies underscore that current-based corrosion methods can indeed diminish both the weight and strength of steel over time.

Several applications are observed for the impressed current method. It helps develop analytical replicas for remaining strength and residual service life for specific corrosion levels [15-19]. This method also evaluates the bond asset between corrosion steel and concrete [20,21], studies the spawlling and cracking-behavior due to the expansion of corrosion goods [20], and estimates the serious time for corrosion initiation then its impact on RC structures [26].

Investigators have explored the suitability and efficiency of the overwhelmed current method by varying example geometry, cathode position, and current strength. As instance, El Maaddawy & Soudki, (2003), found the currents above 200 μA/cm^2 (350 and 500 μA/cm^2) caused advanced concrete-strain at a agreed loss of weight, signifying that advanced currents could produce cracks in concrete in addition to

those caused by corrosion products. Hong et al. [22] used X-ray micro-computed tomography (XCT) to study the efficiency of the impressed current method, observing that advanced applied currents (>600 μA/cm^2) resulted in more uniform corrosion products. They also found that Faraday's law predicted mass damage more accurately at advanced currents, while it overestimated mass damage at lesser currents (20 μA/cm^2). Additionally, lower currents applied over longer durations produced more fatalities than advanced currents applied over shorter durations, given the same total charge.

While the rapt current method is well recognized for RC members, its resemblance to usual corrosion, style of claim concerning cathode location, and conduct of the practical current in multifaceted reinforcement interlocks and concrete mediums need additional study for whole thoughtful and calibration. A significant use of any quickening demean method for RC structural components is to assess the presentation of assimilating and consolidation of materials [15,25-29]. The Carbon fiber reinforced polymers (CFRP) are normally used for this drive [30-33]. The effectiveness of CFRP in restoring the forte of rusted RC components has been established [27,34,35].

Though, when corrosion injury is unadorned, a single CFRP leaf may be insufficient. Xie and Hu (2013) stated that when loss of weight on flexural rebar surpasses 50%, a sole CFRP leaf does not deliver adequate strength to the rusted beam. In likewise cases, it is essential to eliminate the dented concrete cover, un-rust the flexural rebar, and put on an epoxy mortar cover beforehand attaching CFRP covers to the concrete external. Growing the number of practical FRP coatings can improve the load-carrying volume of RC beams [36,37]. Though, CFRP is classy related to GFRP. Hybrid CFRP-GFRP consolidation covers have been observed to upsurge strength while upholding comparatively extra ductility equated to single CFRP coats [37,38]. GFRP is a cost-effective subordinate support laminate together with CFRP consolidation schemes [36]. Therefore, CFRP-GFRP hybrid consolidation is structurally feasible and cost-effective.

Preceding research on the overwhelmed current method has either attentive on small-scale non-structural components or large RC components with protected reinforcement interlocks to isolate flexural steel corrosion. In present study, usual-scale RC beams were exaggeratedly tainted using the overwhelmed current method,

and the corrosion behavior of the complete reinforcement net was examined. Moreover, strictly rusted RC beams were reinforced with two schemes: a single coat of CFRP covers and a cross of CFRP and GFRP covers. The conduct of these FRPs, mainly the CFRP-GFRP hybrid, as consolidation covers on severely rusted RC beams has not been lengthily deliberate and permits further study. Current study aims to enhance understanding of the impressed current method and advance the reliability of CFRP and GFRP epoxy-based consolidation schemes for naturalizing severely rusted RC beams.

The deterioration of concrete structures due to steel rebar corrosion is a critical and pressing issue. However, most existing studies rely on laboratory tests where corrosion is typically accelerated using artificial climate methods [20], [21], [22], [23] or electric (impressed current) methods [13], [24], [25], [26], [27], [28]. Despite significant efforts to simulate natural corrosion of reinforced concrete in laboratory settings [20], [28], the corrosion behaviors observed under artificial conditions often differ from those in real-world environments. Consequently, it is problematic to directly apply laboratory results to scenarios involving natural environments, leading to an incomplete understanding of the long-term corrosion behaviors of reinforced concrete structures in natural settings.

This work aims to provide a comprehensive review of the investigations into steel rebar corrosion in concrete under impressed current technique. The objective is to consolidate current knowledge of the corrosion characteristics of steel rebar in concrete exposed to impressed current, thereby offering fundamental insights for assessing the long-term durability and predicting the service life of existing concrete structures. This review discusses the corrosion rate, loss of weight, and the composition and flexure strength of the rusted concrete beams. It primarily focuses on field corrosion caused by impressed current technique by using on beam soffit.

As a primary factor in the failure of reinforced concrete structures (RCS), rebar corrosion causes the expansion of corrosion products, eventually leading to cracking and damage to the concrete [29]. Typically, the high-alkaline environment provided by concrete helps maintain the passivation of rebar, keeping it stable against corrosion [30], [31]. However, when RCS are exposed to chloride-rich environments, such as seas, salt lakes, and other saline areas, chloride ions gradually

penetrate the concrete's pore structure and macro/micro cracks. These ions reach the rebar/concrete interface, adsorbing on the rebar surface and causing partial de-passivation of the passive film, which initiates rebar corrosion [32], [33], [34]. This process further accelerates corrosion, reducing the durability of reinforced concrete structures [35], [36], [37].

Various strategies have been employed to improve the corrosion resistance of rebar, such as using nanomaterial-incorporated fly ash-based cementitious coatings on steel [38], [39], developing alloyed rebar [40], [41], and employing electrochemical protection methods [42]. Among these, corrosion-resistant alloyed rebars hold great promise due to their excellent anti-corrosion properties and manageable cost. These rebars can be integrated into concrete structures using traditional construction methods. One effective approach to enhancing rebar corrosion resistance is adding chromium (Cr) to the steel matrix. Cr-alloyed steel rebar significantly prolongs the service life of RCS in chloride-contaminated environments [43]. However, the Cr content must be carefully controlled to optimize anti-corrosion efficiency. High Cr levels increase production costs, while low levels may not provide adequate corrosion resistance [44]. Studies have shown that low-alloy steel with 0.13% Cu and 0.10% Cr corrodes two to three times slower than carbon steel in chloride-contaminated simulated concrete pore solutions (SCPS) [45]. Similarly, corrosion-resistant low-alloy steel with 0.82% Cr has demonstrated excellent performance compared to traditional carbon-steel rebar [46]. Research on low-alloy steel containing 1% Cr and 1% Al has shown a 64.08% increase in corrosion resistance compared to HRB400 rebar in coral concrete [47]. Further studies report that alloyed rebar with over 3% Cr offers better corrosion protection in chloride environments [48]. Additionally, a 5% Cr-modified steel bar has shown superior anti-corrosion performance in marine splash zones compared to HRB400 carbon-steel rebar [49]. However, practical engineering applications of corrosion-resistant alloyed reinforcement remain limited, and further investigation into the corrosion behavior and mechanisms of Cr-alloyed steel rebar is necessary.

Studying the corrosion behavior and resistance of steel rebar in real corrosive environments provides more reliable data. However, the complexity and uncontrollability of such environments result in long experimental periods and high resource demands. To address this, various accelerated corrosion tests have been developed

to improve research efficiency, including impressed current accelerated corrosion, salt spray tests, galvanic accelerated corrosion, and dry-wet cycling tests [50], [51], [52]. The impressed current accelerated corrosion (ICCC) test, in particular, has become a standard method for evaluating rebar corrosion resistance due to its efficiency. This method accelerates the corrosion process by applying a current to rebar samples, enabling the study of corrosion behavior and resistance over a shorter period [53]. Research has used ICCC to investigate the long-term passivation capability of reinforcing steels in concrete [54] and the corrosion performance of rebar in carbonation-cured concrete [55]. By adjusting experimental parameters such as current density and salt concentration, this method can control the corrosion rate of rebar [56], [57]. Studies have explored the relationship between applied current density levels and the degree of reinforcing steel corrosion [58], and the efficiency of using impressed current to control expected corrosion degrees during different periods [59].

To examine rebar corrosion resistance under accelerated test conditions, it is essential to observe and analyze the characteristics and evolution of the rebar/concrete interface during corrosion. The rebar/concrete interface is generally considered a weak zone in RCS due to the presence of pores and micro-cracks caused by the interface effect between rebar and concrete. These defects lead to a loss of calcium hydroxide at the interface, making it easier for chloride ions to accumulate on the rebar surface, significantly increasing chloride concentration at the interface. These factors facilitate the corrosion of the passive film on the rebar. Corrosion products primarily accumulate at the rebar/concrete interface, deteriorating the chemical environment and stress status of the interface, leading to gradual performance degradation. Therefore, investigating the corrosion characteristics of the rebar/concrete interface is crucial for understanding and improving the corrosion resistance of reinforced concrete structures.

Corrosion in reinforced concrete (RC) beams, driven by the production of rust, leads to deterioration, reducing their durability and structural capacity. This article provides a comprehensive review of the existing literature on dynamic tests for corroded RC beams and discusses the opportunities and challenges in this research area [60]. Corrosion in these beams is primarily caused by chloride attacks on the reinforcement materials. This paper presents an empirical formula for

TABLE 2.2: External/Internal Cathode Assembly

S. N.	Paper Title	Finding	Reference
1	Numerical Investigation of FRCM-Strengthened Corroded RC Beams under Cathodic Protection	An external impressed current cathode system combined with FRCM strengthens and safeguards corroded RC beams, thereby increasing their load capacity. Internally, a cathodic assembly prevents corrosion of steel bars, preserving the beams' structural strength.	Abdulla et al. (2022) [196]
2	Impressed current cathodic protection of chloride-contaminated RC structures with cracking: A numerical study	To safeguard reinforced concrete beams against chloride-induced corrosion, ensure longevity, and preserve structural integrity, electrical currents are applied through internal and external cathodic methods.	Guo et al. (2021) [197]
3	Cathodic corrosion protection system with rebar mounting assembly	Both external and internal impressed current cathodic assemblies provide effective corrosion protection for RC beams through the supply of ionic current and energy storage elements, thereby improving the durability and lifespan of structures.	David and Tobias (2019) [198]
4	Numerical Simulation to Optimize Impressed Current Cathodic Protection Systems for RC Structures	The study aims to optimize impressed current cathodic protection systems for RC structures, aiming to reduce reinforcement corrosion and improve long-term durability and structural integrity.	Qiao et al. (2017) [199]
5	Numerical Simulation of the Impressed Current Cathodic Protection System for a Reinforced Concrete Structure	External impressed current cathodic protection (ICCP) systems effectively prevent corrosion in RC beams by applying a protective electrical potential, as evidenced in the study.	Qiao et al. (2015) [200]

the stiffness coefficient of the corroded dowel based on experimental data and simulates bond-slip deformation using the infinitesimal algorithm and zero-length fiber section element. A numerical modeling method for corroded RC beams using the SFI-MVLEM approach is also proposed [61].

A two-year study investigated mild steel corrosion in Karachi, Pakistan, comparing the results with other major coastal cities. Karachi is a crucial component

of the China-Pakistan Economic Corridor (CPEC) initiative. Analytical methods measured ambient corrosivity, corrosion rates, time of wetness, contaminants, and corrosion products using standards from the International Organization for Standardization and the American Society for Testing and Materials.

Corrosion rates designated the test sites with categories C3, C5, and C4 for two urban and two industrial areas. Over a 20-year period, corrosion rates and corrosivity categories were predicted using the power-linear function, revealing medium C3 and high C4 for maritime sites. The study suggested that mild steel might be the best material for marine environments [62].

The effectiveness and efficiency of various methods for retrofitting corroded RCC beams depend on multiple factors, including the type of repair material used. Recent research has focused extensively on the durability of reinforced concrete, with probabilistic lifetime design methodologies, such as those developed in projects like Duracrete [63], gaining traction. A common conservative approach assumes a structure's lifetime ends with corrosion initiation, leading to excessively large concrete covers to prevent corrosion. This approach may not be practical.

To create more practical concrete cover sizes, it is crucial to include the structural effects of corrosion in lifetime design models. The most significant effect of reinforcement corrosion is volume expansion, which induces splitting stresses in the concrete, affecting the bond between reinforcement and concrete. Many studies have explored this phenomenon [64], with Li and Zheng [65] finding that bond demean shows more variability than stiffness and strength demean.

Understanding the bond behavior between reinforcement and concrete is complex due to different bond mechanisms and failure modes, complicating the study of corrosion effects on bond behavior. Factors like the surrounding structure and reinforcement type significantly influence both uncorroded bond behavior and the impact of corrosion.

This paper systematically organizes these influential parameters to provide an overview of how corrosion affects bond behavior. Finite element modeling is a crucial tool for developing fundamental insights, and experimental data from the literature are reviewed to validate this overview. The goal is to offer a tool for

understanding corrosion's implications and assessing the risks it poses to existing structures.

The corrosion of steel reinforcement bars is a major factor compromising the strength of structural elements. A study was conducted to investigate large-scale corrosion inducement in reinforced concrete beams using the impressed current technique and their subsequent strengthening with Glass Fibre Reinforced Polymer (GFRP) sheets. Five beams (one uncovered and four covered with GFRP mats in different patterns) were subjected to an accelerated corrosion environment and then tested to structural failure. The beams were partially submerged in a 5% NaCl solution to target the bottom rebar, with the beams acting as anodes and the cathode placed in the tub. A constant voltage of 15 V was applied from an external power supply. One beam from each pattern and one control beam were subjected to this accelerated corrosion process.

After 150 hours of accelerated corrosion, the beams underwent non-destructive testing using a rebound hammer and ultrasonic pulse velocity tests. Following this, they were subjected to destructive testing, including a center-point load flexure test. The reduction in the area of the steel reinforcement was calculated using Faraday's Law. The presence of chloride ions in de-icing salts is a primary cause of passive layer breakdown, initiating corrosion. Corrosion occurs only if chlorides, oxygen, and moisture are present in sufficient quantities at the level of the reinforcing steel. GFRP sheets were wrapped around the beams to protect and strengthen them against the loss of shear strength and confinement due to the corrosion of stirrups [66].

2.3 Methods Used for Strengthening of Corroded RCC Beam

In emerging countries, the high cost of retrofitting buildings poses a significant challenge. One of the most commonly used methods for retrofitting is Fiber Reinforced Polymer (FRP). While various methods have been explored over the years, the use of natural fibers in retrofitting has not been extensively studied. This paper provides an in-depth review of the properties of natural fibers and experimental

investigations on FRP, Carbon Fiber Reinforced Polymer (CFRP), Glass Fiber Reinforced Polymer (GFRP), Fiber Reinforced Mortar (FRM), ferro-cement, and binders.

FRP is widely favored for retrofitting due to its unique features, such as corrosion resistance, ease of handling on-site, and availability. FRP is available in various forms, including sheets and strips of different grades and thicknesses. These attributes have made FRP a leading choice in the construction industry for retrofitting. However, the high cost of FRP retrofitting limits its applicability in many contexts. Numerous modifications have been made to FRP to enhance its properties, but these improvements often come with increased costs. FRP can be tailored to achieve desired properties through modifications such as incorporating glass fiber or carbon fiber.

This paper critically reviews the use of epoxy and natural fibers for retrofitting, highlighting their potential benefits and challenges. The goal is to assess the viability of natural fibers as a cost-effective alternative in retrofitting applications [67].

Reinforced concrete is widely utilized in construction, leveraging the exceptional tensile properties of steel to enhance structural performance. This symbiotic relationship, however, faces challenges from steel corrosion, which can detrimentally impact structural integrity [68]. Steel, being a thermodynamically unstable metal, corrodes over time, leading to significant economic losses for nations, with corrosion costs reported to account for 4-5% of industrial countries' gross national product (GNP) [69,70]. Corrosion in reinforced concrete structures initiates when corrosive elements like CO_2 and chlorine penetrate steel reinforcements, resulting in various forms of concrete deterioration such as spalling, cracking, debonding, delamination, and reduced yield and ductility [68,71]. Normally, the high alkalinity of concrete forms a protective oxide film (Fe2O3) around steel, but this film can be compromised by corrosive agents infiltrating concrete voids, thus exposing steel to moisture and oxygen and triggering corrosion [72,73].

To combat structural degradation, especially corrosion, various strengthening and retrofitting techniques have emerged. Fiber-reinforced polymer (FRP) composites have gained prominence over traditional methods like post-tensioning and steel

plate bonding. FRPs, comprising high-strength fibers embedded in a polymer resin matrix and applied using epoxy resins, offer advantages such as lightweight, high strength-to-weight ratio, fatigue resistance, specific tensile strength, corrosion resistance, and ease of application [74,75,76,77].

Among FRP reinforcements, synthetic fibers like carbon, aramid, and glass are widely used in strengthening and retrofitting concrete structures [78]. Carbon fiber, favored for its high tensile strength and modulus similar to steel, is extensively studied and applied in retrofitting applications [78,79]. Glass fiber, though less strong than carbon, is valued for its cost-effectiveness, deformability, and impact resistance in various strengthening applications [78,80]. Aramid fibers offer benefits such as high modulus, dimensional stability, and corrosion resistance [81,82]. However, synthetic fibers pose health risks due to airborne particles during handling, impacting worker health and posing challenges for recycling and sustainability [78,83].

These challenges have prompted the exploration of natural and renewable alternatives to replace environmentally unfriendly materials. Natural fibers offer promising substitutes for synthetic composites, particularly in strengthening and retrofitting construction materials [83]. The incorporation of natural fibers into composites has gained traction over recent years, encompassing a variety of materials such as kenaf, grass reeds, wood fiber, hemp, flax, jute, and bamboo [84]. Research has shown that hybridizing natural fibers with steel fibers can enhance composite mechanical performance [85]. For instance, laminates using kenaf, jute, and jute rope fibers have demonstrated shear strength comparable to carbon fiber-reinforced polymers [16].

Bamboo emerges as a particularly viable natural fiber option for reinforcing and retrofitting concrete elements. Its attributes including high tensile strength, cost-effectiveness relative to CFRP, wood, and steel, rapid growth cycle, and robust mechanical and durability properties have garnered increasing interest among researchers and engineers [86, 87, 88, 89, 90].

Previous studies have explored the use of natural fibers, including bamboo, in reinforcing RC beams under flexural and shear stresses [91,92,93,94]. However, specific investigations on bamboo as a fiber or laminate in strengthening and retrofitting

RC concrete beams remain relatively scarce. For example, Chin et al. [88] studied the potential of bamboo fiber composite plates (BFCP) in strengthening RC beams under flexural loads. Their experiments, which included testing six RC beams (two controls, two un-strengthened, and two strengthened with BFCP), revealed that BFCP-strengthened beams exhibited significantly enhanced structural capacity compared to untreated beams. Similarly, Chin et al. [89] investigated the behavior of RC beams with and without openings strengthened using bamboo fiber-reinforced composite (BFRC) plates, finding that BFRC effectively restored beam capacity to 98% of the control beam. These studies also highlighted BFRC's ability to redirect crack propagation away from strengthened sections, thereby improving beam ductility.

Bamboo represents a natural solution to enhance concrete structural performance. In ongoing research, bamboo fiber laminate is being used to reinforce structural beams exposed to simulated corrosive conditions in the laboratory. This study involves developing a composite material comprising epoxy resin reinforced with long, unidirectional bamboo fibers to strengthen corroded RC beams under flexural stress. ASTM-standard tensile testing was conducted to evaluate the composite's strength, while experimental validation of bamboo fiber-reinforced polymer (BFRP) laminate performance involved a four-point bending test on strengthened RC beams compared to untreated counterparts. The study's findings are expected to inform concrete designers and constructors on effective solutions for mitigating corrosion-related challenges in practice.

Corrosion in concrete significantly increases rust volume, leading to detrimental effects such as cracking and spalling of the concrete cover due to developing tensile stresses [95,96]. These issues not only affect aesthetics but also impair mechanical performance and load capacity. As cracks widen, water permeation increases, allowing aggressive agents access to reinforcements, initiating the corrosion process with water and oxygen [97]. Steel corrosion requires specific conditions: an electrolyte, metallic connection, and multiple steel locations at different energy levels.

The hybrid technique combining near surface mount (NSM) and external bond (EB) methods has been shown to mitigate drawbacks associated with each technique, enhancing its attractiveness in practice. However, there is limited research

on using this approach with FRP composites, particularly those incorporating natural fibers. Although minimal studies exist on strengthening techniques involving bamboo fibers, those available predominantly utilize the EB technique due to its simplicity and cost-effectiveness.

Bamboo as a reinforcing material is employed in various forms including mats, fibers, powder, and strips, with strips demonstrating superior cohesion on structural members. Most research focuses on bamboo as fiber reinforcement in retrofitting structural elements, with limited exploration of bamboo strips [88,89]. Numerous studies have examined bamboo fibers [98,99,100], highlighting their potential in enhancing the performance and longevity of concrete structures.

The significance of methods employed for reinforcing corroded Reinforced Cement Concrete (RCC) beams is crucial for improving structural integrity, extending the structure's service life, and ensuring safety. These strengthening methods are vital to maintaining the safety and longevity of corroded RCC beams. Table 2.2 provides a summary of the various methods commonly utilized for this purpose.

The corrosion of steel reinforcements is a critical issue affecting the safety and durability of reinforced concrete (RC) structures [14118]. This problem is exacerbated in environments near seashores and cold regions where de-icing salts are used, leading to severe damage [119-121]. Corrosion reduces structural integrity by diminishing cross-sectional areas, weakening material properties, and impairing bond strength [122124]. Furthermore, the accumulation of corrosion products around reinforcements applies outward pressure, causing concrete cover cracking or spalling [125-127]. These factors collectively undermine the load-bearing capacity and longevity of RC structures, necessitating effective strategies to restore mechanical properties.

In recent years, fiber-reinforced polymer (FRP) composites have become increasingly popular for rehabilitating deteriorated RC structures [128,129]. Their advantages include high strength-to-weight ratios, resistance to chemical attack, and adaptability to irregular concrete surfaces. However, FRP composites, typically bonded with organic adhesives like epoxy resin, face challenges such as poor compatibility with concrete and inability to be applied on wet surfaces [130]. As a result, researchers have explored cement-based inorganic materials as alternative

Table 2.3: Methods for Strengthening Corroded RCC Beams

Method name	**Materials involved**	**Advantages**	**Disadvantages**	**Author**
UHPC	Concrete Fibers	UHPC layers applied on three sides exhibited them increase in the ultimate flexural strength in the range of 6 to 63% and an increase in the stiffness in the range of 28 to 112% as compared to that of the un-corroded control beam	high shrinkage of UHPC cracking potentials difficulty in casting UHPC on sloped surfaces tensile strain capacity of UHPC is often limited	Al-Huri et al. (2023) Abid Hossain and Carlos M. Chang (2023) Yue Huang et al. (2023) [67]
NSM	FRP sheets Splay anchors Steel plate with bolts	postpone/prevent the debonding failure between NSM FRP and concrete thus largely increase the strengthening efficiency of NSM FRP method.	debonding failures do not achieve full potential of FRP	Jedrzejko, M. J et al. (2023) [68]
Polyurea GFRP	Bonding agents Sprayed polyurea GFRP	No slippage No debonding No early cracks	Manual layup of polyurea Not suitable for hight load caring members	Yu, P., Silva et al. (2023) [69]
HSFRC	High strength fiber reinforced concrete	The peak load- carrying capacity and initial stiffness of rehabilitated specimens showed a significant increase up to 36 % and 84 % respectively, when compared to control specimens. High compressive strength, high tensile strength, and high Workability	brittle failure retrofitting with side face jacketing retrofitting	Dangwal, S., & Singh, H. (2023) [70]

Method name	**Materials involved**	**Advantages**	**Disadvantages**	**Author**
FRP sheets	Fiber reinforced polymers in sheets or leafs	high tensile strength non-corrosive lightweight easy to handle and install increasing the load-carrying capacity of reinforced concrete structures, with some studies showing an increase of up to 47%	strengthening efficiency of FRP sheets can be reduced when the relative eccentricity increases limited fire resistance premature debonding	Jacobs, R. R., & Williams, C. S. (2023) [71]
DE bars	Deep embedded bars	significantly enhanced the beam shear capacity, with an extra strength gain of almost 26% serviceability performance of the beams was also improved	tensile capacity of the DE bars may not be fully utilized, leading to underutilization careful consideration of bar anchorage lengths for effective shear transfer may require additional labor-intensive methods for installation and retrofitting	Bhanugoban, M et al. (2021) [72]
SHCC U-Jacket	Strain-Hardening Cementitious Composites (SHCC)	with 20 mm thick U-shaped SHCC jackets shear-crack response of the repaired beams was improved	inability to restore the initial stiffness of uncracked beams	Hassan, A et al. (2021) [73]

Method name	Materials involved	Advantages	Disadvantages	Author
Metakaolin-based alkali- activated concrete (AAC)	Concrete Alkalies	The metakaolin-based AAC with 15% metakaolin had a high stiffness and increased flexural strength up to 14.4% compared to the specimen before repair. significant bonding with the concrete substrate with less shrinkage and improved strength	Effects on slump flow and workabili can lead to a decrease in compressive strength can also increase the setting time of AAC	Karmegam, A et al. (2022) [74]
EBROG	CFRP sheet Grooves Pressing mechanism	Increase flexural resistance Enhance bond behavior	Need large surface area for grooves making Pressing assembly to press CFRP sheet in grooves	Moshiri, N et al. (2023) [75]
PTMS	Post tensioned metal straps	PTMS can effectively alter the type of failure of the beams from a brittle shear failure to a ductile bending failure load-carrying capacity of the beam can increase by 143%, 170%, and 182% by using two, four, and six strips of PTMS Reduction in the number of cracks	mostly on small specimens debonding failure need assembly on sight to apply this method	Abdullah, W. (2023) [76]
Crack Fill Method	Epoxy, cement mortar	Increase flexural strength Load bearing capacity	Mostly depend upon size, shape, location of crack	Farouk et al 2023 [77]

Method name	Materials involved	Advantages	Disadvantages	Author
Steel Bracing	Steel angles, plates, bolts	improve flexural capacity of (RC) beams high ductility in SMFs seismic force-resisting systems	fatigue failure in the brace or bolted connection due to multiple earthqual	Attia et al. 2023 [78]
Jacketing Method	Steel bars, steel fiber, concrete	enhancing ductility, stiffness, and energy absorption capacity increase the load capacity of beams in existing buildings steel-concrete composite jackets containing steel fiber can increase the tensile strength	formation of shear cracks in coupling beams consideration of factors such as yield strength, concrete strength, rebar size, and jacket thickness	Junhui Cao et al. 2023 [79]

bonding agents, such as fabric-reinforced cementitious matrix (FRCM) or textile-reinforced mortar (TRM) systems. These alternatives effectively address several drawbacks of FRPs but encounter issues like reduced tensile strain in dry fibers within cementitious matrices compared to epoxy, limiting their flexural strengthening efficacy [131-134].

A novel approach for strengthening RC beams, termed FRP grid-reinforced engineered cementitious composite (FGREM), has recently been introduced. FGREM embeds an FRP grid within an engineered cementitious composite (ECC) matrix, optimizing material performance and interface treatment beyond traditional FRCM configurations. The FRP grid, fabricated with interlaced fibers and epoxy resins, provides robust textile reinforcement, preventing premature fiber rupture typical in inorganic matrices. ECC, chosen for its exceptional tensile deformation capacity and strain-hardening properties, effectively suppresses early cracking, maintaining stable tensile strains of 3%8% at low fiber volumes [135-138].

ECCs microcracking behavior (crack width ¡ 100 m at ultimate state) further inhibits aggressive substance penetration, protecting against secondary corrosion in aggressive environments [139-142].

Despite the success of FGREM in enhancing normal RC structures, its application in repairing corrosion-damaged members remains underexplored. Initial studies using basalt and carbon fiber-reinforced grids have shown significant improvements in the flexural bearing capacities of RC beams [143,144]. However, challenges persist, including potential impacts on specimen dimensions and the risk of debonding due to long stress transmission paths during application on corroded beams.

To address these challenges, researchers are integrating FGREM with patch repair methods for corrosion-damaged RC beams. This approach involves removing damaged concrete, cleaning oxidized steel, applying anticorrosion coatings, and reinstating with repair mortar. It effectively restores bond performance without altering specimen dimensions, leveraging ECCs strain-hardening and microcracking characteristics to mitigate interfacial stress concentration and suppress crack-induced debonding more effectively. Comprehensive tests evaluate the strengthening efficacy, assessing flexural behavior, failure modes, load-deflection responses, FRP grid strain, ductility, and energy absorption under varied reinforcement ratios, corrosion levels, strengthening extents, and FRP grid types. In summary, integrating FGREM with patch repair methods represents a promising approach for enhancing the resilience of corrosion-damaged RC structures. This synergistic method not only restores structural integrity but also enhances durability against future deterioration, offering significant potential for practical application in civil engineering. In recent years, there has been increasing interest in rehabilitating and repairing Reinforced Concrete (RC) structures, driven by the escalating issue of premature demean under severe environmental conditions and heavy mechanical loads.

Relying solely on CFRP or BFRP external support for corroded beams without addressing the steel's rust condition is not recommended [188-192]. Rust on the steel surface significantly affects how well the composite material bonds with it, thereby influencing the overall effectiveness of strengthening efforts. Research

indicates that various surface treatments and rust removal techniques are pivotal in optimizing the bond between corroded steel and CFRP composites [191]. Therefore, it is crucial to first eliminate rust from the steel surface using appropriate methods before applying CFRP or BFRP wraps. This ensures a robust and durable bond, ultimately improving the beams' load-carrying capacity and flexural performance [188-190]. Carbon Fiber Reinforced Polymers (CFRPs) and Basalt Fiber Reinforced Polymers (BFRPs) display mechanical properties that vary with temperature. CFRP maintains its strength up to temperatures of 150-200 °C, but beyond this range, there is a rapid decline in strength due to degradation of the matrix and interface [194].

In contrast, BFRP bars exhibit decreased stiffness and flexural strength as temperatures increase, particularly near their glass transition temperature [193]. Moreover, the tensile strength of CFRP decreases nonlinearly with rising temperature, and a tanh function serves as a suitable model for correlating temperature-dependent experimental data [195]. These findings underscore the significance of considering temperature effects when employing CFRP and BFRP in diverse applications, notably in aerospace, automotive, and construction sectors, to ensure optimal structural integrity and performance across varying thermal conditions.

2.4 Applications of CFRP and BFRP in Corroded Beams Re-strengthening

Carbon fiber-reinforced polymers (CFRPs) are widely used in strengthening and rehabilitating reinforced concrete (RC) structures due to their advantageous properties: lightweight, corrosion resistance, and high tensile strength [145]. These materials significantly enhance the mechanical propertiessuch as flexural, shear, and axial strengthof RC members [145]. However, the long-term durability of CFRP systems under harsh environmental conditionssuch as high temperature, humidity, and exposure to saline waterrequires further investigation to understand their degradation mechanisms [145]. Concerns primarily revolve around the behavior of fiber-reinforced polymers (FRPs), the bond between FRP composites and concrete interfaces, and the overall durability of strengthened elements throughout

their service life in severe conditions [145]. Researchers, such as Karbhari (2003), have identified significant gaps in understanding the long-term performance of FRP materials, particularly concerning durability. [145] This lack of comprehensive data raises concerns within the engineering and research communities about the widespread use of epoxy-based composite materials in repairs and strengthening of RC structures.

Moreover, existing data present conflicting conclusions regarding the durability of epoxy-based composite materials. For example, Al-Tamimi et al. (2011) observed strength gains in CFRP-strengthened samples exposed to saline water and sunlight over two years, [145] while Hanna and Jones (1997) found no strength loss in FRP-wrapped specimens under moisture and temperature exposure for extended periods. [145] Researchers reviewed degradation indices from various studies, noting instances of complete strength loss and, conversely, strength gains up to twice that of control samples. [145] As a result, widespread adoption of FRP-epoxy materials for RC structure repairs and strengthening remains tempered by these durability concerns.

Two critical areas lacking reliable data to conclusively assess the durability of fiber-reinforced polymers (FRPs) are their performance under direct sunlight and exposure to saline water. [145] Dolan et al. (2009) extensively studied CFRP systems in twelve different environments, highlighting immersion in high-temperature water and exposure to high humidity without water accumulation at the FRP interface as critical conditions leading to severe and rapid degradation. [145] Table 2.3 and Table 2.4 are showing the results of different researches on flexure strength increased by using the single layer of CFRP and BFRP, respectively.

In regions where temperatures reach up to 50°C, the surface of concrete can exceed 60°C to 70°C, approaching or surpassing the glass transition temperature (Tg) of most commercially available epoxy adhesives. This thermal condition causes epoxy adhesives to lose tensile strength and modulus [145]. Furthermore, moisture ingress disrupts cross-linking within the epoxy matrix, damages CFRP laminates and fibers, and weakens the bond between the epoxy and concrete substrate. The fiber-matrix interface also suffers under moisture exposure [145]. Myers et al. (2001) noted a stiffness loss of up to 60% in CFRP-strengthened beams subjected to temperature and humidity cycles. Helbling et al. (2006) observed increased

Table 2.4: Flexure Strength Increased by Using CFRP Single Layer

S. N.	Paper Title	Finding	Reference
1	Flexural behavior of RC beams contains rubberized pieces and strengthened with CFRP sheets	The flexural strength demonstrated an increment of 8.57% when a sole layer of CFRP sheet reinforcement was applied to rubberized concrete beams, as reported in the research focusing on the flexural performance of RC beams.	Adday et al. (2023) [157]
2	Flexural Strengthening of Reinforced Concrete Beams with Variable Compressive Strength Using Near-Surface Mounted Carbon-Fiber-Reinforced Polymer Strips [NSM-CFRP]	The enhancement in load-carrying capacity of reinforced concrete beams is observed through the application of near-surface mounted carbon-fiber-reinforced polymer (NSM-CFRP) strips, resulting in an increase in flexural strength ranging from 10.36% to 52.28%.	Al zu'bi (2022) [158]
3	Flexural Behavior of Reinforced Recycled Aggregate Concrete Beams Strengthened by CFRP	The beams' flexural strength demonstrated a 23% enhancement through the application of a singular layer of CFRP utilizing the EBR technique, and a 40.4% improvement when employing the EBROG approach.	Dawood and Asadi (2022) [159]
4	Flexural Strengthening of Prestressed Girders with Partially Damaged Strands Using Enhancement of Carbon Fiber Laminates by End Sheet Anchorages	The flexural capacity demonstrated a notable increment of around 13% when a solitary layer of CFRP laminates was applied, thereby amplifying the structural integrity of partially deteriorated prestressed girders within the investigation.	Abbas et al. (2022) [160]
5	Simulation Behavior of Flexure in Reinforced Concrete Beams Strengthened with Carbon Fiber Reinforced Polymer (CFRP)	The flexural strength of beams enhanced by the application of a sole layer of CFRP experienced a significant increase of up to 32.8% as outlined in the simulation analysis carried out in the study.	Al fahdawi et al. (2015) [161]

Table 2.5: Flexure Strength Increased by Using BFRP Single Layer

S. N.	Paper Title	Finding	Reference
1	Flexural performance of RC beams externally strengthened with a single-layer of basalt fiber reinforced polymer sheets	The flexural strength of beams experienced a significant increase of 78% after being reinforced with a sole layer of Basalt Fiber Reinforced Polymer (BFRP) sheets, according to the findings of the study.	Kadhim and Ozakca (2022) [162]
2	Efficacy of CFRP/BFRP laminates in flexurally strengthening of concrete beams with corroded reinforcement	The flexural strength of beams was enhanced by a maximum of 41% through the utilization of a solitary layer of Basalt Fiber Reinforced Polymer (BFRP), demonstrating its cost-efficient viability as a reinforcement solution for deteriorated reinforcement.	Do-dai et al. (2022) [163]
3	Flexural Strengthening of Reinforced Concrete Beam Bonded with Built-in T Type BFRP Plate	The flexural strength of the beam showed a noticeable enhancement ranging from 14% to 30% upon reinforcement with a singular layer of Basalt Fiber Reinforced Polymer (BFRP) plate in comparison to the beam under standard conditions.	Chhorn et al. (2022) [164]
4	An anchorage technique for flexural strengthening of RC beams using NSM BFRP bars	According to the study on using NSM BFRP bars for flexural strengthening, applying a single layer of BFRP with ETS end anchorage increased the flexural capacity of RC beams by 90%.	Diab (2022) [165]
5	Flexural Behavior of Glulam-Concrete Composite Beams Reinforced Using CFRP Sheets	Applying a single layer of BFRP increased the flexural strength of the composite beam by 3.07%.	Hakiki and Mujiman (2020) [166]

moisture absorption in the FRP matrix under high-temperature strain, with localized fiber damage becoming more pronounced after 18 months of hygrothermal exposure.

The durability of concrete members strengthened with FRP sheets using various

epoxy adhesives has been explored by researchers [145]. Choi et al. (2012) investigated three epoxy systems and two types of CFRP sheets, subjecting prism specimens to diverse environments including alkaline solutions, saline water, UV light, outdoor exposure, and hygrothermal conditions (30°C to 60°C) over 18 months. They found that each adhesive system responded uniquely to environmental stresses, with mixing ratios, resin types, and application amounts significantly impacting durability at the interface and within laminated fibers. [145] Grace and Singh (2005) observed differing impacts of 100% humidity on CFRP plates versus fabrics, noting a slight load-carrying capacity enhancement for CFRP fabrics under such conditions [145].

Studies evaluated the performance of various epoxy and CFRP/GFRP sheet combinations on flexural strength after wet/dry cycles in saline water. They highlighted the critical role of epoxy adhesives and their bond with concrete under harsh climate conditions [145]. El-Hawary et al. (1998, 2000) investigated epoxy-strengthened concrete under different environments and found initial strength losses followed by recovery attributed to seasonal temperature and humidity effects, emphasizing the influence of epoxy type on concrete strength. [145] Table 2.5 is showing the significance of BFRP over GFRP and FRP.

Pan et al. (2015) examined water immersion effects on CFRP systems, noting increased water uptake and reduced mechanical properties with longer exposure times and higher temperatures [145]. Li et al. (2019) reviewed epoxy degradation under saline conditions, emphasizing rapid strength loss with increased sodium chloride concentrations and prolonged exposure times.

Long-term studies by Nishizaki et al. (2005) over five years showed slight reductions in CFRP tensile strength initially, followed by recovery, while Sen (2015) reported minimal degradation in CFRP tensile strength over ten years in real-world applications. [145] Al Azzawi et al. (2018) observed durable performance of CFRP-strengthened masonry under hot and humid climates over two decades.

Overall, these studies underscore the complex interplay of environmental factors and epoxy properties in determining the durability of FRP systems, highlighting the need for further research to enhance understanding and inform practical applications in structural strengthening.

Table 2.6: Significance of BFRP

S. N.	Paper Title	Finding	Reference
1	A comparative life cycle assessment of fiber-reinforced polymers as a sustainable reinforcement option in concrete beams	BFRP outperforms GFRP and CFRP in 10 out of 14 environmental performance categories, making it a more sustainable reinforcement option for concrete beams.	Sbahieh et al. (2023) [167]
2	Development of Basalt Fibre Reinforced Polymer (BFRP) Rebar Infused with Geopolymer Binder	BFRP is superior to GFRP and FRP due to its non-corrosive nature, high tensile strength, and improved interfacial bonding with concrete, enhancing durability and structural performance in various applications.	Subhani (2023) [168]
3	Experimental and Numerical Investigations of BFRP-Reinforced Normal and High Strength Concrete Beams	BFRP is favored over GFRP and FRP because of its high performance, non-metallic composition, corrosion resistance, and cost-effectiveness, making it a durable option for reinforcing concrete structures.	Bigenwald (2023) [169]
4	Failure Study of BFRP Joints with Two Epoxy Adhesives under Hygrothermal Coupling	BFRP offers advantages such as being lightweight, having high strength, cost-effectiveness, and environmental friendliness, making it superior to GFRP and FRP in civil applications.	Niu et al. (2023) [170]
5	A review on basalt fibre reinforced polymeric composite materials	BFRP better than GFRP and CFRP due to its cost-effectiveness, higher strength, and improved adhesion properties, making it a viable alternative in composite materials.	Fegade et al. (2022) [171]

Studies have indicated that the bond between FRP and concrete substrates deteriorates significantly under the combined influence of harsh climates and applied loads. [145] However, these studies often focused on small prisms and single-lap shear test samples, lacking extensive investigation into the durability of typical-scale beams. Current research underscores that temperature and moisture adversely affect the bond strength, tensile strength, and modulus of elasticity of FRP-epoxy systems, with moisture ingress particularly initiating epoxy matrix plasticization and strength reduction. Variations in FRP types and epoxy systems also yield differing responses under these conditions.

This study aims to assess the long-term durability of CFRP-strengthened RC

beams under the harsh environmental conditions typical of Qatar and similar regions, characterized by sustained sunlight exposure, saline water, and airborne chlorides. Specimens underwent exposure to laboratory conditions, outdoor sunlight, and immersion in 3% NaCl solution for durations of 6, 12, and 24 months. Strength reduction factors (CE) for the exposed CFRP beams were established by comparing strength retention against un-strengthened and unexposed specimens, as well as controlled laboratory-strengthened specimens and unexposed control specimens subjected to the same environmental conditions for the same periods. To the authors' knowledge, this study provides a comprehensive examination of typical-scale CFRP-strengthened RC beams' long-term durability under real-world harsh climates, filling a significant gap in existing research. Table 2.6 is showing the results of different researches on the u se of CFRP and BFRP on RC Beams, Columns, and Slabs.

For the design and analysis of CFRP-strengthened beams, the strength reduction factors (CE) derived from this study are recommended and compared with those recommended in the American Concrete Institute (ACI) 440.2R-17 guidelines (ACI, 2017). This research aims to bolster confidence in the use of CFRP strengthening techniques and alleviate concerns regarding their performance in severe climatic conditions.

The utilization of Basalt Fiber Reinforced Polymer (BFRP) proves highly effective in significantly enhancing the ultimate load-carrying capacity of flexural dominated reinforced concrete (RC) beams. Comparative studies have demonstrated that BFRP outperforms Glass Fiber Reinforced Polymer (GFRP) composites in enhancing the ultimate load-carrying capacity of RC beams. Both types of strengthening techniques effectively alter the load-carrying capacity of RC beams. However, in direct comparison, Strengthening Technique B exhibits superior performance over Strengthening Technique A [146].

Basalt fiber-reinforced polymer (BFRP) sheets have also been employed to strengthen beams, improving their flexural performance and damage tolerance. Experimental assessments involving various failure load percentages utilized multi-view digital image correlation to monitor deformation and crack propagation. Additionally, compressive and flexural strengths were enhanced with the inclusion of BFRP in oil well cement, showing improvements of 15.9% and 13.5% respectively over

TABLE 2.7: Use of CFRP and BFRP on RC Beams, Columns, and Slabs

S. N.	Paper Title	Finding	Reference
1	Flexural Behavior of Corroded Concrete Beams Strengthened with Carbon Fiber-Reinforced Polymer	The flexural capacity of corroded concrete beams reinforced with CFRP diminished as corrosion levels rose, with a relative strength of 52.5% observed at a corrosion level of 25.6%.	Wang and Wu (2023) [172]
2	Strength of Hybrid Steel-BFRP Reinforced Concrete Beams with Openings in the D-Region Strengthened Internally and Externally	The addition of BFRP reinforcement substantially enhanced beam load capacity: internal BFRP bars increased load by 60%, while BFRP sheets at corners increased it by 76%. When combining internal steel with external BFRP, the load capacity rose by 137%.	Yehia (2023) [173]
3	Performance evaluation and FRP strengthening of concrete-filled steel tubular columns subjected to vehicle impact	Wrapping CFRP around CFST columns enhances their performance during vehicle impact by orienting fibers at 90°C for flexure and shear resistance, and at 0°C to prevent flexural failure. This approach improves performance significantly without requiring complete wrapping coverage.	Hu and Wang (2024) [174]
4	Experimental-numerical study on axial compression performance of square concrete columns confined by new-type BFRP	The research indicated that BFRP wrapping improved the axial compression capacity of concrete columns by 28.45% to 64.73%, demonstrating a lesser effectiveness when compared to CFRP reinforcement.	Chen et al. (2024) [175]
5	Behavior of Reinforced Lightweight Concrete Slab with Initial Cracks	The application of CFRP sheets boosted the ultimate load capacity by 17.7% and reduced deflection by 31.4%, effectively restoring reinforced lightweight concrete slabs and halting the propagation of cracks.	Khadim and Abdulridha (2024) [176]
6	Short-Term Efficiency of Using Sustainable BFRP Bars in Post-Tensioning Systems for One-Way RC Slab	The implementation of BFRP post-tensioning systems notably improved load capacity and reduced deflection in RC slabs. Hybrid reinforcement combining BFRP and steel bars enhanced energy absorption and ultimate load capabilities.	Yehia (2023) [177]

unmodified cement [147]. Analytical methods, experimental observations, and numerical simulations were utilized to comprehensively study the bonding behavior of these sheets [148]. Table 2.7 is showing the literature review on external and internal cathode assembly of current.

The findings underscored that BFRP sheets significantly increase flexural strength and ductility of beams. Debonding at the end of the bonding zone was identified as a primary failure mode due to high interfacial stress. Effective bonding zones were evidenced by strain distributions along BFRP sheets, supporting numerical modeling efforts. Models were developed to predict failure loads and determine effective bond lengths between sheets and concrete [149, 150]. When combined with reinforcement materials like PVA fibers, basalt fiber-reinforced sheets enhance load-carrying capacity and extend beam service life [151].

CFRP materials are widely used globally for flexural strengthening of concrete structures, enhancing their load carrying capacity through passive repair methods involving non-prestressed CFRP materials.

Over the past few decades, extensive research has been conducted on enhancing the flexural strength of reinforced concrete (RC) beams using various strengthening techniques, including concrete, steel, and artificial fiber reinforced polymer composites (FRP) [146]. Among artificial FRPs, glass, carbon, and aramid fibers have been extensively studied [146]. For instance, Attari et al. (2012) investigated the strengthening of RC beams using glass FRP sheets, carbon FRP sheets, and hybrid FRP sheets. They constructed seven simply supported RC beams of identical dimensions and reinforcement details: two 10-mm diameter steel bars (1.6% steel ratio) for bottom flexural reinforcement, two 8-mm bars for top reinforcement, and 6-mm diameter stirrups spaced at 120 mm intervals for shear reinforcement.

The beams had dimensions of 160 mm in height, 100 mm in width, and a span length of 1300 mm within a testing rig limited to 1500 mm overall length. The study found that a dual-layer glass-carbon fiber composite significantly enhanced the strength of the beams, increasing their capacity by 114% without significant ductility loss. The U-anchorage strengthening configuration was particularly effective in redistributing internal forces through increased beam deformations [146].

Michael et al. (1994) experimentally investigated fourteen RC beams, including control beams and beams reinforced with aramid fabric, E-glass fabric, and graphite fiber fabric. They observed enhancements in flexural capacity ranging from 36% to 57%, with corresponding increases in flexural stiffness between 45% and 53% [10]. Grace et al. (2002) studied thirteen rectangular beams strengthened with various carbon fiber materials, observing differences in yield load and ductility between uniaxial carbon fiber sheets, carbon fiber fabric, pultruded carbon fiber plates, and hybrid fabric configurations.

In contrast to synthetic fibers, natural fibers such as jute and basalt fibers are gaining popularity in structural strengthening and repair [146]. Alam et al. explored the use of kenaf fiber reinforced polymer (KFRP) laminate for shear strengthening of RC structures, finding that KFRP laminates with 25% fiber content exhibited significantly higher tensile strength (119.6 MPa) compared to epoxy laminates without kenaf fiber, demonstrating potential for enhanced structural performance [146].

The present study aims to investigate the flexural response of RC beams strengthened with natural jute fiber and basalt fibers, continuing the exploration of alternative fiber reinforcement strategies in structural engineering.

Two critical areas lacking reliable data to conclusively assess the durability of fiber-reinforced polymers (FRPs) are their performance under direct sunlight and exposure to saline water [145]. Dolan et al. (2009) extensively studied CFRP systems in twelve different environments, highlighting immersion in high-temperature water and exposure to high humidity without water accumulation at the FRP interface as critical conditions leading to severe and rapid degradation.

To enhance the strength of corroded beams without using external fiber wrapping, several techniques can be employed. One method involves utilizing a durable cementitious composite matrix embedded with randomly distributed plastic fibers. This approach aims to retard metal degradation caused by corrosion, thereby improving the residual anchorage capacity [186]. Furthermore, in the case of reinforced concrete beams, a combination system of carbon fiber-reinforced polymer (CFRP) laminates and ultrahigh-performance concrete (UHPC) layers has been proven to significantly boost both load-bearing capability and rigidity. This hybrid

system offers an alternative to traditional external fiber materials for reinforcing corroded beams [187]. These approaches highlight viable strategies for enhancing the strength of corroded beams without relying on external fiber wrapping, offering effective solutions for structural rehabilitation and upkeep.

The economic viability of repair, replace or retrofitting of existing buildings is influenced by several key factors, particularly the extent of damage, cost considerations, and energy performance improvements. Understanding these factors can guide decision-makers in optimizing retrofitting strategies. The level of damage significantly dictates the choice of retrofit strategy. Minor damages may only require basic interventions, while major damages necessitate comprehensive retrofitting efforts. For instance, minor retrofits (RS1) achieved a 16.7% energy reduction, while major retrofits (RS3) resulted in a 24.12% reduction in energy consumption.

Minor Damage (RS1): A retrofit strategy addressing minor damage can yield a 16.7% reduction in energy consumption, suggesting that even slight damage can justify retrofitting efforts.

Moderate Damage (RS2): For moderate damage, retrofitting can achieve a 19.87% reduction,indicating that as damage increases, the potential benefits of retrofitting also rise.

Major Damage (RS3): When damage is significant (over 30%), retrofitting strategies can lead to a 24.12% reduction in energy use, making it a more compelling economic choice [201].

A common threshold for initiating retrofitting is around 30% damage, as this level often leads to significant economic losses if not addressed promptly [202]. Seismic Risk and Economic Loss: In urban settings, buildings with higher damage percentages face greater economic losses during seismic events. A study on 98,618 buildings in Xian highlighted that neglecting indirect economic losses can lead to underestimating the benefits of retrofitting, especially for unreinforced masonry structures [203]. Cost-Effectiveness of Strategies: In Surabaya, retrofitting strategies that reduced damage by 4.75% yielded a high cost-benefit ratio, emphasizing that lower damage levels correlate with more favorable economic outcomes [204].

Here question arises Why are you focusing on the corrosion due to current artificial method? How often concrete structures are subjected to DC currents? Steel corrosion is by far the biggest durability issue for reinforced concrete structures, although other deterioration mechanisms will lead to attack of the concrete itself, he notes, such as freeze-thaw scaling, moisture, acid or sulfate attack, thermal cracking, shrinkage from drying, impact, erosion, and wear. That is why controlled and accelerated corrosion mechanism is adopted without disturbing concrete properties to carryout corroded steel efficacy on the structural behavior of structure [205].

Stray current (DC) induced corrosion is a major technical challenge for modern electrified railway systems. It can lead to corrosive damage to railway tunnel segmental linings and surrounding infrastructure. For an electrified railway, the transmission of power is normally provided by an overhead wire or a conductor rail.. The leakage of stray current to surrounding structures, e.g. tunnel lining segments and reinforced concrete sleepers, can lead to steel reinforcement corrosion and the disintegration of concrete. Stray current can also accelerate corrosion of neighboring infrastructure such as underground service cables, water mains and gas pipes which will ultimately reduce their service life. The corrosive damage due to stray current will become more prominent in the UK as the government is committed to developing more electrified rail networks to provide sustainable and cleaner services for the public (an electric train consumes 20% less power compared to a diesel-powered train, along with a reduced CO2 emission by at least 20% [206]. The most common types of RC structures susceptible to damage from DC currents-induced corrosion in steel are those with steel reinforcement, such as bridges, buildings, and parking structures [207].

Chapter 3

Experimental Program

3.1 Sample Geometry and Testing Matrix

The beam's geometry and reinforcement are shown in Fig. 3.1. This phase of the project focuses on artificial corrosion, strengthening and flexural testing of beams. Beams have rectangular shape having 1000mm length, 150 mm width and 200mm depth and designed using the American Concrete Institute (ACI) codes ACI CODE-31819 as tension-controlled sections. Furthermore, Idea to cast beam of such dimension is to meet actual behavior of beam under four-point loading and deflection. Keeping above in view, available resources limitation is also a point of concern because laboratory apparatus available at CUST comprises of UTM with 1m span between externals supports. Total 16 beams were casted with 4000 psi plant mix concrete.

Fig 3.1(a) illustrates the reinforcement details that is 4 bars of #4 are used as main flexural bars while #3 bars are used as stirrups spaced at 100mm making it total 9 in numbers. Longitudinally cover of 50mm is provided at both ends so the length of each main bar is 900mm. Fig 3.1 (b) shows cross section cut at location A-A and cover at the bottom of beam is kept 37mm and 25mm at sides of beam. CFRP and BFRP wraps are applied at the soffit of beams and their width is 100mm and length 900mm as shown in Fig 3.1 (a) (b). The clear cover provided is 25mm and 50mm at lateral side and longitudinal side respectively. Thickness of CFRP/BFRP laminate was 0.12mm $\pm$ 0.02mm. But, after applying paste epoxy and adhesive total thickness of the strengthening system reaches to 1.5mm.

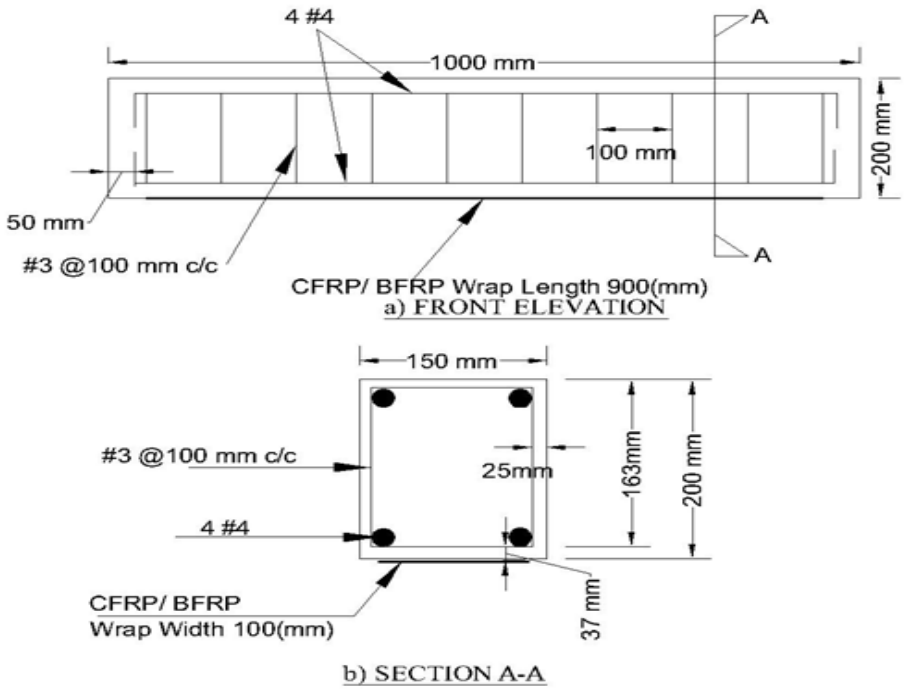

FIGURE 3.1: Geometry and Reinforcement of The Beam

Table 3.1 illustrates nomenclature of beams based on the strengthening system, applied current, the proposed weight loss, period of current application and strength deficient beams. Total 16 beams were casted out of which 6 were corroded with induced current, whereas remaining 10 are un-corroded that also includes 2 control beams. Beams were corroded or degraded till 15 days at 8 hours interval with AC power supply running at 220V. Control beams are referred as CB, while corroded beams are symbol as C. Controlled beam strengthened are CBS, corroded beams Strengthened CS and further BFFRP and CFRP is attached with them subjected to strengthening system. There are 4 beams which were pre-cracked by applying 70% of ultimate load of the control beam. Then these were strengthened 2x with BFRP and 2x with CFRP. Total number of four point loading tests performed is 20 out of which 16 are tested till fracture point while 4 are tested till 70% controlled beams ultimate load. Beams are categorized as Corroded, Controlled beam, Pre cracked Beam, corroded strengthened with BFRP, corroded strengthened with CFRP, Controlled strengthened with BFRP, Controlled strengthened with CFRP and last 70% cracked beam strengthened with BFRP and CFRP. Each category has two beams specimen.

**CB= Control beam, C= corroded, CBS= control beam strengthened, CS= corroded beam strengthened, 0.7 shows beam is pre-cracked with loading applied 70%*

TABLE 3.1: Nomenclature matrix for beams corroded, controlled and strengthened with CFRP/BFRP

Sr No	**Designation**	**Applied Current (μA/cm^2)**	**Current application in days (8 Hours/day)**	**Expected Weight Loss %**	**Strengthening system**
1	CB-1	-	-	-	-
2	CB-2	-	-	-	-
3	C-1	1650	15	10	-
4	C-2	1650	15	10	-
5	CS BFRP-1	1650	15	10	BFRP
6	CS BFRP-2	1650	15	10	BFRP
7	CBS BFRP-1	-	-	-	BFRP
8	CBS BFRP-2	-	-	-	BFRP
9	CS CFRP-1	1650	15	10	CFRP
10	CS CFRP-2	1650	15	10	CFRP
11	CBS CFRP-1	-	-	-	CFRP
12	CBS CFRP-2	-	-	-	CFRP
13	0.7 CB-4 BFRP-1	-	-	-	BFRP
14	0.7 CB-2 BFRP-1	-	-	-	BFRP
15	0.7 CB-3 CFRP-1	-	-	-	CFRP
16	0.7 CB-1 CFRP-1	-	-	-	CFRP

of the ultimate load of controlled beam.

After current induced to the required level, appearance of the beam was investigated visually. The cracks in concrete were measured.

3.2 Materials

Project involves different kind of materials ranging from locally available to imported from other country. Most advanced epoxies and adhesives are used in this research. Materials used are; Concrete (cement, sand, aggregate), Mild Steel,

Stainless steel plate (cathode), Carbon Fiber Reinforced Polymer (CFRP), Basalt fiber Reinforced Polymer (BFRP), Epoxy each material is detailed below.

3.2.1 Concrete

All beams and cylinders were cast with 4000 psi ready-mix concrete. This concrete also termed class A3 as per NHA General Specifications 1998 (401-1) . Ordinary Portland Cement (OPC) were used weighing 400 Kgs whose specific gravity is 3.12, Coarse aggregate total weight was 1061 Kgs with size range of the aggregates 5mm, 12mm to 20mm and weight 318 Kg, 636 Kg, 106 kg respectively. Fine sand weighs 732 Kgs. While water used is 168 Kgs that shows water cement ratio 0.42. Slump of the concrete was between 100-125 mm. Average Compressive strength observed after 28 days is 4300 psi.

3.2.2 Mild Steel

Steel of Locally available steel manufacturing firm was used. #3 and #4 steel were used for all sixteen beams. #3 was used for stirrups and #4 for main flexural bars at top and bottom. Given below Table 3.2 illustrates chemical composition of batch of steel manufactured.

Table 3.2: Steel rebar's chemical composition

C	**Si**	**Mn**	**P**	**S**	**V**	**Nb**	**Cu**	**Ni**	**Cr**	**Mo**	**N**	**Ce**
0.291	0.414	1.38	0.038	0.024	0.0026	0.0005	0.12	0.051	0.08	0.0029	0.009	0.55

3.2.3 Stainless Steel Plate

Stainless steel plate SS304/ SS304L is used as cathode for current inducement circuit. Current is supplied by the power supply and it flows through steel bars embedded in beam and ends at the stainless steel plate (cathode) externally attached to beam through an electric wire. Concept behind to use stainless steel is that it is not a good conductor of electricity so iyt will absorb ions and will be corroded less. It also acts an earthing rod, that controls and dispose off electrons,

once the current flow circle is completed. Chemical composition of stainless steel is;

TABLE 3.3: Chemical composition of Stainless steel

Chemical Composition %								
Garde	**C**	**Mn**	**P**	**S**	**Si**	**Cr**	**Ni**	**N**
304	≤0.08	≤2	≤0.045	≤0.03	≤0.75	18.0 ∼ 20.0	8.0 ∼ 10.5	0.1

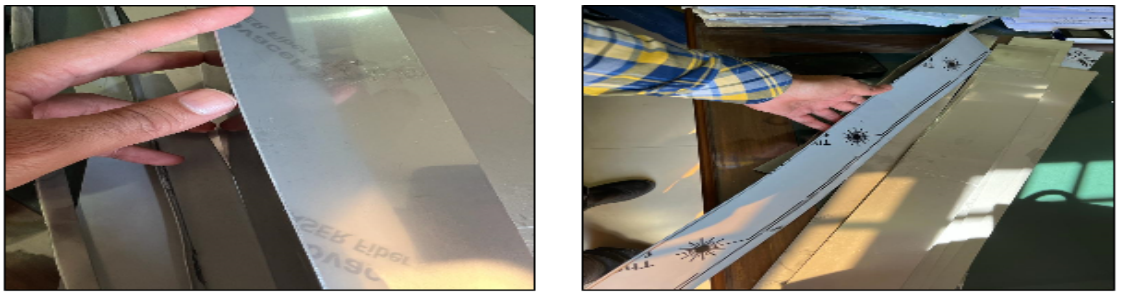

FIGURE 3.2: Stainless Steel Plate as Cathode

3.2.4 DC Power Supply & Electric Connections

DC Power supply TN3010D operating on 30 volts and current 10 Amp with manual adjustable regulators was used. As our max requirement was 5 Amp per beam so this power supply was sufficient to work. Moreover electric cable 2.5mm 2 core, having 7 conductors and each conductor diameter 0.29mm was used. locally available electric cable manufacturer was selected for this purpose whose cable is pure copper and having good insulation so that chances of short circuit can be eliminated when intact with water. This cable can withstand up to 25 Amp current.

3.2.5 Carbon Fiber Reinforced Polymer (CFRP)

Fig 3.3. Shows one of the main ingredient of this project. It is available in different forms e.g 230gsm, 300gsm, 450 gsm and 600gsm. Each have its own characteristics. But, for this project we used 300gsm unidirectional (UD) CFRP locally aviable in the market. Its elastic modulus is 230 to 250 GPa. Thickness of the wrap is 0.167mm and tensile strength is approx 4000 MPa. But after application of adhesives the laminate thickness approximately reaches to 1.4mm. Elongation at

failure is approx 1.9 % as per manufacturer summary sheet. Sheet was cut into the strips of 900mm length and 100mm wide as required at the soffit of beam Fig 3.4.

FIGURE 3.3: Carbon Fiber Reinforced Polymer (CFRP) Uni-Directional

FIGURE 3.4: CFRP & BFRP Strips

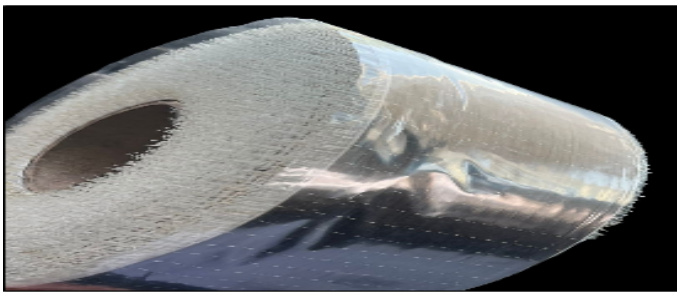

FIGURE 3.5: Basalt Fiber Reinforced Polymer (BFRP) 100mm width roll Uni-Directional

3.2.6 Basalt Fiber Reinforced Polymer (BFRP)

BFRP shown in Fig 3.5 was not locally available in the market so it was imported from china. It is also available in different weights and forms but we choose 300gsm BFRP. Its thickness is approx 0.12mm and tensile strength is 2200MPa. Elastic modulus is approx 95GPa and % elongation at break is approx 2.13 according to manufacturer sheet. This sheet was already available in the form of 100mm wide strips so only it was cut into the length of 900mm.

TABLE 3.4: Comparison of BFRP and CFRP Properties

Test Name	**BFRP**	**CFRP**
Weight	310 grams/sqm	310 grams/sqm
Width	100 mm	110 mm
Thickness	0.12 mm	0.167 mm
Tensile elastic modulus	95 GPa	165 GPa
Elongation	2.13%	2.15%
Tensile strength	2200 MPa	2500 MPa

3.2.7 Base Epoxy & Adhesives

Base Paste Epoxy shown in Fig 3.6 is a trowel able, sag resistant patching compound for concrete and other substrates. This is applied to give CFRP/BFRP wraps a smooth surface. This compound is two components, 100% non-volatile filled epoxy/amine resin system. Part A and Part B is mixed with ratio 1:1 and its gives thick grey appearance when its wet and white once its dry. Compressive strength: ASTM D695 $\geq$ 70 MPa @ 7 days , E-Modulus (compression): ASTM D695 $\geq$ 12000 MPa @ 7 days , Tensile strength: ASTM D638 $\geq$ 27 MPa @ 7 days , Adhesive strength: ASTM D4541 $\geq$ 3.5 MPa (Concrete Failure), Pot life (F.I.P.) 50 - 70 min @25°C Mixing ratio 1:1 (Base: hardener) , Slant shear bond strength: AASHTO T-237-73 $\geq$ 25 MPa (Old / New Concrete) ,Heat deflection: ASTM D648 $\geq$ 50°C.

FIGURE 3.6: Base Paste Epoxy Part A and Part B, mixing ratio 1:1

This adhesive also comes in two parts and mixed with ratio of 2:1 which gives dark blue glossy appearance Fig 3.7. Adhesives are used to stick CFRP/BFRP wraps with base epoxy which is applied at soffit of beam or concrete substrate surface by rollers at the rate of 0.25 - 0.30 kg/m^2 . XPERT PROFIBER CW ADHESIVE is 100% solids, low viscosity epoxy material that is used to encapsulate Profiber carbon,basalt, glass, and aramid fibre fabrics. Adhesive cures to provide a high performance FRP laminate. The resulting FRP laminate can provide additional strength to concrete, masonry, steel, and wood structural elements. It is Used to encapsulate any fabric and acts as a substrate primer for the wet application it is 100% solids epoxy Low odor, low VOC's .its Yield Strength is (55 MPa) Strain at Yield 2.5%. Elastic Modulus (3034 MPa), Ultimate Strength (55.2 MPa) and Rupture Strain 3.5%. While at flexural its Yield Strength Is (138 MPa), Elastic Modulus (3724 MPa) and Ultimate Strength (138 MPa). Crack filler with Low

FIGURE 3.7: Adhesive in two parts and mixed with ratio of 2:1

Viscosity Two Component Injection Resin thin cracks & pin holes is also used for the beams which are pre-cracked upto 70% of the ultimate strength of control beam. It is low viscosity epoxy grout based on specially selected epoxy resins and hardeners to produce a highly fluid grout for injection into cracks in masonry and concrete. This method is suitable for repair to floor slabs or other horizontal surfaces. At 20°C its Pot Life is 35 minutes, Viscosity 350 Centi poise and Specific Gravity 1.05. Fig 3.7.

3.3 Sequence of Works

Following is the sequence of works.

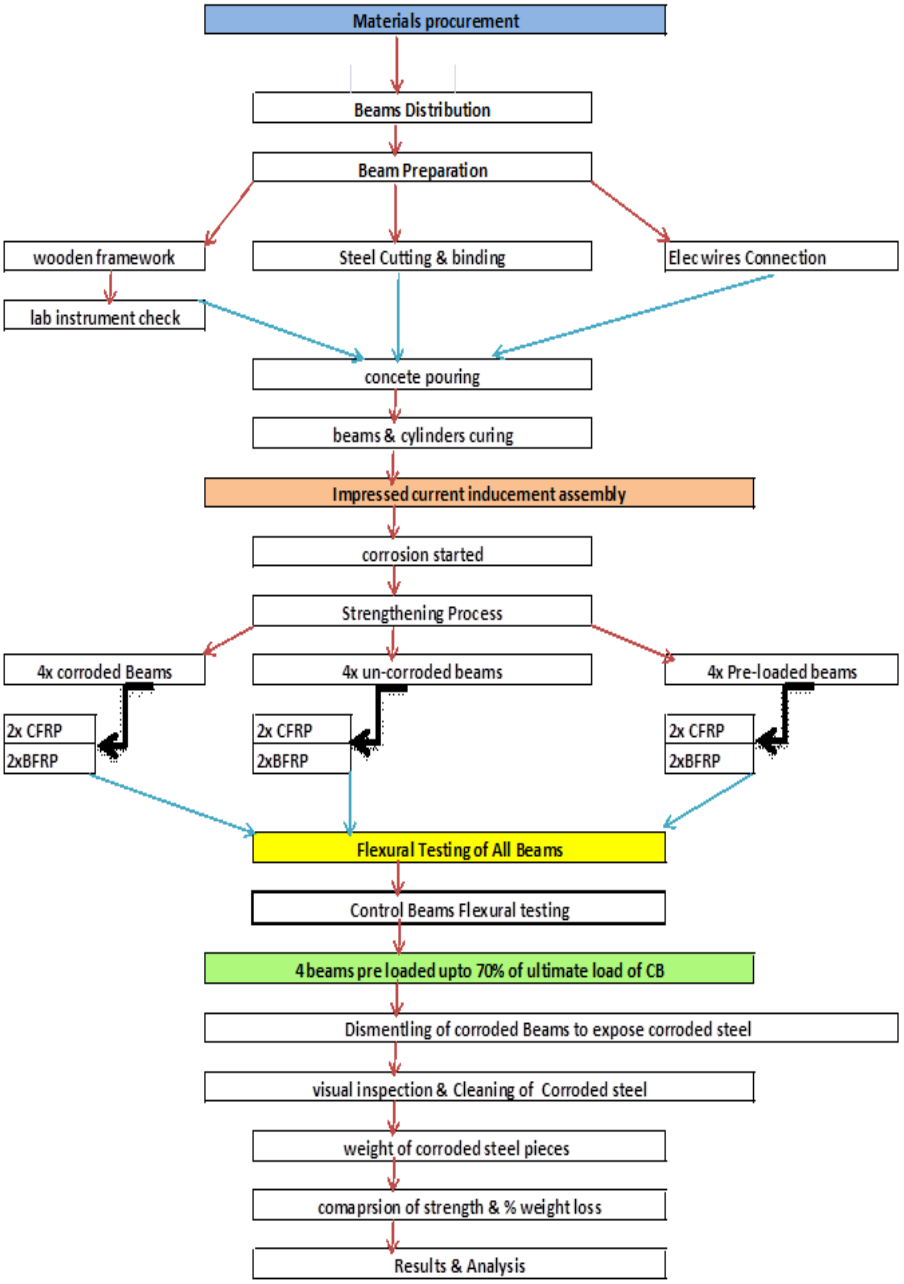

FIGURE 3.8: Flow chart of activities to be conducted during this experimental research

3.4 Beams Distribution

3.4.1 Beams Sample Preparation

Total 16 beams were casted. 6 beams are corroded by impressed current technique while, remaining 10 beams is un-corroded. These beams are further dvided into sub sets of controlled, corroded, pre cracked beams and strengthened beams. Their nomenclature is already discussed above in Table 3.5.

Table 3.5: Beams sample preparation

16x beams	6x Corroded beams	2x corroded	
		4x corroded & strengthened	2xCFRP 
			2x BFRP 
	10x Un-corroded beams	2x controlled	
		4x 70% Pre-loaded & strengthened	2x BFRP 
			2x CFRP 
		4x controlled & strengthened	2x BFRP 
			2x CFRP 

3.4.2 Steel Cutting and Binding

Steel used is 60 grade having good quality and tensile strength. #3 and #4 bars were used and cut into lengths desired. 4 flexural bars each having length 900mm and 9 stirrups each has length 600mm longitudinally and laterally steel skeleton is shown in Fig 3.8. Binding wires were used to tie up flexural bars and stirrups. And one loop handle of #4 were attached with steel skeleton to make handling easy once beam cures and transported. PCC spacers of thickness 37mm were used at sides of reinforcement as concrete covers Fig 3.9.

FIGURE 3.9: Beam steel skeleton longitudinal face

FIGURE 3.10: Lateral face of steel skeleton & electric cable connection

3.4.3 Electric Wires Connecting

2.5mm cable 2xcore was used to supply current within beam bottom bars. One end of the wire is peeled off and attached to bottom steel bars and rest portion of the steel wire is kept insulated because it will be embedded in the concrete shown in Fig 3.9. To keep other end of the wire safe from environmental effect it is tapped and sealed until it is connected in current inducement assembly.

3.4.4 Concrete Pouring Activity

Beams reinforcement was properly placed in wooden frame shown in Fig 3.10 (a)(b) and then concrete activity was started. Ready mix concrete of 4000 psi is ordered from locally available plant. Mix formula of 4000 psi concrete has already discussed in 3.2.1. 16 beams and 4 cylinders were casted. Temperature was between 20-25°C during time of pouring. Scoops were used to pour concrete from wheel barrow where concrete was collected from Truck mixture. Manual Roding was applied to remove air voids and to help concrete spread evenly Fig 3.11, Fig 3.12. Once concrete was poured, steel trowel was used to give top surface smooth finish Fig 3.13. Cylinders Fig 3.14 was also casted for compressive strength testing. Fig 3.15 shows, once all the beams were poured.

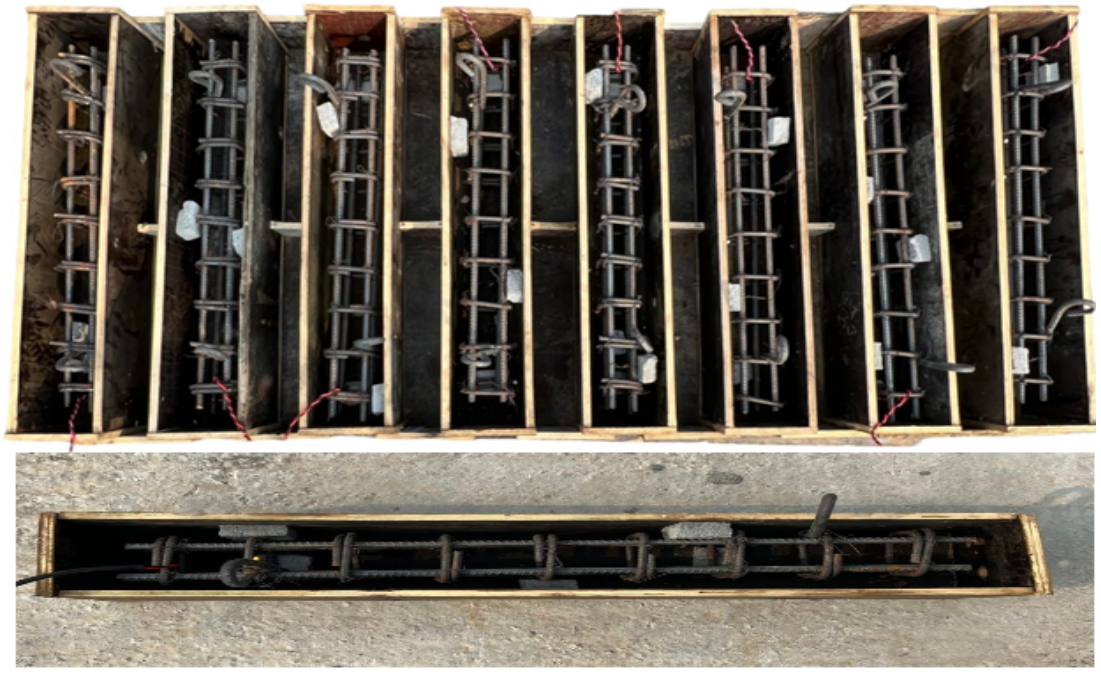

FIGURE 3.11: Beam steel skeleton placement in wooden Frame

FIGURE 3.12: Manual Roding to remove air voids

FIGURE 3.13: Scoop to pour concrete from TM

3.4.5 Beams and Cylinders Curing

All the beams and cylinders that were casted at site transported to curing tank available at university. They will be cured for 28 days and then further process of corrosion and strengthening shall be started.

3.4.6 Impressed Current Inducement Assembly

This is most crucial part of this project. Accelerated corrosion of mild steel used in beams using impressed current technique. First question comes into mind how much steel we want to corrode or how much percentage of weight loss we are

FIGURE 3.14: Surface troweling & Leveling

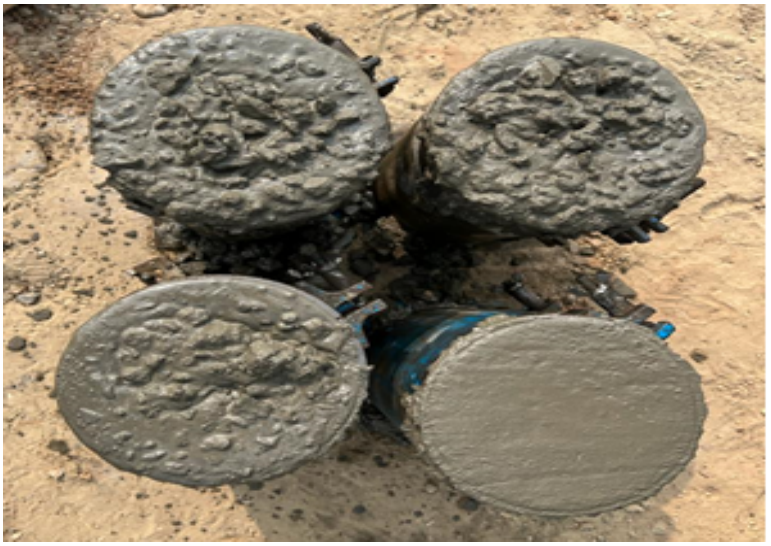

FIGURE 3.15: Cylinders Casting

expecting from this technique? This is followed by how much current should be applied to achieve expected weight loss of steel? All of this achieved using this formula:

$$\Delta m = \frac{MIt}{ZF} \tag{3.1}$$

In this equation, Δm represents weight loss (g or%), M represents the equivalent weight of iron (55.56 g), I represent current required (A), t indicates time (s), Z represents the number of electrons released (iron has 2), and F represents the faradays constant (96487 C).

In our case we expected 10% theoretical weight loss of the steel bars. Total weight of the beam was 6511 g Fig 3.16 , so the δm= 651 g. Time decided to apply current was 8 hours per day for consecutive 15 days. So t= 432000s. Regardless of

FIGURE 3.16: All Beams after concreting and surface leveling

the various cross-sectional areas, the reinforcement skeleton's overall surface area was taken into account in this context. Therefore, it was determined that 1650 μA/cm^{-2} (i_{app}) of impressed current would be needed for 15 days at 8 hours per day to achieve this weight loss. Based on the surface area of the steel bars, a total of 5.02 A of current was needed per beam. The AC power supply could only handle 10 A of current and 30 operating volts, but it could handle 160 V (V) of direct electrical potential from the power plug (Fig. 3.17). According to a review of the literature, applied impressed current ranges from 100 to 3000 μA/cm^{-2}.

FIGURE 3.17: Total weight of beam steel skeleton before corrosion

FIGURE 3.18: DC Power Supply operating above 5A current

Once we calculated the amount of current required per beam. It was time to transform this idea into practical. Assembly consists on Power supply, beams, water, NaCl, pan etc had to be assembled at site. First of all large pan sized 1200mm x 1500mm was taken and filled with water to check if it has leakage somewhere. Then all the side and corner of the pan was sealed with silicone gel .

We had six beams to be corroded so It was necessary to make compartments of size 200mm spaced for each beam to be separated so 2cm thick plywood was used. Polythene sheet of 1mm thickness was spread all over the compartments to make steel pan safe from current and water intact. Before placing beams 2 inch thick wooden spacers were used to lift beams from body of pan and suspended in air . Water was filled with 5% of NaCl to accelerate electrons. 2.5 inches wide Stainless steel plate was attached longitudinally to each beam one side externally in such a way it is half immersed in water Fig 3.18. It is important to mention here that this stainless steel plate is also called as "cathode".

The power supply's positive terminal was connected to the steel rebar. This is due to the fact that, similar to natural corrosion, induced corrosion requires the removal of electrons from the steel. Fe^{2+} ions flow through the pores in the concrete and towards the cathode plate as a result of the current balance caused by the electron flow.

The cathode plate that was positioned next to this beam was connected to the anode of the second beam in the compartment beyond it, while the bottom steel

FIGURE 3.19: Stainless Steel cathode attached with beam

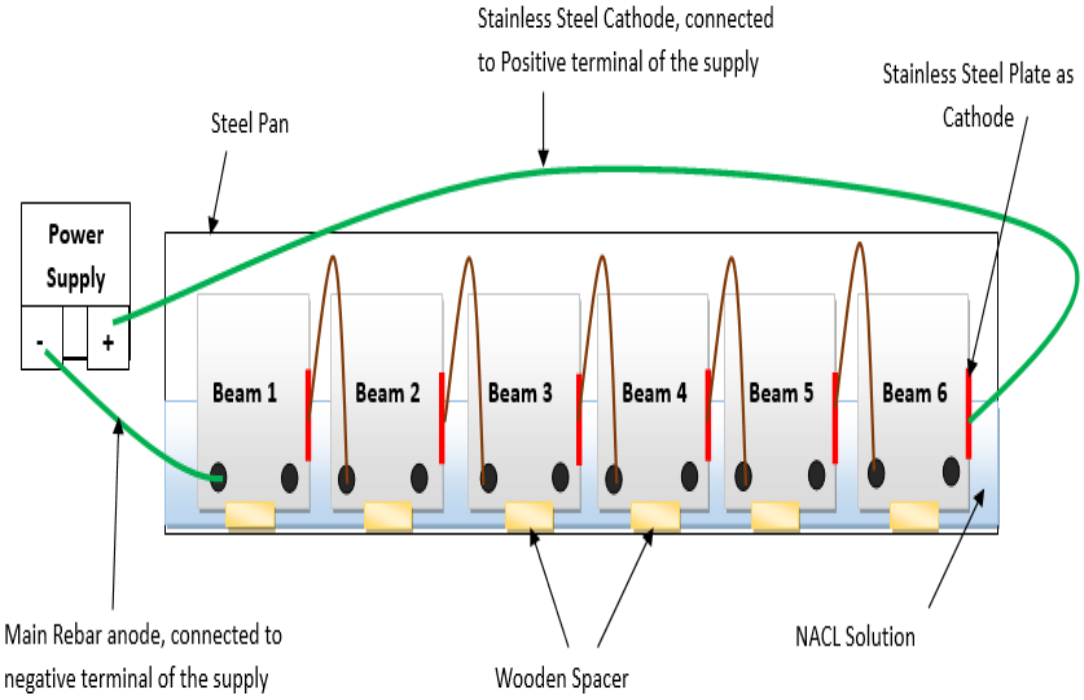

FIGURE 3.20: Diagram showing the impressed current technique with beams positioned in different compartments and connected in series with the DC power supply while submerged in 5% NaCl

of the first beam, which served as an anode, was initially connected to the power supply's negative terminal. Subsequently, the anode of the third beam was linked to the cathode of the second beam. The anode of the fourth beam was linked to

FIGURE 3.21: Physical interpretation of Schematic circuit of beams connected in series

the cathode of the third beam in turn. Ultimately, the circuit and current flow were completed when the sixth beam's cathode was linked to the power supply's positive terminal. Figure 3.19. The entire system demonstrates that the electric circuit's beams are made up of series-connected resistors, where the applied current stays constant while the potential at the terminals varies (Fig. 3.20).

3.4.7 Real Time Corrosion Started

Interval base current was applied for 15 days at 8hr/day. With the passage of time we can see clearly corrosion firstly appears externally due to NaCl present in water and environmental effect. Then slowly it goes into the flexural bars of the beam which are embedded in the beam and visually not present. We can see bottom of the beams got reddish in color and some portion of the cathode also deteriorated. That shows current is flowing even the end beam has turned its bottom side appearance into rusty color. Ammeter is also used to check whether current is flowing or not. Current was kept 5.01 A constant, through manual regulators attached at the face of power supply. The real-time, continuous deterioration process in the beams installed in the steel tank is shown in Fig. 3.21(a), (b), and (c). The corrosion behavior of the reinforcement mesh is said to be unaffected by the number of connected flexure rebar [35].

FIGURE 3.22: Beams under corrosion stage

3.4.8 Strengthening Process

This process main ingredients are CFRP, BFRP, Base Epoxy, Adhesive and Crack Filler. Characteristics of each material are briefly elaborated above in 3.2. Here we will discuss how these are applied at the surface of beam and what requirements and precautions should be made for strengthening of beams. All the steps followed are same for CFRP and BFRP except a little change when dealing with pre-cracked beams which involves cracks filling activity also.

First of all beams soffit will be visually inspected whether there are cracks or concrete cover has fallen out. Once it is satisfied surface of beam is grinded with steel blade to remove humps and impurities attached with the surface Fig 3.22. Then base repair epoxy is applied evenly in 1:1 ratio using scrapper to fill any depression created at the soffit of beam Fig 3.23. Surface must be clean, sound and dust-free. So, remove unsound concrete with small pneumatic or electric steel grinder. Light sandblasting can also be used. Repairs made on marginal concrete

FIGURE 3.23: Beam soffit surface grinding

may not be successful and are not usually recommended. Thats why applied base Paste Epoxy to the area to be patched to enhance the adhesion of the epoxy mortar and to prevent binder starvation at the interface. Epoxy is dark grey in color but gives white appearance once it is dry. This is kept for drying upto 20-24 hours. Then sand paper is used to remove air bubbles or overlapping epoxy stains that are visible at the surface Fig 3.24. . Moreover border layout using paper tape is ensured to maintain adhesives within desired place Fig 3.25. Then CFRP & BFRP is cut into desired dimension 100mm wide, 900mm length shown in Fig 3.26.

FIGURE 3.24: Base Epoxy mixing and application

Now adhesive with mixing ratio of 2:1 (Part A to Part B) by volume or 66.67 : 33.33 (Part A to Part B) by weight, dark blue in color with 0.25Kg/m^2 application

FIGURE 3.25: Sand Paper

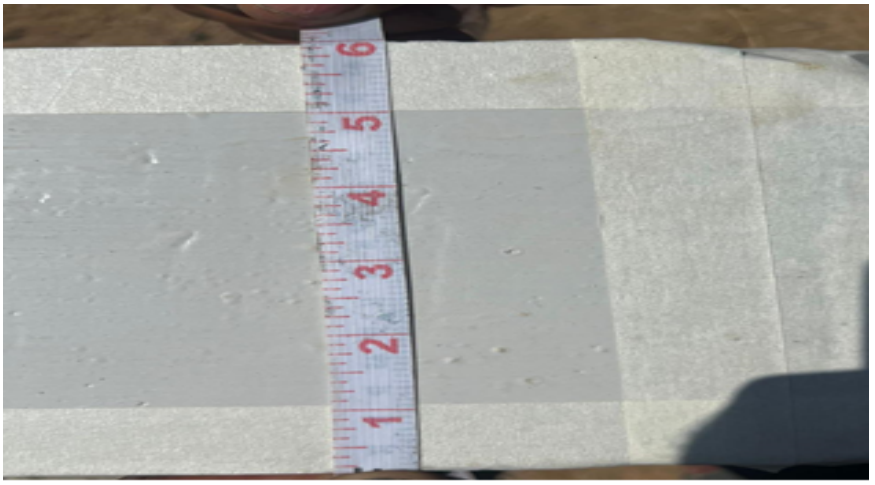

FIGURE 3.26: Border layout with paper tape

FIGURE 3.27: CFRP/ BFRP pieces

rate is applied with 3/8" nap roller and let it dry and sticky for 35 minutes Fig 3.27. Mix only the amount of material that can be used within the working time of the material. Then CFRP/ BFRP soaked in this solution is evenly spread at

the soffit before saturate becomes tacky Fig 3.28 (a) (b). Apply a second layer of adhesive using the same roller. Now, For 3 hours let CFRP/ BFRP wrap be dry and check it with bare hand either it is properly hard with the surface. Fig 3.29 illustrates once it is confirmed one last time roller dipped in adhesive solution is applied at the surface and let it dry for 15 days. Only apply XPERT PROFIBER CW ADHESIVE when the ambient temperature is between 50 and 120 °F (10 and 50 °C). All beams are strengthened by following the same steps. Distribution of

FIGURE 3.28: First coat of adhesive

FIGURE 3.29: (a) BFRP application, (b): CFRP application

FIGURE 3.30: Final coat of adhesive

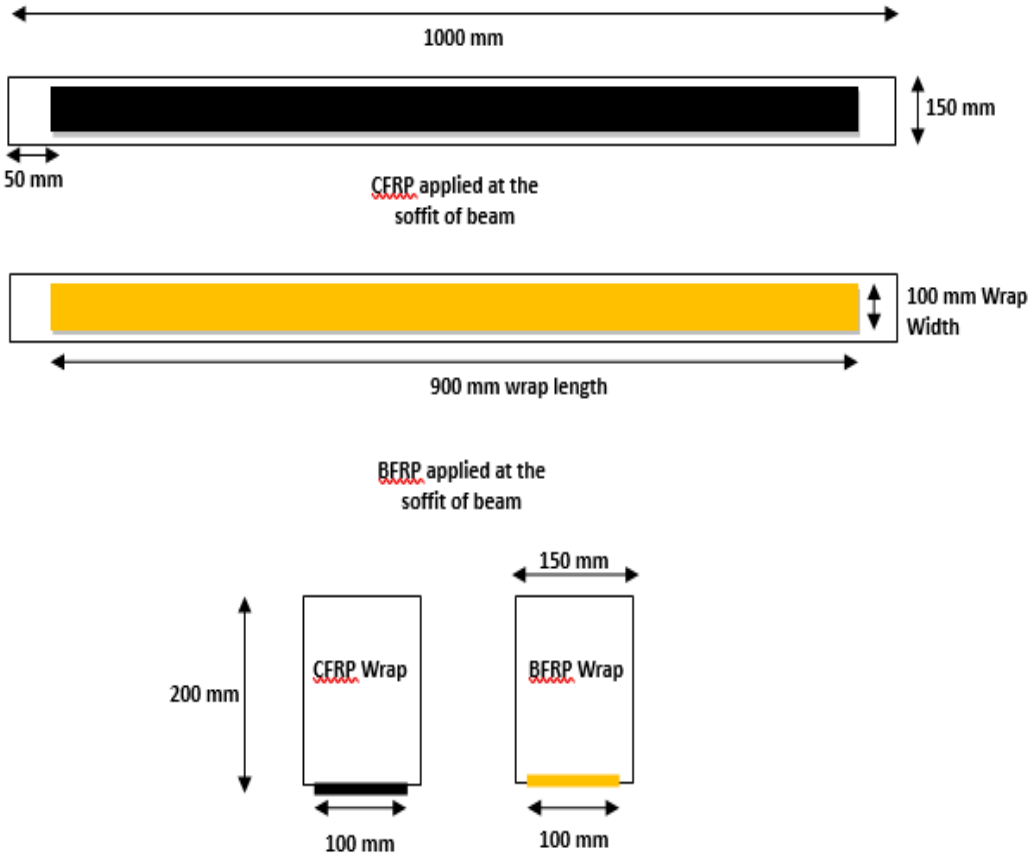

FIGURE 3.31: (a) (b) Longitudinal & X-Section view of CFRP/BFRP wrap at soffit of beam

beams are 4x Corroded Beams i.e 2x CFRP & 2x BFRP. Then 4x Un-corroded Beams i.e 2x CFRP & 2x BFRP are strengthened. Fig 3.30 (a) (b) illustrates beam dimension and place where these CFRP and BFRP wraps are attached to beam.

3.4.9 4x Pre-loaded Beams

All the strengthening procedure for these is same as above except one step must be ensured before strengthening of these beams. Low Viscosity two Component resin is filled in cracks & pin holes with Injection Fig 3.31. This is done so that beams which are loaded up to 70% of ultimate load shows cracks when de-loaded from lab apparatus. If we fill these cracks with this resin it might help to increase its strength also. Further follows the same procedure for both CFRP and BFRP wraps. 2x preloaded beams are strengthened with CFRP & two with BFRP.

FIGURE 3.32: Cracks filling with filler resin using injection

3.4.10 Flexural Testing

3.4.10.1 Control Beams Testing

Two control beams are tested with four point loading to get their ultimate load value in (KN). So, that this value can be used for those beams who are needed to loaded upto 70% of this ultimate load value. To keep beam perfectly placed and equally spanned beam side face is marked and distributed in rectangular boxes of 50mm x 50mm Fig. 3.32. Then beam is lifted with the help of loading facility and placed in UTM and at the top of beam 2 rods of 75mm diameter and a balanced plate of 50mm thickness is used to make it four point loading assembly shown in Fig. 3.33.

FIGURE 3.33: 50mm x 50mm Grid

FIGURE 3.34: Rods & Wrought iron plate for four point loading

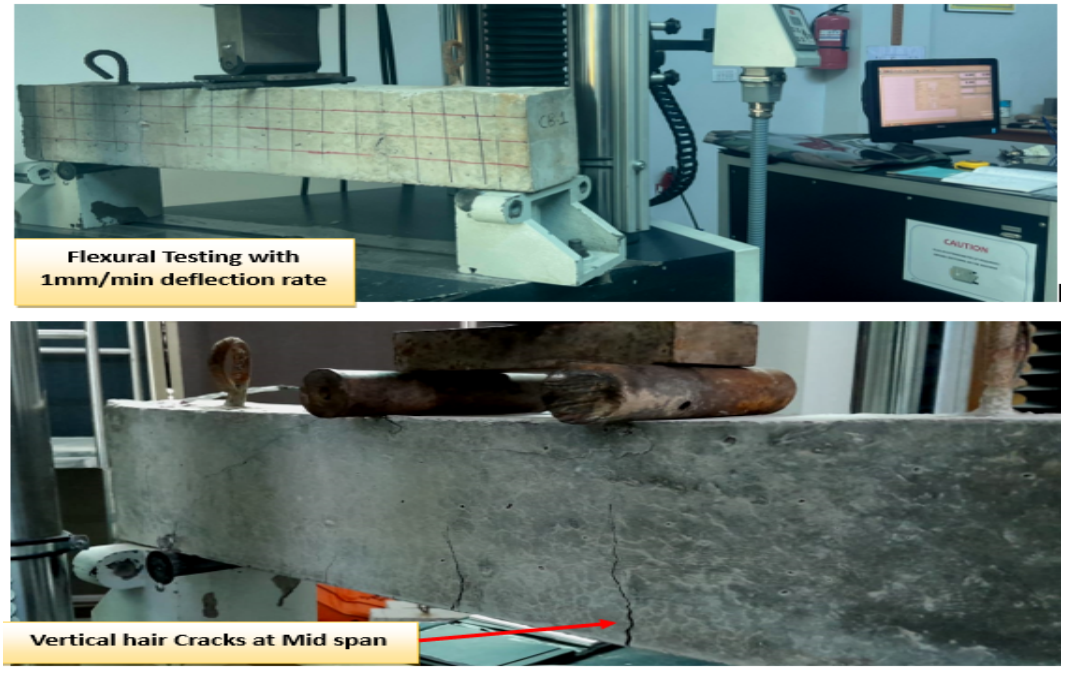

FIGURE 3.35: Flexural Testing with 1mm/min deflection rate

3.4.10.2 Pre Loaded Beams Up to 70% of Ultimate Load of CB

Four beams are loaded up to 70 percent of the ultimate load of the control beams Fig. 3.34. Value of ultimate load was derived from test conducted in 3.3.8. This is done so that a real time beam can be stimulated because these beams would be strengthened with CFRP and BFRP at later stage and then will be tested till their fracture load. It is evident that real life beams also have small hair cracks somewhat due to any prevailing conditions. So, by producing pre cracks before strengthening will give use to summarize our research more close to real time scenario Fig. 3.35 and Fig 3.36. Moreover, same testing procedure will be adopted as before. All beams are tested till there fracture point. Different beams

FIGURE 3.36: Beam to be loaded 70% of CB ultimate load

FIGURE 3.37: Vertical hair cracks

show different stress strain curve. Failure mode was different and deflection when

FIGURE 3.38: Diagonal cracks originating from tension zone

loaded up to fracture point varies significantly from beam to beam. Four-point loading apparatus were used instead of three point. Because for deep beams which have depth to mid span ratio equal or more than 2 must be loaded four point when testing their flexural strength. This testing approach is specifically designed to assess the bending strength and behavior of the materials incorporated into the beams. By subjecting each specimen to controlled loading at four distinct points along its length, the test aims to meticulously measure and analyze how the beams react to applied forces. The loading setup for the four-point bending tests is shown in Fig. 3.37. A 1500 kN load capacity serve-tech universal testing machine (UTM) was employed. Deflection control loading was applied, and it increased at a rate of one millimeter per minute. The machine's roller supports replicate the circumstances of a simply supported beam. There was a 1000 mm testing span and a 100 mm shear span.

The primary objective of this flexural testing is to gather critical data on the structural performance and durability of the materials under simulated real-world conditions. It provides insights into how well the beams withstand bending stresses, indicating their ability to support anticipated loads, to resist deformation, mechanical properties and load-bearing capacities of the beams. This information is essential for evaluating the suitability of the materials for the intended construction application, ensuring that they meet design specifications and safety. The results obtained will be discussed in chapter 4. Ultimately, this rigorous testing approach plays a pivotal role in validating the reliability and functionality of the

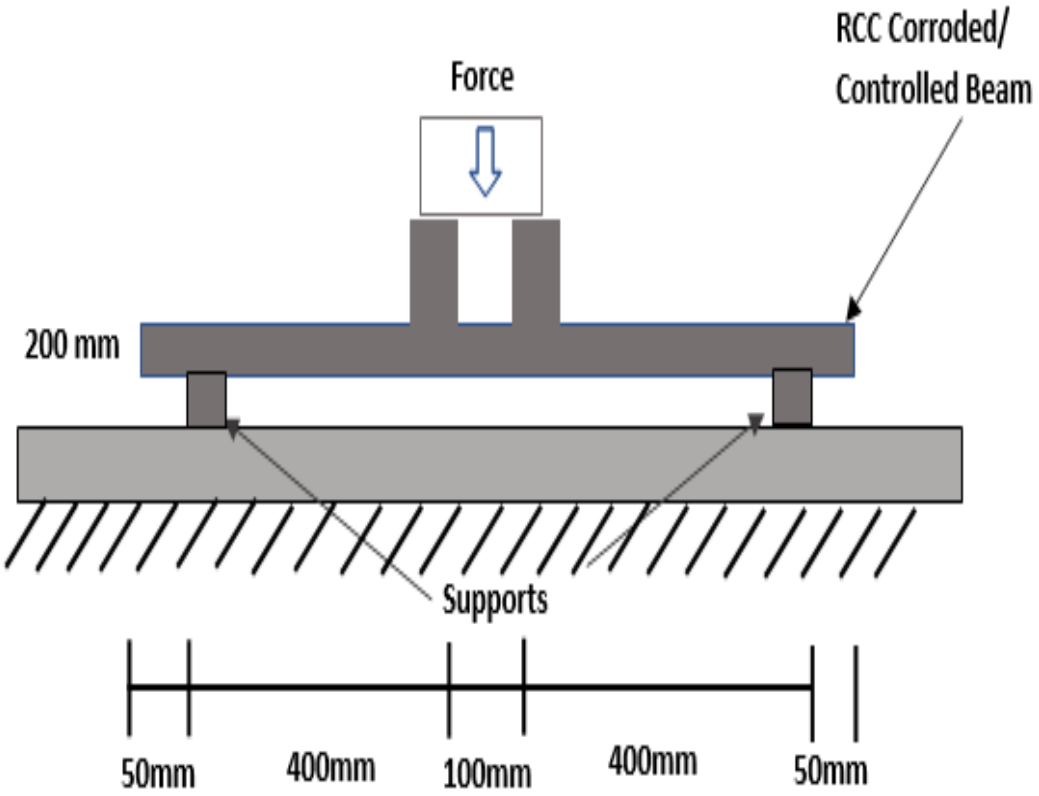

FIGURE 3.39: Four-point flexure test setup sketch

construction materials, thereby enhancing the overall quality and longevity of the project.

3.4.11 Dismantling of Corroded Beams to Expose Corroded Steel

Once, the corroded beam is strengthened and tested flexural tested. Here it comes the moment when whole research that is based on accelerated corrosion, reinforcement weight loss and strength deficiency might be proved physically. This is only possible if we extract corroded steel that was embedded out of the beam, so, beam is dismantled and crushed using hilti machine shown in Fig 3.38.

3.4.12 Visual Inspection & Cleaning of Corroded Steel

After dismantling and crushing of beam whole skeleton of corroded reinforcement were extracted shown in Fig 3.39 (a)(b)(c). Now it was time to select locations

FIGURE 3.40: Flexural testing of CS and BFRP

from where small bars varying 5 cm to 16 cm length have to be cut from main flexural bars at three positions named as near connection, middle and far corner and two sides named as Bar- facing cathode and Bar-Far from Cathode. Flexural bar which is close to cathode is called as Bar facing cathode corner of bar which is connected to main supply is named as near connection corner shown in Fig 3.40. We had selected two beams and their main flexural bottom bars were cut from 3 locations. So total cut lengths fro flexural bars under weight loss testing are 12 shown in Fig 3.41. Moreover two stirrups were selected one was from near connection and other was from far end. Cut lengths from each stirrup were four. From bottom side, Vertical side near bottom, vertical side middle and top side shown in Fig 3.42. Cut bars are undergone cleaning process so that rust can be removed from these bars and actual weight can be measured. That will help to

FIGURE 3.41: Flexural testing of CBS BFRP and CS CFRP

FIGURE 3.42: Flexural testing of CB-CFRP

FIGURE 3.43: Flexural testing of other CFPR and BFRP beams

FIGURE 3.44: Extraction of corroded steel using hilti

make comparsion between nominal weight and weight loss. After that, the bars are rinsed in bleaching agents based on chlorine, such as 200 g/l sodium hydroxide, ammonium hydroxide, and sodium alkyl (C10-13) benzene sulfonate, as advised by ASTM G-I-90 (1999) [37] standard to get rid of the rust products. After drying,

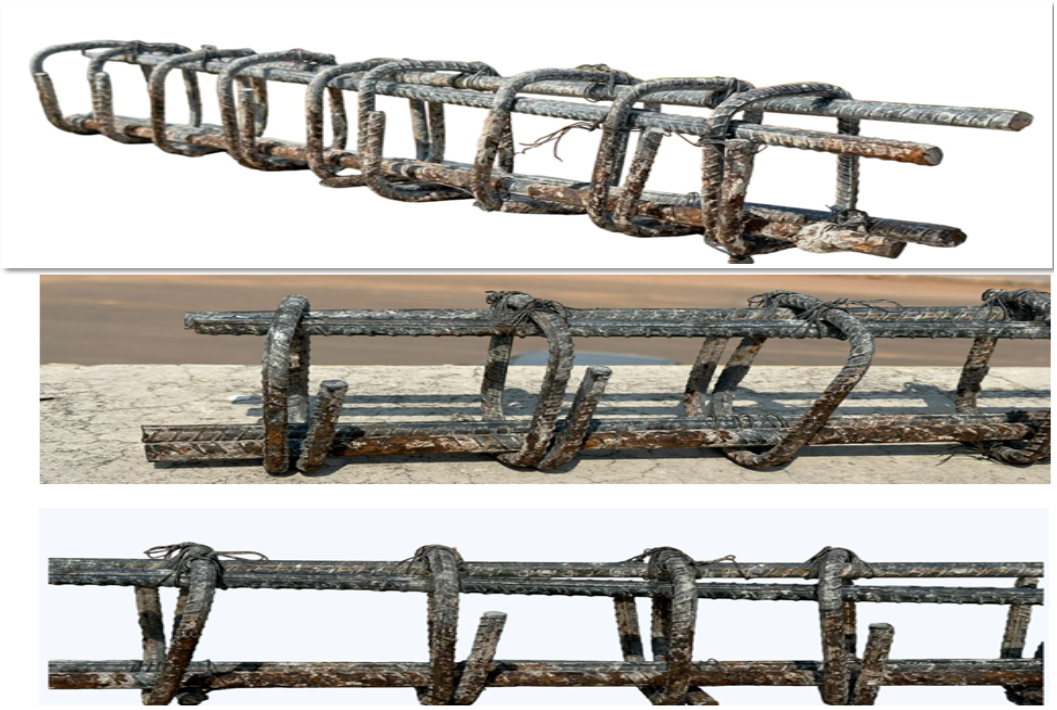

FIGURE 3.45: Extraction of corroded steel skeleton

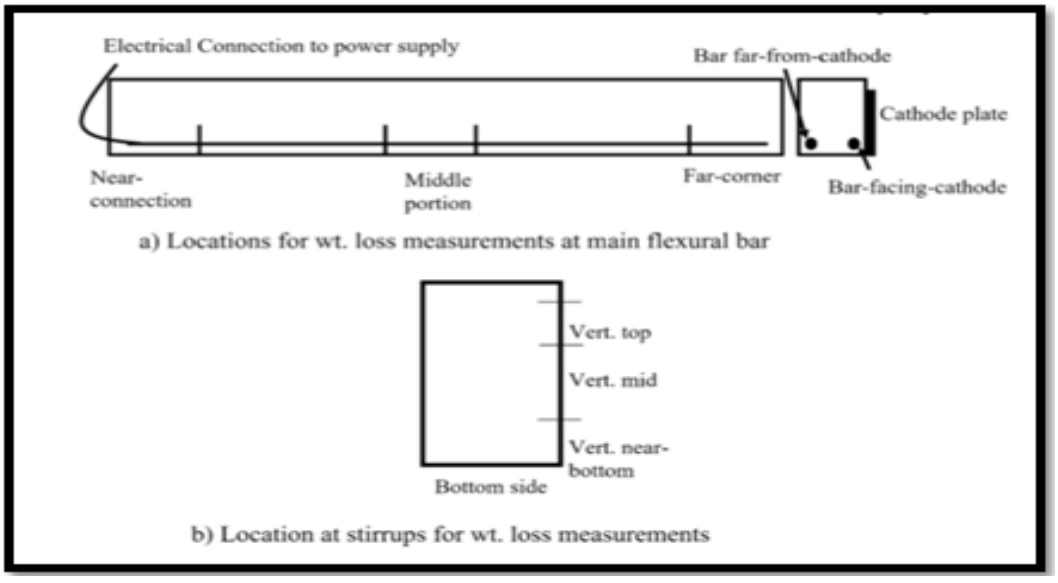

FIGURE 3.46: Location decided to cut corroded steel pieces

rebars were softly brushed with a fine brass brush. This process was carried out repeatedly until all adhered concrete was gone. Process is shown in Fig 3.43.

3.4.13 Weight of Corroded Steel

Weight loss was measured until two cycles of constant values were reached. By using Faraday's law, the applied impressed current was linked to the weight loss.

FIGURE 3.47: Cut pieces from flexural bars

FIGURE 3.48: Cut pieces from Stirrups

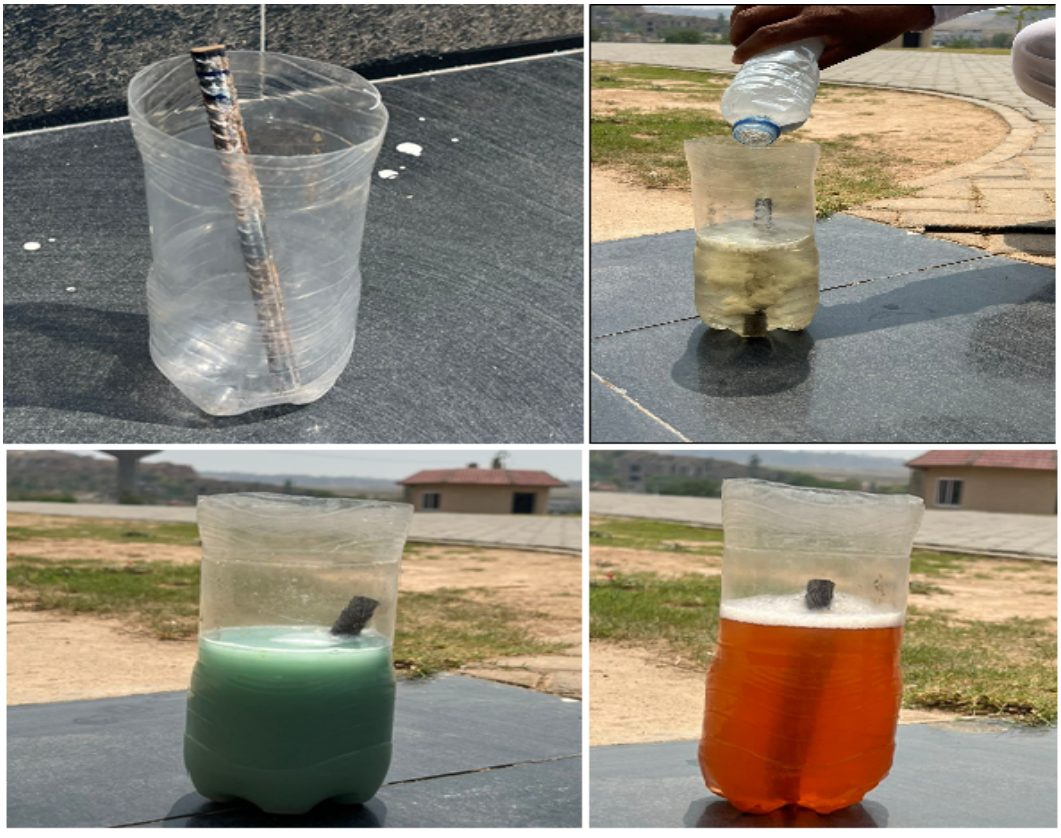

FIGURE 3.49: Procedure to remove rust from corroded steel pieces

Next, the nominal diameter of the ribbed bars with the same length was used to calculate the original weight of the steel bar of the same size, which was then compared to the weight of the corroded cut pieces. Figures 3.44 and 3.45, respectively, display the weight of cut pieces from flexural bars and stirrups that are corroded and those that are not. It is possible to determine the actual corrosion current that the rebars experienced by using weight loss measurements. Due to current losses to overcome the high resistance of the concrete, water hydrolysis around the steel rebars, and resistance provided by deterioration products at a later stage of the corrosion procedure, the i_{corr} is counterbalanced from the i_{app}.

FIGURE 3.50: Comparison of weights from flexural bars away from cathode and far corner

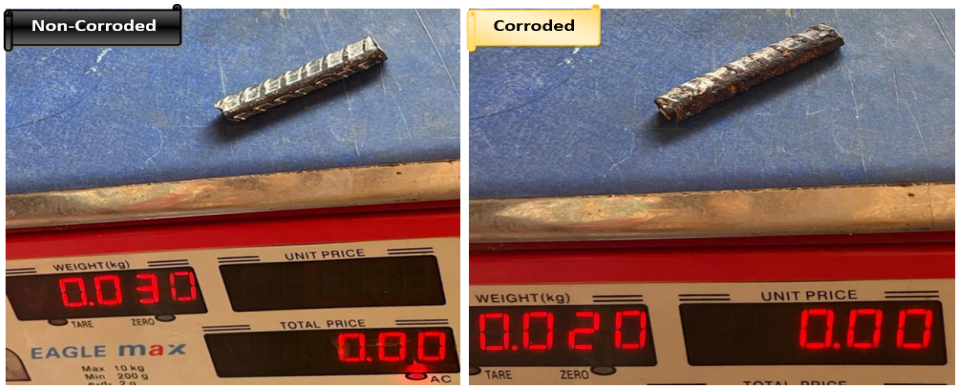

FIGURE 3.51: Comparison of weights from stirrup 2 & Far End (Bottom Leg)

3.4.14 Comparison of Strength & % Weight Loss

Shall be discussed in next chapter 4.

3.4.15 Results & Analysis

Shall be discussed in next chapter 4.

In conclusion, the detailed timeline and systematic approach ensure that each phase of the project contributes to the validation and optimization of construction practices. By adhering to this sequence of works, the project team can make informed decisions based on empirical data, enhancing the reliability and longevity of the constructed infrastructure while meeting stringent safety and performance standards.

Chapter 4

Results and Analysis

Results are presented in the form of real time failure modes of controlled, corroded, strengthened, pre-loaded strengthened beams and load-deflection curves are elaborated then ultimate strength and deflection values are tabulated and compared. Weight loss of steel due to corrosion and the comparison between i_{app} and i_{corr} are discussed.

4.1 Visual Inspection and Loss of Weight

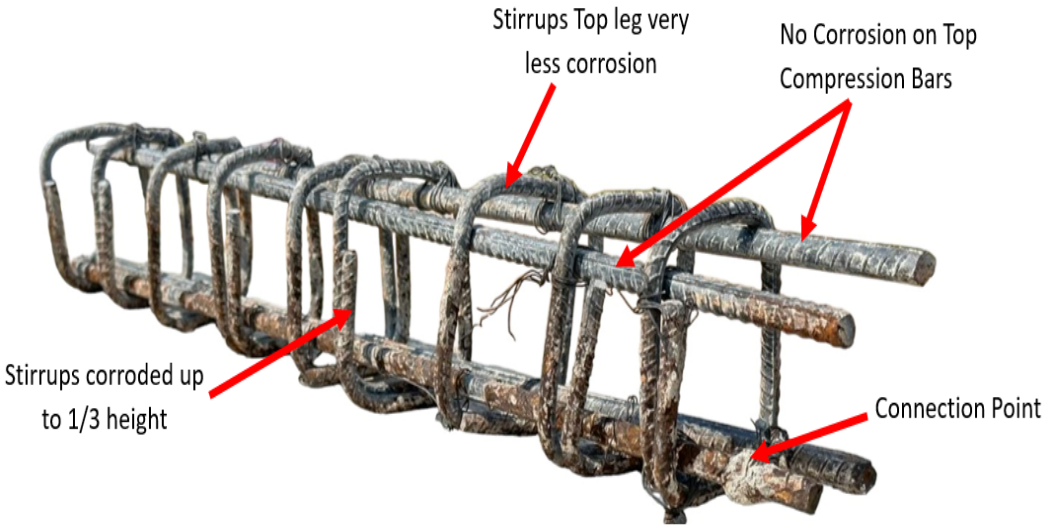

FIGURE 4.1: Extraction of corroded steel skeleton

A 15-day-old corroded reinforcement skeleton taken from a beam is shown in Fig. 4.1. Whole beam is visible in this beam and cathode side bar and anode side bar

is visible here. The impressed current's electrical connection was positioned in the bottom left corner of the reinforcement. Both connected and unconnected bars of the main flexural reinforcement exhibited corrosion along their entire lengths. The bar nearest to the cathode showed more severe corrosion compared to those farther away, irrespective of its connection or lack thereof. This is because of a phenomenon known as face-to-face polarization, which is caused by the arrangement of the anode and cathode. In comparison to its opposite side, the side of the active steel (anode) facing the cathode (stainless steel plate) saw higher rates of corrosion. Laurens S, Sohail MG, and others (2015). Additionally, ASTM C876-09 (2015) clarifies that the cathode has a greater influence on the anode that is closest to it and less of an impact on the anodes that are farther away when numerous anodes are arranged parallel but at different spans from it.

The stirrups were corroded up to 1/3 of their height, corresponding to the coverage area of the cathode steel plate attached to the side of the beam. The bottom side of the stirrups suffered severe corrosion, leading partial dissolution of some portions. The vertical sides of the stirrups facing stainless-steel plate (cathode) corroded more extensively compared to opposite sides. Meanwhile, top compression main bars and stirrups upper portion remained unaffected by the applied current and exhibited no signs of corrosion after the 15-day period. Several factors contributed to these observations: the proximity of metal to the electrical connection supplying electrons caused rapid corrosion initiation, resulting in uneven corrosion along the steel reinforcement. This phenomenon aligns with findings by Wang et al. Study conducted by Almusallam AA, Al-Gahtani AS et al (1996) noted advanced corrosion rates near the connection point compared to farther areas. It was also observed the presence of chloride ions is vital for initiating corrosion during impressed current application El Maaddawy TA et al. At the beam's soffit and up to specific height of the stirrups, chloride ion flow was maintained due to partial immersion. As the rebars lost their passivity due to the current and chloride presence, their polarization resistance decreased, facilitating easier current flow compared to the non-passivated top compression bars. Fig 4.2 exhibited that this experienced corrosion less as compared to other corner which was connected with direct power supply. It is clearly visible as we move from right to left of the picture corrosion exposed at bottom flexural bars and stirrups vertical legs are

FIGURE 4.2: Connected corner side of anode (steel)

decreasing in a non-uniform manner and it gets almost zero at the flexural bars far corner where no sign of pitting corrosion or loss of cross section is noticeable. Even grooves of the rebar are well maintained. There are two bottom flexural bars one which is severely corroded is facing cathode and the other one showing less signs of corrosion were the bar away from cathode in impressed current assembly.

In addition, the uppermost bulk concrete was drier and showed more resistance close to the steel-concrete boundary, which prevented ionic current from passing through the concrete voids and onto the cathode plate. This arrangement played a role in the localized corrosion that was mainly noticed on the vertical faces of the stirrups next to the stainless-steel plate. In conclusion, the corrosion pattern seen in the top compression bars and stirrups following a 15-day impressed current application highlights the intricate interactions between the presence of chloride, the distribution of current, and the moisture content of the concrete that speed up the erosion processes inside reinforced concrete structures.

Furthermore, the height of the stainless-steel plate (cathode) did not extend to reach the compression steel shown in Fig 3.28: Schematic assembly of the impressed current technique, and there was no established electrical connection through the concrete due to dry conditions and a space between the stainless steel and concrete surface. Li et al. (2021) noted that during accelerated corrosion, steel bars closer to the concrete surface, where moisture content was higher, experienced more significant corrosion compared to bars away from the concrete surface. To

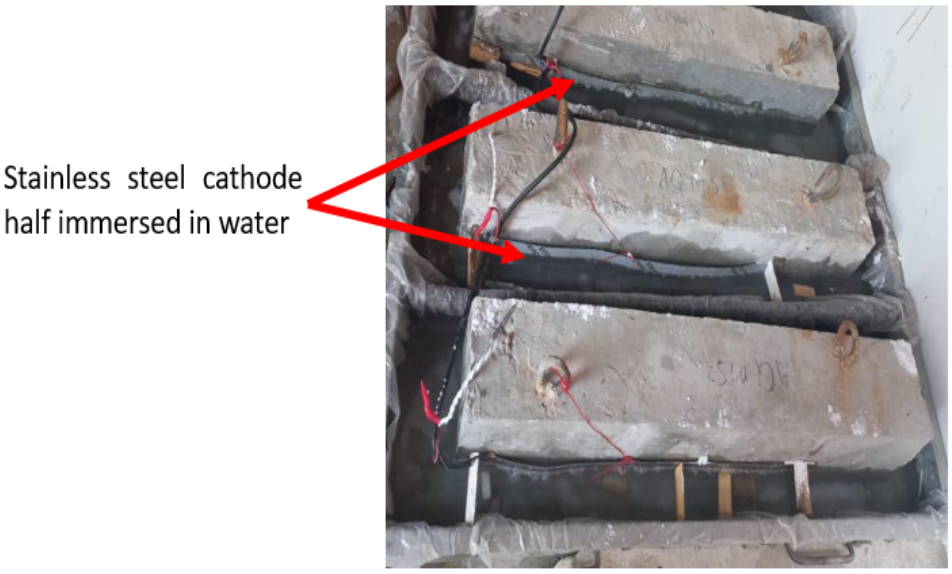

FIGURE 4.3: Cathode (stainless steel plate) half immersed in water

ensure uniform corrosion rates across the reinforcement net, it is suggested to maintain concrete members moist and ensure the cathode plate covers the entire concrete surface Ahmad S. (2017). However, the current experimental setup demonstrated targeted corrosion induction on specific portions of the reinforcement, such as the outer steel layer can be targeted to natural corrosion phenomena. Fig 4.4 displays steel samples cut for loss of weight measurements, visual inspection of rust products that are overlaid on steel bars. Damages occurred to the bar and loss of cross-sectional area etc. Two RC corroded beams were dismantled and their flexural bars were extracted and bottom flexural bars of each beam was cut into 3 pieces so total number of cut pieces we got four flexural bars weight loss and rust inspection were 12. They were named as near connection, middle and far end for each bar facing cathode or away from cathode. In addition, the uppermost bulk concrete was drier and showed more resistance close to the steel-concrete boundary, which prevented ionic current from passing through the concrete voids and onto the cathode plate. This arrangement played a role in the localized corrosion that was mainly noticed on the vertical faces of the stirrups next to the stainless-steel plate. In conclusion, the corrosion pattern seen in the top compression bars and stirrups following a 15-day impressed current application highlights the intricate interactions between the presence of chloride, the distribution of current, and the moisture content of the concrete that speed up the erosion processes inside reinforced concrete structures. Figure 4.5 also illustrates

FIGURE 4.4: Cut pieces from flexural bars

FIGURE 4.5: Cut pieces from Stirrups

corrosion on the stirrups, with significant loss of weight and cross-sectional deterioration observed particularly on the bottom legs. Corrosion decreased in this order Bottom side, near Bottom vertical side, middle vertical side and top side bar. The rust products observed were principally orange-yellow and brownish-black, typical of erosion products found in concrete exposed to saline water Arya C, Vassie PR (1995). The electrochemical conditions of natural and artificially induced corrosion somewhat differ, resulting in varying rust product compositions. Zhang et al. Azad AK, Ahmad S (2007) reported advanced proportions of iron oxides (FeO, Fe2O3, Fe3O4) in accelerated corrosion compared to natural corrosion, where iron hydroxide oxides (Fe(OH), αFe(OH), βFe(OH), γFe(OH)) dominate.

During impressed current application, the lack of oxygen supply under high corrosion rates can lead to phase changes in rust products. However, due to lower current densities, corrosion products resemble those formed during natural erosion, as observed in this study. This similarity indicates that the rust products observed were largely influenced by oxygen availability from partial water immersion and the specific current intensity applied.

Figure 4.6a & 4.6b depicts samples from flexural bars facing the cathode after cleaning, revealing visible pitting erosion. The pits, ranging up to 3-5 mm in length and 1.5-2 mm in depth, were distributed along the entire length of the flexural reinforcement and stirrups. Pitting corrosion is indicative of chloride-induced erosion in concrete Nguyen W, Duncan JF et al. (2018). Pits found during impressed current application indicate that the border between the concrete and steel was penetrated by chloride ions. However, in contrast to localized natural corrosion brought on by chloride attack, some studies indicate uniform erosion distribution in impressed current methods Hai T, Nguyen Y, Hong V et al. (2021). These results highlight the usefulness of impressed current in researching and reducing erosion in reinforced concrete structures by indicating that it can replicate real-based corrosion phenomena in chloride-contaminated concrete quite well. Figure 4.7a and 4.7b depict the %age losses of weight at various positions

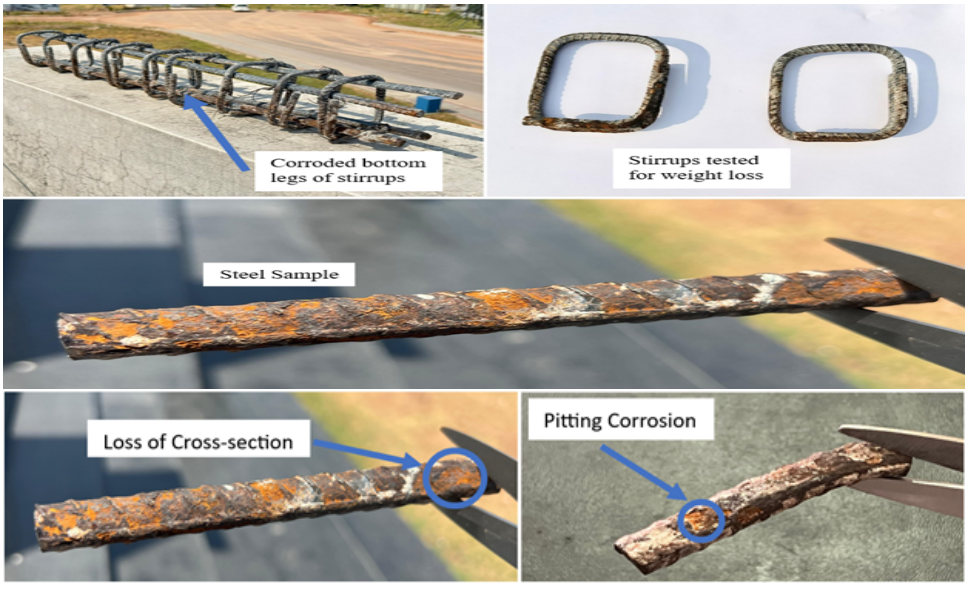

FIGURE 4.6: (a) Removed samples of corroded steel from various places, (b) After rust removal and cleaning the steel samples

along the flexural reinforcement bars of two fractured beams, beam-I and beam-II,

both subjected to a 15-day demean process. For beam-I, the bar facing the cathode exhibited losses of weight of 19%, 15%, and 12% at the near the connection, middle of the portion, and the far corner locations, correspondingly. In contrast, the bar beyond from the cathode experienced losses of 16%, 12%, and 9% at these same points. Similarly, for beam-II, the bar facing the cathode showed loss of weight 17.5%, 13.6%, and 10.4% at the near the connection, middle of the portion, and far from the corner spots, correspondingly, while the bar farther from the cathode experienced losses of 14.4%, 11.5%, and 8.5% at these locations.

These loss of weight values highlight uneven erosion laterally the length of the rebars. Advanced resistance at the steel-concrete border creates frictional confrontation to the stream of current, subsequent in irregular circulation of current on the reinforcement rebars. The specific resistivity of the steel rebar increases the resistance encountered by the impressed current from the connection point to the far corner. If length of the bar increases, so does its resistance, leading to reduced polarizing current at the far corners. Bulk concrete resistivity also plays a significant role by hindering the flow of Fe2+ ions away from the steel rebar, creating a +ve charge barrier that makes electron extraction from the steel more challenging. This results in increased current demand at the points near the connection, where more erosion products accumulate on the steel surface Azarsa P, Gupta R (2017).

Figure 4.7c displays the loss of weight observed on the stirrups. The bottom horizontal side of the stirrups exhibited a loss of weight of 39% near the connection and the far corner, with some portions were deteriorated due to severe corrosion. The vertical sides of the stirrups experienced comparatively less corrosion damage, although loss of weight in the vertical leg near bottom & middle of the vertical legs reached up to 31% & 27 % respectively. Loss of weight decreased with height, reflecting the varying exposure to moisture and chloride ions. The more loss of weight percentages on stirrups comparatively to main bottom flexural rebars can be attributed to their smaller cross-sectional area, where smaller bars experience greater loss of weight at the same impressed current density compared to larger bars.

Additionally, current tends to flow through the path of least resistance, facilitated by the damp concrete at the sunken soffit, which offers better bridge and lower resistance for ionic current flow from anode to cathode. This environment promotes

circulation of chloride ions, resulting in advanced loss of weight at the stirrups' base in the moist concrete near the cathode plate.

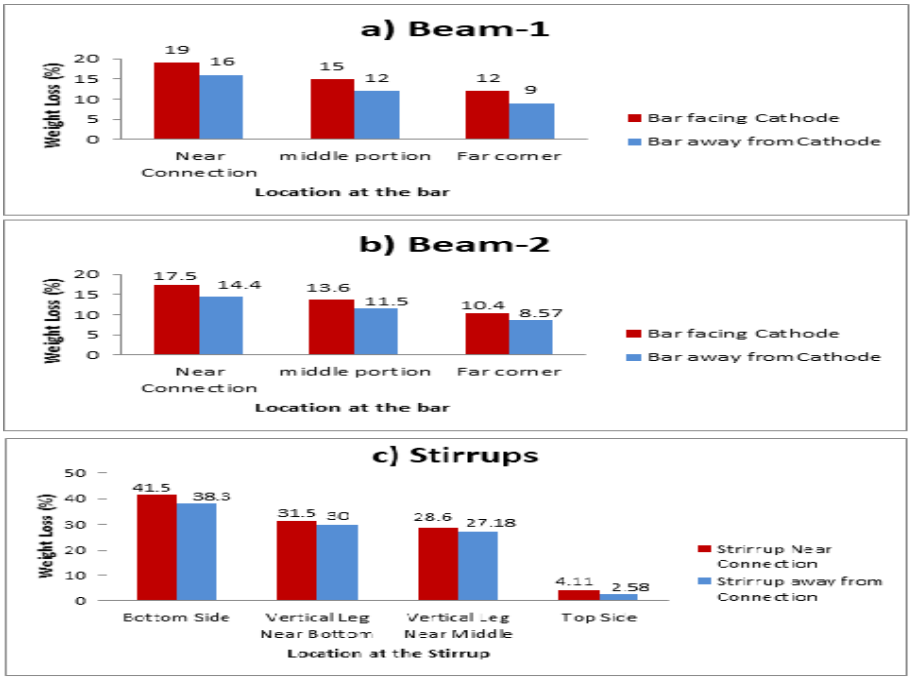

FIGURE 4.7: Explains % weight loss at diff locations of a) beam-1, b) beam-2, c) stirrups

4.2 Actual Corrosion Current Density

Initially weight loss was expected 10 percent by applying 1650 μA/cm^2 current on the surface are and total current required per beam was calculated as 5.01 A.But after 15 days corrosion it was observed that neither the weight loss was uniform nor the current consumed by the steel bars at different locations was same. According to the loss of weight using faraday's Law actual corrosion current was measured (i_{corr}). It was observed that it was very higher at some points and zero at the locations where no weight loss was observed just like top compression bars. The irregular distribution of the actual applied current along the length of the flexure rebars at the near-connection, middle portion, and far end is shown in Figure 4.8 and Table 4.1. For beam-1, the values ranged from 3907 μA/cm^{-2} at the near-conneciton to 1910 μA/cm^{-2} at the far-corner of the bar facing the cathode.

It is also observed that the actual applied currents vary from the bar facing the cathode to the rebar located far from the cathode. At the far corner of the flexural

rebars, there is less corrosion current because steel resists corrosion better the further it is from the connection point. Because the total current applied of 5.01 A was calculated using the entire surface area of the reinforcement mesh, the i_{corr} values at most of the locations on the flexure reinforcement are higher than the 1650 μA/cm^{-2}. Nevertheless, during the 15-day application, the impressed current was not applied to the top compression steel or certain sections of the stirrups.

For beam-2 (i_{corr}) was 3685 μA/cm^{-2} , 2878 μA/cm^{-2} , 1477 μA/cm^{-2} for bar facing cathode and at locations near connection, middle, far corner respectively. It is pertinent to mention here current consumed by the bar away from cathode beam-2 was 3057 μA/cm^{-2} , 2442 μA/cm^{-2} , 1740 μA/cm^{-2} for locations near connection, middle, far corner, respectively. Since the top bars were unable to draw current and the same amount of current was supplied at intervals of eight hours each day, the bottom portion of the reinforcement mesh had to draw more current than what was theoretically calculated. The variable moisture conditions in both beams and the heterogeneous nature of concrete may be the cause of the difference in current values between beam-1 and beam-2 in Figure 4.8(a)(b) & Table 4.1.

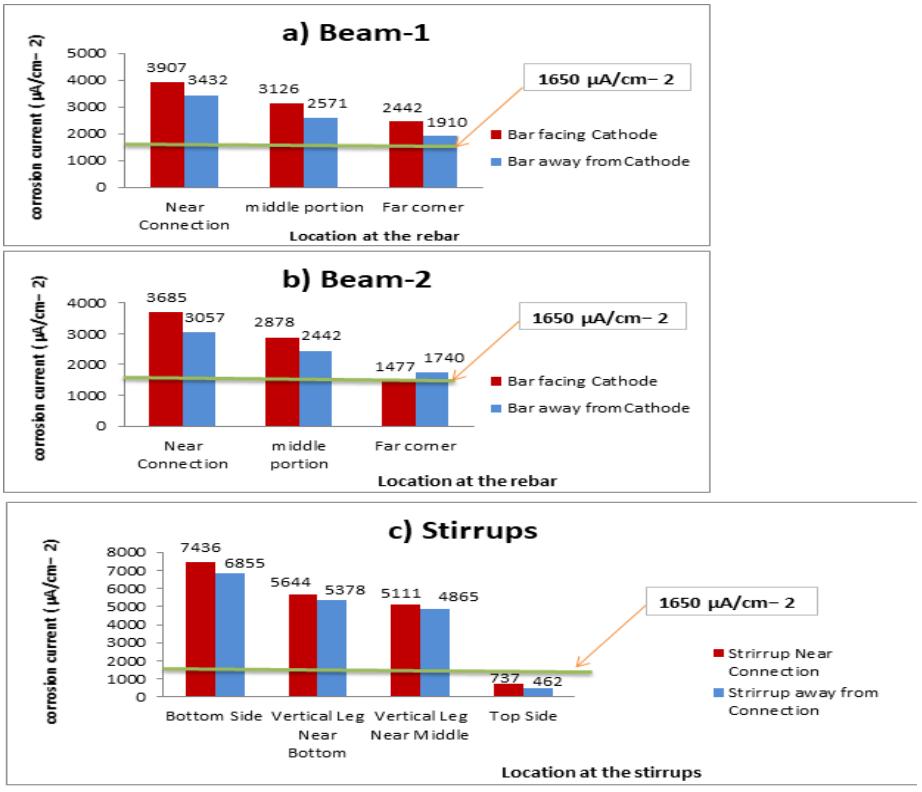

FIGURE 4.8: Explains actual corrosion current at diff locations of a) beam-1, b) beam-2, c) stirrups

TABLE 4.1: Explains at different locations of a bar & stirrups, diameter, radius, nominal weight, final weight, % loss of weight, and actual applied current & density

	Location	Bar portion	Length (L)	Dia (cm) D	Radius (cm) R	Nominal wt (g)	Final Weight (g)	Wt. loss (g)	Percent wt loss (%)	Surface Area (cm2) (2x3.1416xR XL)	Wt. loss per unit area (g/cm2)	Actual app current (Amp)	Amp/cm2	Actual Applied current, Icorr, (n /cm2)
Beam 1	Bar Facing Cathode	Connected comer	16.00	1.2	0.6	158	129	29	19	60	0.49	0.236	0.0039	3907
		Mid	13.05	1.2	0.6	129	110	19	15	49	0.39	0.154	0.0031	3126
		Far Corner	12.00	1.2	0.6	119	105	14	12	45	0.30	0.110	0.0024	2442
	Bar Away from Cathode	Connected comer	14.00	1.2	0.6	139	116	23	16	53	0.43	0.181	0.0034	3432
		Mid	14.50	1.2	0.6	143	126	17	12	55	0.32	0.141	0.0026	2571
		Far Comer	16.00	1.2	0.6	158	144	14	9	60	0.24	0.115	0.0019	1910

	Location	Bar portion	Length (L)	Dia (cm) D	Radius (cm) R	Nominal wt (g)	Final Weight (g)	Wt. loss (g)	Percent wt loss (%)	Surface Area (cm2) (2x3.1416xR XL)	Wt. loss per unit area (g/cm2)	Actual app current (Amp)	Amp/cm2	Actual Applied current, Icorr, (n /cm2)
Beam 2	Bar Facing Cathode	Connected comer	12.00	12	0.6	118.8	98	20.75	17.5	45.24	0.46	0.167	0.0037	3685.4
		Middle	11.00	1.2	0.6	108.9	94	14.86	13.6	41.47	0.36	0.119	0.0029	28782
		Far Corner	15.00	12	0.6	148.4	133	15.44	10.4	56.55	027	0.084	0.0015	1477.8
	Bar Away from Cathode	Connected comer	13	12	0.6	128.6	110	18.65	14.5	49.01	0.38	0.150	0.0031	3057.0
		Middle	12	12	0.6	118.8	105	13.75	11.6	45.24	0.30	0.110	0.0024	2442.3
		Far Corner	10.50	12	0.6	103.9	95	8.91	8.6	39.58	0.23	0.069	0.0017	1740.0

	Location	Bar portion	Length (L)	Dia (cm) D	Radius (cm) R	Nominal wt (g)	Final Weight (g)	Wt. loss (g)	Percent wt loss (%)	Surface Area (cm2) (2x3.1416xR XL)	Wt. loss per unit area (g/cm2)	Actual app current (Amp)	Amp/cm2	Actual Applied current, Icorr, (n /cm2)
Stirrup-1	**Near Connection**	Bottom Leg	55	0.8	0.4	30.8	18	12.79	41.5	13.82	0.93	0.103	0.0074	7436.5
		Vertical Leg Near	6	0.8	0.4	33.6	23	10.59	31.5	15.08	0.70	0.085	0.0056	5644.4
		Vertical Leg Near	5	0.8	0.4	28.0	20 20	8.00	28.6	12.57	0.64	0.064	0.0051	5111.7
		Top Leg	4.75	0.8	0.4	26.6	25.5	1.10	4.1	11.94	0.09	0.009	0.0007	737.3
Stirrup-2	**Near Connection**	Bottom Leg	5.5	0.8	0.4	30.8	19	11.79	383	13.82	0.85	0.095	0.0069	68553
		Vertical Leg Near Bottom	6	0.8	0.4	33.6	23.5	10.09	30.0	15.08	0.67	0.081	0.0054	5378.0
		Vertical Leg Middle	6.5	0.8	0.4	36.4	26.5	9.89	272	16.34	0.61	0.079	0.0049	4865.8
		Vertical Leg near Top	5.5	0.8	0.4	30.8	30	0.79	2.6	13.82	0.06	0.006	0.0005	462.0

Table 4.2: Behavior of all beams under four point load testing

Sr. No	Beam Name	First Crack (KN)	Additional Cracks			Fracture	Time (Sec)
1	**CB-1**	25KN 1.0 mm small hair crack	80KN 3mm Diagonal cracks	127KN 6mm Vertical & diagonal cracks at mid span of beam	136 KN 6.4mm Multiple cracks throughout the beam.	118 10.3mm Cracked in tension. As cracks are wider at bottom side. But not significant cracks appear at top side of beam	620
2	**CB-2**	24KN 0.9mm crack at top due to uneven surface	76KN 2.6mm Bottom Vertical	129 KN 6.1mm Due to Weak point Sudden drop of load	132 6.25mm Cracks are not much wider, no cracks appeared at top of beam	116 10mm Cracks at supports in diagonal position but at center of beam bottom vertical cracks	600
3	**C-1**	64.3KN, 2.3mm, Vertical hairs	118KN, 4.6mm, diagonal cracks	121KN Cracks at supports moving from bottom to top	126KN 6.4mm Bottom side of beam	117KN 8.5mm Wider cracks in the middle originating	528
					cracked in full width, but no failure in reinforcem ent, multiple cracks originated	from bottom to reaching at the top surface of beam, Diagonal cracks at supports	

Sr. No	Beam Name	First Crack (KN)	Additional Cracks			Fracture	Time (Sec)
4	**C-2**	6KN, 1.8mm, Top crack	67 KN, 3.8mm, Bottom hair cracks	115KN 6.3mm Vertical cracks at center of beam and diagonal cracks at supports	120KN Cracks width is less but whole body of beam shows cracks vertical and diagonal as well	110KN, 11.11mm At the center of beam this time both vertical and diagonal cracks are originated from bottom and reached to top . diagonal cracks starting from supports also touching center of shear span at the top side of beam	660
5	0.7 CB- 1	48KN, 2.1mm, Bottom Hair Cracks	65 KN, 2.7mm, Bottom Crack	70KN 3.5mm Diagonal cracks hair line	95 KN Visually no cracks in graph of computer	-	213
6	0.7 CB- 2	36 KN, 2.3mm, Bottom hair crack	50 KN, 2.9mm, Bottom Crack	67KN, 2.5mm, bottom vertical cracks	95 KN, 5.05mm	-	301

Sr. No	Beam Name	First Crack (KN)	Additional Cracks			Fracture	Time (Sec)
7	0.7 CB- 3	40KN, 3.5mm, Bottom Cracks		57 KN, 4.4mm, Top cracks in bulging of concrete	96.8KN, 5.8mm	-	349
8	0.7 CB- 4	25KN, 1.9mm	46KN, 2.4mm, bottom crack	74KN, 3.2mm, Multiple cracks	96 KN	-	235
9	CS BFRP-1	7KN, 2mm	39KN/4.5mm horizontal cracks 58KN/ 7.3mm bottom vertical 80KN/6.4mm vertical uptill center half of beam	96KN/7.3mm diagonal bottom to top full crack 0.25cm crack width 113KN/7.3mm cracking completely diagonal	132.59 KN/ 10.2mm	126KN/ 15mm De-lamination in one end/ rest of the beam was ok	502
10	CS BFRP-2	80Kn, 5mm crack bottom vertical	102KN, 5.8 mm Diagonal bottom to top 123KN, 7mm no delamination but top to bottom crack	135KN, 6.5 mm Massive cracks in beam but no delamination yet	138KN, 8.7 mm No Delaminati on but cracks at support is developed	123KN 14mm BFRP breaks from center	459

Sr. No	Beam Name	First Crack (KN)	Additional Cracks			Fracture	Time (Sec)
11	CBS BFRP-1 504 Sec	25KN/2. 3mm top crack due to uneven surface	66KN/3.9mm bottom vertical hair in the mid portion of beam 97KN/5.3mm diagonal cracks from top to bottom at the supports	121KN/6.3mm more diagonal cracks de- lamination at small stage 134/7mm de- lamination at support, concrete almost crushed but BFRP is still maintanied	156.75 KN 10.4mm	122KN 11.5mm BFRP tears up in parts	463
12	CBSBFRP-2	53KN/3 mm Top concret e falling due to uneven surface, bottom hair vertical cracks	103KN/5.3mm diagonal hair cracks at support and middle but no delamination	139KN/ 6.7mm Cracks at supports but no delamination	155.3KN 9.5mm	154KN/10.5m m No delamination but cracks are visible at supports in beam 150KN/11mm Delamination at supports 129KN/12mm Delamination at center 117KN/15mm Only Delaminated at center and supports but no tear out in BFRP	471
13	CS CFRP-1	67KN/4 mm vertical hair cracks	84KN/4.5mm Diagonal hair cracks 121KN/6mm full diagonal cracks from bottom to top	143KN/ 7.2mm full diagonal crack at the support	148KN 8.5mm	133KN/13.7m m/ 829 Seconds de- lamination at one end support 120KN/14.7m m/(865 sec) no de-lamination or tear out at center only one support CFRP breaks at some extent	865

The distribution of i_{corr} at the various stirrup locations is shown in Figure 4.8(c). The stirrups' lower legs experienced the greatest corrosion current, measuring 7436 μA/cm^2 and 6855 μA/cm^2, respectively, for stirrups that were closer to the connection (Stirrup-1) and farther away from the connection (Stirrup2). The consumed current values for the stirrups at the near connection and far end of the top side leg is 737 μA/cm^2 and 462 μA/cm^2, respectively. For both stirrups, the icorr values at the bottom sides were higher than the ones on the vertical sections, ranging from 4865 to 5644 μA/cm^2. It is evident from Figure 4.8(c) that there is no variation in the weight loss between the two stirrups' vertical legs. There is another factor, though, which is that regardless of where the stirrup is in relation to the connection, the leg facing the cathode plank should typically corrode more.

The wet concrete pores made it simpler for the ionic current to pass through and react with oxygen, water molecules, and hydroxyl ions to produce rust products. Because of this, compared to the top bars, where the ionic current had to overcome the higher concrete resistivity to reach the wet concrete and form a connection with the cathode plates, the impressed current was able to extract electrons (negative current) from the bottom bars more readily. Because of this, top compression bars had very little weight loss and were in their original condition, while bottom rebars had severe corrosion. The aforementioned considerations should be kept in mind when creating a striking current technique application. Similar findings were reported by Li et al. (2021), who attributed the stirrups' increased corrosion to their smaller diameter and closer proximity to the cathodic mesh that encircled the concrete prism samples.

4.3 Failure Modes of RC Beams

Results are presented in the form of graphs, tables, and curves. Results are discussed in certain way; first of all real time failure modes of controlled, corroded, strengthened, pre-loaded strengthened beams are elaborated then their strength values are tabulated and compared in the form of table and curves. Following this; weight loss of steel due to corrosion and the comparison between iapp and icorr are discussed. The loaddeflection and curves are also elaborated.

4.3.1 Background and Summary of Physical Behavior of Beams under Loading

A total of 16 beams were casted for 4000psi strength with dimensions of 1000 mmx150 mm x200 mm. Which includes, 2 control beams, 2 control beams strengthen with BFRP, 2 control beams strengthen with CFRP, 2 corroded beams, 2 corroded beams strengthen with BFRP, 2 corroded beams strengthen with CFRP, 2 control beams were loaded 70% of ultimate load and then strengthen with BFRP, and 2 control beams with 70% loading and then strengthen with CFRP.

Beams were loaded under four point loading at constant load rate of 1mm/ minute. During loading each beam shows its own behavior and failure mode, crack propagation behavior was different. Some of the beams were failed under laminate tear out, adhesive and concrete failure in tension zone. Table 4.2 shows crack pattern and deflection under loading since the beam started carrying no further loads. It represents physical observation of beam recorded during testing.

Table is self explanatory that how beams were behaving and resisting loading. Some shows wider racks, few shows deflection in beams and rest were failed in de-bonding of laminates. Fig 4.9 comprises on eight sets of beams represented in tabular form and pictorial view. Fig (a) shows failure of control beams CB were cracks in tension zone. Firstly the cracks were developed diagonally and then vertical cracks as the load increased. Initial cracks that were developed in control beam were due to uneven surface at top of the beam. Slowly the crack propagates from tension zone and travelled towards compression zone near loading points. Shear cracks were vertical but not inclined and shear cracks did not reached till the top of beam & they stopped in the mid height of the beam. Steel yielding was not occurred and no failure in reinforcement was observed, load was increasing and so deflection. But at certain point beam stopped taking further loads but cracks width and deflection was increasing so it was perceived that concrete was failed because cracks widths are reached at that dimensions where beam failure is imminent. Fig (b) shows the failure of beam was in shear zone and vertical cracks were developed. Contrary to control beams corroded beam initial cracks was occurred at 6KN and 1.8mm deflection while CB first crack was developed at 24KN and 0.9mm deflection.Ductility index decreases significantly with 12%

reinforcement corrosion. Failure mechanism shifts from flexural to shear failure with corrosion [208]. Stirrups typically corrode before longitudinal bars, leading to a significant reduction in shear strength. This early corrosion can result in a transition from bending to shear failure modes [209]. Reason behind generation of cracks at very initial loads is due to already existed stress due to corrosion products in the concrete around the bars. It is important to consider that slope of curve from yield to ultimate limit in control beams was steeper as compared to corroded beams. Corroded beams exhibit greater deflection and less increase in load while approaching from yield limit to ultimate load limit. Finally the degraded/corroded beam with average 15% weight loss in flexural rebar failed with full width wide crack at center of shear span approaching from bottom to top of beam. At fracture point multiple diagonal cracks were also produced at supports approaching towards loading point. Fig (c) (d) shows corroded beams strengthened with BFRP and

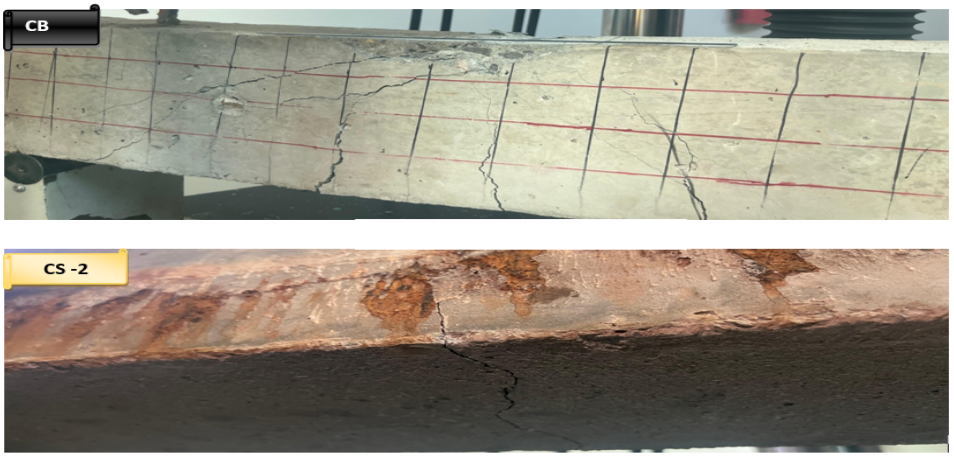

FIGURE 4.9: (a) Failure in tension zone (b) Cracked shear zone/wider cracks

CFRP respectively. Both shows laminate tear out or splitting failure due to wider cracks at tension zone. But strengthening laminate in corroded beam was tear out at mid span of the beam when it was strengthened with BFRP and tear out at supports when it was strengthened with CFRP. This type of failure is called splitting/ tear out failure where laminates are de-bonded at the point where multiple cracks are originated and splits. Before the de-lamination, BFRP and CFRP laminate experienced splitting rupture in the transverse direction at the soffit of the beam. This shear rupture in laminates could be due to non uniform stress distribution as one flexural rebar is corroded more as compared to other and also each end of on rebar also shows different weight loss in a single beam.

Loads were transferred by flexural rebar to the CFRP and BFRP laminates this generates shear and tension in laminates and cause splitting in transverse direction. Beam shows cracks more than 1cm. Based on these results it could be concluded that laminate thickness can be increased in corroded beams or multiple layers of hybrid system can be used. Conversely, strengthened corroded beams where only

FIGURE 4.10: Laminate tear out at mid span, at supports, and 0.5cm cracks

wider cracks were originated and propagated at any end of the beam, strengthened Controlled beams exhibits multiple minor and major cracks shown in Fig (e) (f). Failure observed in these beams were adhesive type in which laminates are de-bonded from the soffit of beam but not break out or splits. Mostly this happens when large number of minor cracks is originated at substrate and laminates slips from the surface. In our case when these beams were strengthened with CFRP and BFRP, both materials shows same behavior none of them splits out. In the case of BFRP strengthened beams initial crack developed at 53KN and 3mm deflection. Then diagonal cracks at support and middle originated at 103KN. Upon reaching ultimate load, cracks at supports reaches up to middle span of the beam in compression zone. At fracture vertical cracks in shear zone also propagated

across the full depth of the beam. In the case of CFRP strengthened beams initial crack developed at 80KN and 4.5mm deflection. Then vertical bottom cracks started originating throughout the beam. At fracture point cracks width reaches almost at 2cm but no rupture in laminate was observed only adhesive failure was occurred. Fig (g) shows that beams who were preloaded and then strengthened

FIGURE 4.11: Adhesive failure and de-lamination

with BFRP shows increase in flexural strength even as compared to control beams. But upon fracture it has been observed that BFRP laminate splits and tear out at supports and delaminates at center portion of beam. Also some portion of concrete also sticks to the laminate catering it into interfacial failure. In properly

FIGURE 4.12: Cohesive de-lamination at supports

applied CFRP and BFRP strengthening systems, corroded RC beams experience

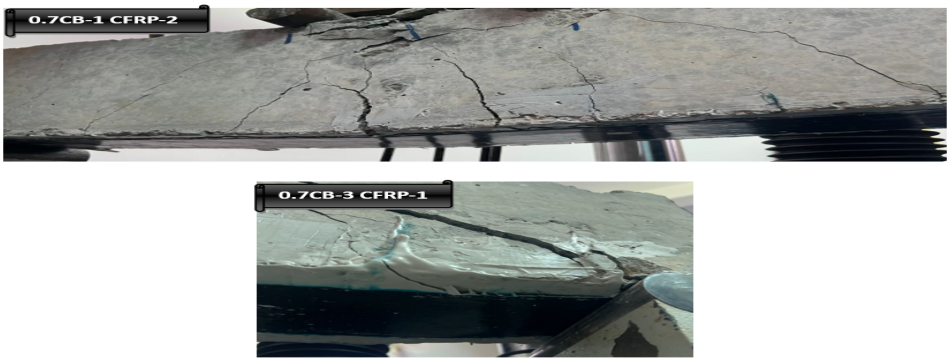

FIGURE 4.13: Adhesive de-lamination/wider cracks

cohesive or interfacial failures. If the epoxy is not applied sufficiently, bond breaks between the laminates and substrate could occur, which would be an adhesive failure. Similarly, the failure changes from adhesive or interfacial to fully cohesive as the thickness or number of layers of the strengthening laminates increases. Flexural reinforcement that had corroded was combined with CFRP and BFRP strengthening in the study of beams with insufficient strength. Still, the failure modes resembled those commonly found in the reinforced control RC beams.

The numerical outcomes are aligned with experimental results, confirming the validity of the developed constitutive models. The findings reveal that a low corrosion level (5%) in steel stirrups exhibits a limited impact on the overall structural shear capacity (-4%-0.9%). However, a higher corrosion level (12%) in stirrups induces a more pronounced reduction in structural shear capacity. This reduction is particularly prominent in scenarios involving a high shear span-to-depth (av/d) ratio. Furthermore, it is observed that a higher corrosion rate corresponds to a smaller mid-span deflection when the RC beam reaches its peak shear force. This phenomenon is attributed to the corrosion-induced degradation of stirrup performance, resulting in an overall reduction in deformation capacity. The av/d ratio significantly influences the failure mode, altering from deep beam failure to shear-compression failure and flexural-shear failure as av/d increases from 1.0 to 3.0. This observation remains unchanged even after the corrosion of steel stirrups at different corrosion levels (5% and 12%) [210].

Corroded RC beams exhibit a marked decrease in bending stiffness and flexural capacity compared to intact beams, as demonstrated by experimental investigations using a Rigid Body Spring Method (RBSM) model [211]. This implies that

flexural strengthening with CFRP laminates enhanced the strength but significantly reduced the ductility of the RC beam which resulted in a brittle failure. As the material gets stiffer its ductility reduced. The elastic modulus measures a material's stiffness. as the elastic modulus goes up, the stiffness of a material also goes up. Ductility is not related to elasticity. Ductility is a dimensionless material property that measures how much a material can be stretched (in terms of length, or L/L before it breaks, whereas elasticity expresses how difficult it is (i.e. how much force is required) to stretch the material [212]. The experiment conducted on Flexural and shear strengthening of RC beams reinforced with externally bonded CFRP laminates postfire exposure, reveals that the CFRP reinforcement increases considerably the ultimate strength and stiffness capabilities. Additionally, they have the potential to heal partially cracks [213].

4.4 Load-deflection Behavior

Fig 4.10 (a), (b), (c), (d) presents the load deflection curves of controlled beams and strengthened with BFRP & CFRP, Corroded beams and strengthened with BFRP & CFRP. It provides comparison of load deflection of pre loaded beams strengthened with BFRP & CFRP. Whereas Fig 4.11 (a), (b) gives us the ultimate and yield load of all 16 beams. Table 4.4 summarize all the parameters of four-point bending such as critical loads, deflections at yield, ultimate loads and fracture loads and also gives the failure modes of the beams. Table 4.3 compares percentage of strength increase or decrease when different strengthening systems are applied on controlled and corroded beams.

Figure 4.10 (a) The yield loads for CB-1 and CB-2 were 121 and 116 kN, respectively, and the ultimate loads were 136 and 132 kN. Both the CBS BFRP-1 and CBS BFRP-2 demonstrated yield loads of 139 and 143 kN, ultimate loads of 157 and 155 kN, and fracture point deflections of 13.5 and 14.1 mm, respectively. The ultimate loads for the CBS CFRP-1 and CBS CFRP-2 were 159 and 169 kN, with yield loads of 142 and 154 kN and fracture point deflections of 16.1 and 14.5 mm, respectively.

Curve clearly shows that slope of the curve for BFRP strengthened beams has been identical such as controlled beams when reaching from yield limit to ultimate limit.

While beams strengthened with CFRP shows greater slope because it carried more load and shows less deflection at ultimate load point shows in Table 4.3. After ultimate limit when entered in the phase of fracture almost each beam exhibits same declination in graph. Sudden drops in the curve shows weak points in the RC beam that occurs due to non uniform material distribution of coarse aggregates under loading points or air voids etc.

Figure 4.10 (b), the average yield strength of the concrete beams was lost by 8.23% after corrosion caused the steel rebars at the flexural steel to lose 17% of their weight. In comparison to the control beams, the ultimate strength was also reduced by 8.94%. It is clearly exhibited that curve of corroded beams becomes flat when it crosses yield limit and not much bear strength after it crosses ultimate load limit. Angle of slope for controlled beam at region between yield and ultimate limit is approx 30 degree but for corroded beams it is approx 20 degree which shows more deflection and less load increment. The CS BFRP-1 and CS BFRP-2 showed yield loads of 118 and 122 kN, and ultimate loads of 133 and 138 kN, and deflection 10 mm and 8.7 mm at Ultimate load limit respectively. The CS CFRP-1 and CS CFRP-2 showed yield loads of 130 and 128 kN, and ultimate loads of 148 and 142 kN, and deflection 8.5 mm and 7.8 mm at ultimate load limit point, respectively. The unequal corrosion rates close to the mid-span may be the cause of the variation in final deflections between two identically sized corroded beams. Given the differences in the concrete conditions, the deflections show that the corrosion with impressed current in the two different beams may not be the same. Greater flexural steel corrosion at the mid-span would result in less ultimate deflection and load carrying capacity for the beams. induced in it. Then it was strengthened with BFRP and CFRP to check which material gives better results and can we achieve strength equivalent or more than the control beams.

Most of real beams have cracks with the passage of time due to any prevailing conditions so this methodology of preloading resembles real life beam and helps to correlate these results for design of strengthening systems. Table 4.3 shows Corroded and controlled beams strengthened with CFRP shows 7.20% and 5.01% higher value in load bearing capacity as compared to when these were strengthened with BFRP. That clearly shows CFRP is ahead of BFRP but in this case of preloaded beams strengthening there is not much difference between strengths

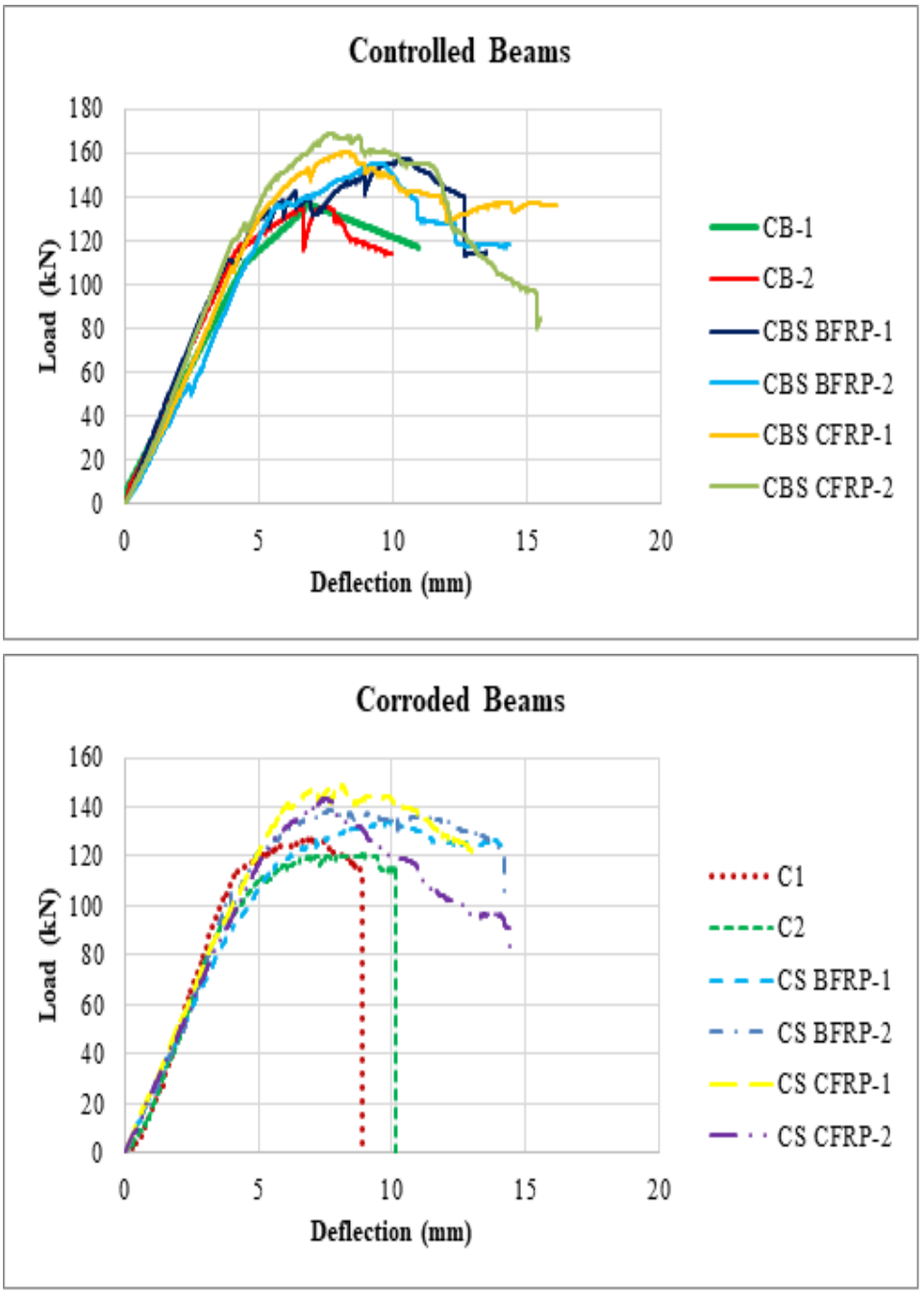

FIGURE 4.14: (a): Load-Deflection curve of controlled and controlled beams strengthened with BFRP & CFRP, (b): Load-Deflection curve of corroded and corroded beams strengthened with BFRP & CFRP

achieved with CFRP and BFRP. Preloaded beams strengthened with CFRP shows 2.15% higher ultimate load as compared to BFRP strengthened. El Maaddawy and Soudki (2005) found that strengthened corroded RC beams with CFRP laminates experienced a 73% gain in load capacity despite losing 32% of their weight on the flexure rebars. In contrast, in our instance, we were able to regain 17.88% of the ultimate load of the corroded beam strengthened with CFRP despite a 17% weight loss of the flexural bars. And it regains up to 9.8% with BFRP. The

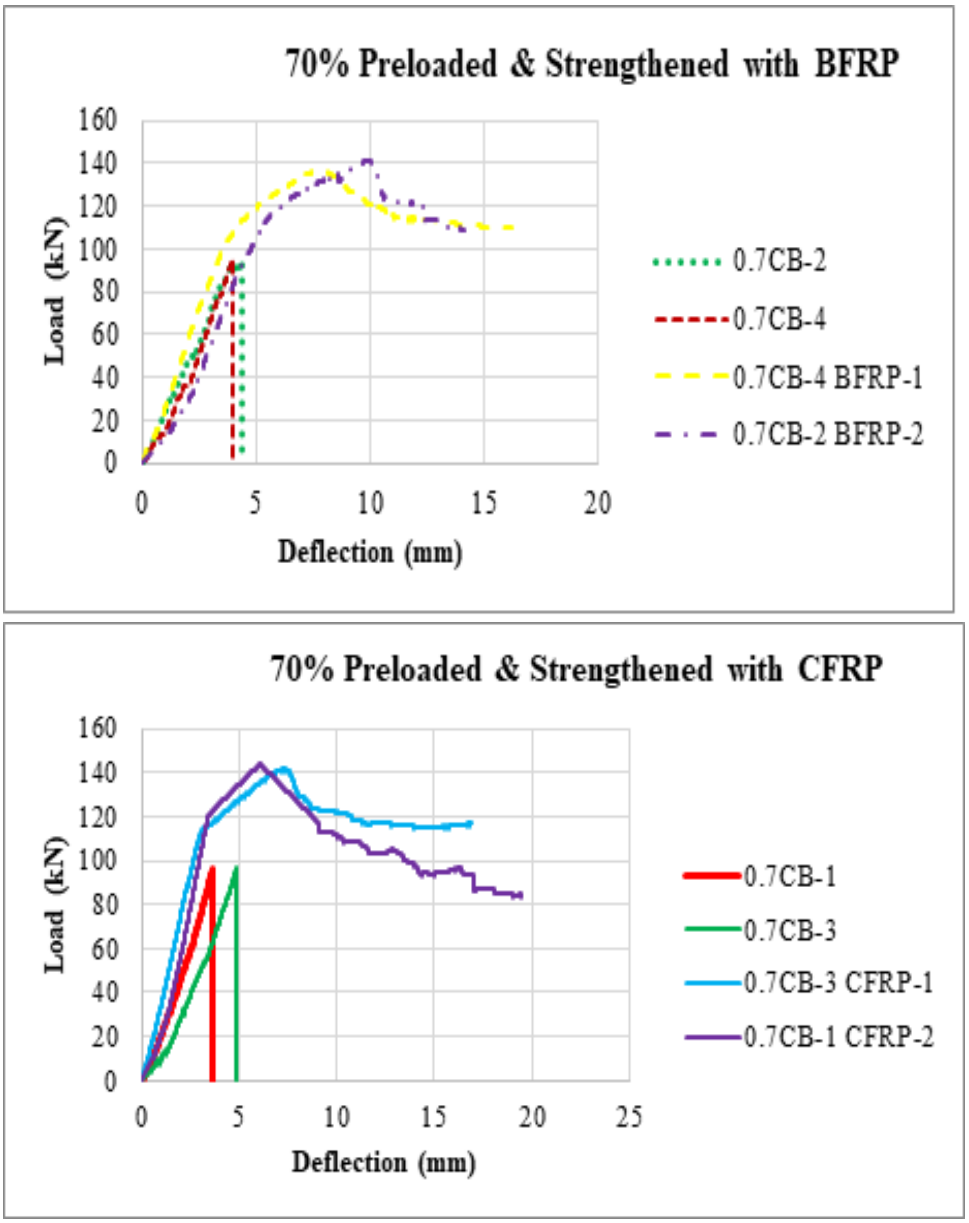

FIGURE 4.15: (c): Load-Deflection curve of pre-loaded beams strengthened with BFRP, (d): Load-Deflection curve of pre-loaded beams strengthened with CFRP

beams deteriorated with 1650 A/cm 2 for 15 days. As can be seen in Table 4.3, their yield and ultimate loads were lowered to 108 and 122 kN, respectively. In comparison to the controlled beams, that represents a 9.25% and 8.93% loss in yield and ultimate strength, respectively. It is connected to decreased yield loads as a result of the cross-sectional loss of corroded main rebars. According to Hong S. and Zheng F. (2020), the loss of weight and steel area does not increase linearly with the duration of the application. As the current application time increases, it increases in a non-linear manner. The primary flexure reinforcement's varying level of corrosion is the cause. This emphasizes how crucial the main flexure rebars are

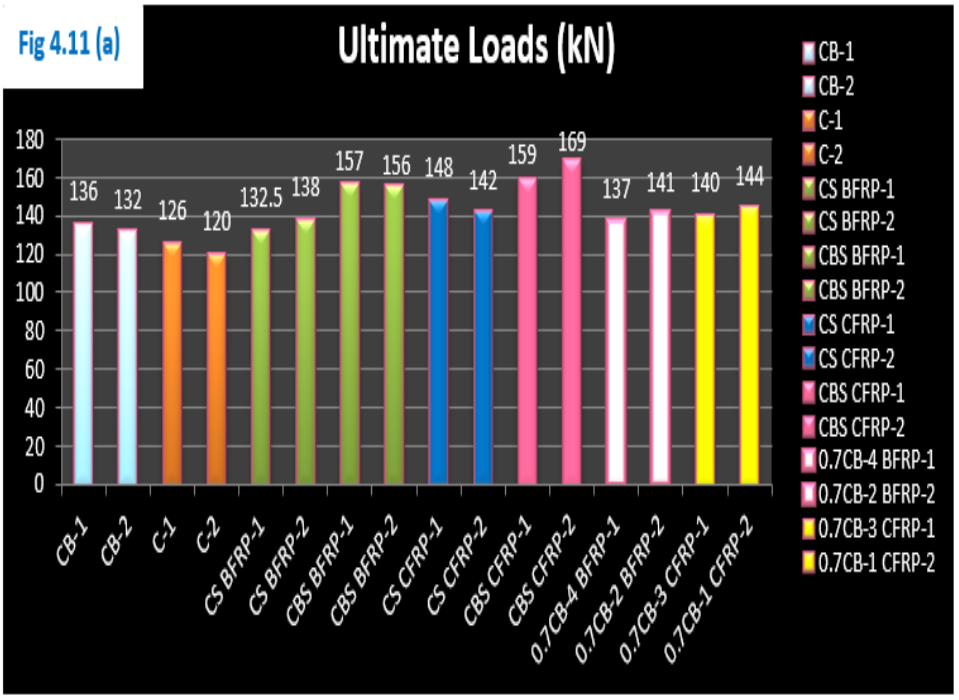

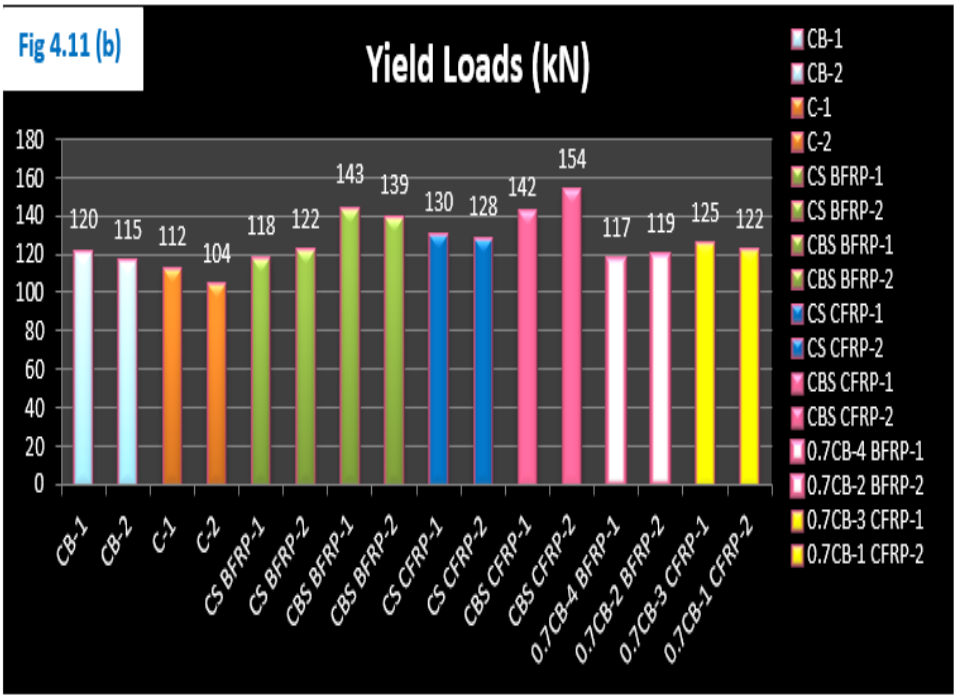

FIGURE 4.16: (a): Ultimate Load , (b): Yield Load

because, even with external strengthening, the stiffness may be lost if the rebars corrode too much.

Different beams shown different failure moods and are discussed briefly above. Few are failed in Debonding and others are failed in laminate splitting. More the beam is corroded less will be its ultimate deflection and load carrying capacity. From table 4.4 it is also evident that beams which are strengthened have higher

TABLE 4.3: Comparison of % ultimate strengths of all beams

S. N.	Beam Samples	Ultimate Loads (kN)	Average (kN)	Comparison of Ultimate Strengths (-ve) shows Lesser than (+ve) shows more than
1	CB-1	136	134	-
2	CB-2	132		
3	C-1	126	123	(*-ve) 8.94% of CB
4	C-2	120		
5	0.7CB-4	96	95.7	70 % Preloaded for BFRP strengthening
6	0.7CB-2	95.4		
7	0.7CB-3	96.8	95.9	70 % Preloaded for CFRP strengthening
8	0.7CB-1	95		
9	CS BFRP-1	132.5	135.25	(*+ve) 0.9% of CB
10	CS BFRP-2	138		(*+ve) 9.8% of C
11	CBS BFRP-1	156.75	156.025	(*+ve) 16.4% of CB
12	CBS BFRP-2	155.3		(*+ve) 26.84% of C
				(*+ve) 15.36% of CS BFRP
13	CS CFRP-1	148	145	(*+ve) 8.20% of CB
				(*+ve) 17.88% of C
14	CS CFRP-2	142		(*+ve) 7.20% of CS BFRP
				(*-ve) 7.58% of CBS BFRP
15	CBS CFRP-1	159	163.85	(*+ve) 22.27% of CB
				(*+ve) 32.21% of C
				(*+ve) 21.14% of CS BFRP
16	CBS CFRP-2	168.7		(*+ve) 5.01% of CBS BFRP
				(*+ve) 13.0% of CS CFRP
17	0.7CB-4 BFRP-1	137	139	(*+ve) 3.73% of CB
				(*+ve) 13.01% of C
18	0.7CB-2 BFRP-2	141		(*+ve) 45.24% of 0.7% CB
19	0.7CB-3 CFRP-1	140	142	(*+ve) 5.97% of CB
				(*+ve) 15.44% of C
20	0.7CB-1 CFRP-2	144		(*+ve) 48.07% of 0.7% CB
				(*+ve) 2.15% of 0.7% CB-BFRP

ratio of Ultimate to yield loads and deflections. That shows they travelled more vertical and less horizontal (deflection) which shows this strengthening system provided more stiffness to the beam by providing extra reinforcement in the form of CFRP and BFRP laminates.

When corroded beams were strengthened with CFRP & BFRP both were failed in tear out (split) failure of laminates. But when controlled beams were strengthened they only show de-lamination of laminate at the substrate of beam, it exhibits that the maximum capacity of CFRP laminates was not utilized.

The reinforced beams experienced concrete crushing upon failure; this occurred due to adhesive laminate debonding, laminate splitting, or delamination of the concrete cover and laminate combined. Since the beam collapsed in the concrete when it was compressed, yielding or steel fracture was not seen in any of the aforementioned tests, nor was it attempted. And the beam ceased to support additional weight. The laminates' load-strain behavior was tri-linear at the tension face. Because of the steel, concrete, and laminates' resistance to tensile stresses, the slope was initially steeper. The slope was lessened after the laminate cracked or de-bonded. It was reduced even more after crushing the concrete.

BFRP has been shown to improve the shear capacity of corroded reinforced concrete (RC) beams, particularly when applied strategically. Studies indicate that BFRP can significantly enhance the flexural behavior of corroded beams, suggesting that its application at the bottom can be beneficial [214].

Applying BFRP only to the bottom may not fully address shear deficiencies, as shear forces are distributed throughout the beam. The lack of reinforcement on the sides could lead to inadequate performance under certain loading conditions [215]. If BFRP is applied at the bottom side of the beam and extending it to the mid height of the beam at both vertical sides will help to increase shear capacity of the beam.

Corrosion of steel bars leads to a notable decrease in bond strength, which is critical for the structural performance of reinforced concrete (RC) structures [216] Interestingly, mild corrosion (below 2.5%) can enhance bond performance, particularly when combined with fly ash in concrete [217].

Table 4.4: Properties of the loaddeflection behavior & failure modes of controlled, corroded, and strengthened beams

S.N.	**Designation**	Py (KN)	Pu (KN)	σy (mm)	σu (mm)	σf (mm)	σf/σy	σf/σu	**Failure Modes of beams**
1	CB1	120	136	6	7	11	1.83	1.57	Failure in tension zone/wider cracks
2	CB2	115	132	4.6	7.6	9.9	2.15	1.30	Failure in tension zone/wider cracks
3	C1	112	126	5	6.7	9	1.80	1.34	Cracked in shear zone/wider cracks
4	C2	104	120	6	6.4	10.1	1.68	1.58	Cracked in shear zone/wider cracks
5	CS BFRP1	118	133	4	10	14.1	3.53	1.38	Laminate split at Mid span/ Concrete Rupture/ Delamination
6	CS BFRP2	122	138	4	8.7	14.1	3.53	1.62	Laminate split at Mid Span/ Concrete Rupture / Delamination
7	CBS BFRP1	143	157	3.9	10	13.5	3.46	1.30	Adhesive failure/ wider cracks
8	CBS BFRP2	139	155	4.8	9.5	14.2	2.96	1.49	Adhesive failure / wider cracks
9	CS CFRP1	130	148	6	8.5	13	2.17	1.53	Laminate Tear Out at supports / Wider Cracks
10	CS CFRP2	128	142	5	7.8	14.2	2.84	1.82	Laminate Tear Out at supports / Wider Cracks
11	CBS CFRP1	142	159	4	8.2	16	4.00	1.95	Adhesive/ Wider cracks/ Delamination

S.N.	Designation	Py (KN)	Pu (KN)	σy (mm)	σu (mm)	σf (mm)	σf/σy	σf/σu	Failure Modes of beams
12	CBS CFRP2	154	169	4	7.6	14.5	3.63	1.91	Adhesive/ Wider cracks/ Delamination
13	0.7CB4 BFRP1	117	137	4	8.1	16.5	4.13	2.04	Interfacial/ Delamination/ tear out at supports
14	0.7CB2 BFRP2	119	141	5.5	10	14.2	2.58	1.39	Interfacial/ Delamination/ tear out at supports
15	0.7CB3 CFRP1	125	140	3	7.5	17	5.67	2.27	Delamination/Adhesive/ Wider Cracks
16	0.7CB1 CFRP2	122	144	3	6.6	19	6.33	2.88	Delamination/Adhesive/ Wider Cracks

Chapter 5

Conclusions and Recommendations

5.1 Conclusions

Corroded and strength deficient reinforced concrete beams were strengthened with basalt fiber reinforced polymer (BFRP) and carbon fiber reinforced polymer (CFPR). Impressed current technique was applied on normal scale RC beams for 15 days and 8hours/day. Current value was kept uniform at 1650 μA/cm^2. Weight loss on the rebars was calculated to substantiate which portion of steel reinforcement had consumed more or less current and what degree of extent those parts were corroded. Secondly, few beams were pre-loaded up to 70% of ultimate load of normal beams to induce cracks in them. Strengthened beams were tested under four-point bending in a UTM.

Following important conclusions were extracted:

1. Impressed current technique on interval-based application caused non-uniform corrosion at different parts of reinforcement. Expected weight loss was 10% but we experienced 15% and 35% weight loss in flexural rebars and stirrups of the beams corroded, respectively.

2. It was observed that corrosion followed same pattern as in literature. Part of the rebar facing cathode was damaged severely as compared to bar which

is away from the cathode. Moreover, compression bars which were away from bottom of the beam (soaked portion) experienced less or zero corrosion. Corner of the reinforcement which was connected to the power supply also experienced greater value of corrosion during 15 days impressed current application.

3. Average loss of weight in flexural rebars facing cathode was 15.3% and bars away from cathode was 12% and top compression bars shown no significance in corrosion. Similarly stirrups bottom and vertical legs near bottom were showed weight loss 39% and 28% respectively. Top leg of stirrups shows approx 2.5% weight loss.

4. Average loss in yield and ultimate strength of the corroded beams were 8.79 and 9% respectively as compared to control beam. Due to 35% weight loss in steel its cross section was reduced but steel rupture was not observed in this case and beam was failed when wider cracks were observed at shear zone of beam and it no longer take further loads.

5. Single layer of BFRP regained the strength of corroded beam having approx 35% weight loss in flexural bars up to the virgin strength of control beam. when corroded beam was strengthened with BFRP, raise in strength was observed 1% as compared to Control beam and 9.8% increment in ultimate strength as compared to corroded beam,. Same was observed when corroded beam was strengthened with single layer of CFRP. Average increase in ultimate strength was 8.20% of CB, 17.88% of Corroded and importantly 7.20% higher of the corroded beam strengthened with BFRP.

6. When controlled beams were strengthened with BFRP and CFRP, strengths improvement was 16.4% and 22.27% as compared to Control un-strengthened beams. And 15.36% and 21.14% strength upgrading as compared to corroded beams strengthened with BFRP and CFRP, respectively.

7. When pre-loaded beams were strengthened with BFRP and CFRP it exhibited 3.73% and 5.97% higher value of ultimate strength as compared to control beams.

8. In general BFRP shows less increment in ultimate strength as compared to CFRP due to its own tensile properties. But, BFRP always gave better results to regain strength of corroded, controlled as well as pre-loaded beams and in each case strength was achieved higher than control beams strength. Keeping economical aspects in consideration BFRP was available in 40% less cost as compared to CFRP.

9. The results designate that the BFRP and CFRP laminates are competent rehabilitation and strengthening materials and can be widely useful in the scenario of corroded reinforced members.

Table 5.1: Market Prices and Availability of CFRP and BFRP

Material Name	**Dimensions Unit**	**Market Price (Pkr/sft)**	**Adhesives Price (Pkr/sft)**	**Source of Availability**
CFRP	Sft	850-1100	200-250	Local
BFRP	Sft	500	200-250	Imported from China

5.2 Recommendations

On the basis of conclusions drawn, following recommendations are made:

1. Hybrid CFRP-BFRP for strengthening the corroded and control beam should be examined.

2. Experiments need to be performed to gain more control over artificially induced corrosion level. Which may be achieved by placing the cathode (stainless steel) plate at appropriate location.

3. Application of BFRP in comparison to CFPR on the columns should also be done.

Bibliography

[1] A.M.H. Kolio, et al., "Corrosion products of carbonation induced corrosion in existing reinforced concrete facades," *Cement & Concrete Research*, vol. 78, pp. 77-86, 2015.

[2] R. Su, et al., "A double-cylinder model incorporating confinement effects for the analysis of corrosion-caused cover cracking in reinforced concrete structures," *Corrosion Science*, vol. 96, pp. 101-111, 2015.

[3] C. Cao, et al., "Modelling of interaction between corrosion-induced concrete cover crack and steel corrosion rate," *Corrosion Science*, vol. 73, pp. 168-176, 2013.

[4] W. Zhu, et al., "Corrosion of the reinforcement and its influence on the residual structural performance of a 26-year-old corroded RC beam," *Construction & Building Materials*, vol. 69, pp. 124-132, 2014.

[5] H. Ye, et al., "Performance of reinforced concrete beams corroded under sustained service loads: A comparative study of two accelerated corrosion techniques," *Construction & Building Materials*, vol. 162 pp. 521-531, , 2018.

[6] L. Huang, et al., "Corrosion-induced shear performance degradation of reinforced concrete beams," *Construction & Building Materials*, vol. 246, pp. 118529, 2020.

[7] Z. Ye, et al., "Deterioration of shear behavior of corroded reinforced concrete beams," *Engineering Structures*, vol. 164, pp. 308-318, 2018.

[8] H. Ye, et al., "Rust distribution and corrosion-induced cracking patterns of corner-located rebar in concrete cover," *Construction & Building Materials*, vol. 148, pp. 499-509, 2017.

[9] Y. Zhao, et al., "Comparison of uniform and non-uniform corrosion induced damage in reinforced concrete based on a Gaussian description of the corrosion layer," *Corrosion Science*, vol. 53, pp. 3670-3680, 2011.

[10] C. Fu, et al., "Non-uniform corrosion of steel in mortar induced by impressed current method: An experimental and numerical investigation," *Construction & Building Materials*, vol. 182, pp. 714-723, 2018.

[11] T.U.H.H. Mohammed, "Relationship between free chloride and total chloride contents in concrete," *Cement & Concrete Research*, vol. 33, pp. 167-173, 2003.

[12] M. Thomas, et al., "Performance of lightweight aggregate concrete containing slag after 25 years in a harsh marine environment," *Cement & Concrete Research*, vol. 42, pp. 1475-1485, 2012.

[13] M. Alexander, et al., "Service life prediction and performance testing Current developments and practical applications," *Cement & Concrete Research*, vol. 75, pp. 1-12, 2015.

[14] P. Castro, et al., "Interpretation of chloride profiles from concrete exposed to tropical marine environments," *Cement & Concrete Research*, vol. 31, pp. 135-142, 2001.

[15] G.R. Meira, et al., "Durability of concrete structures in marine atmosphere zones The use of chloride deposition rate on the wet candle as an environmental indicator," *Cement & Concrete Composites*, vol. 32, pp. 555-562, 2010.

[16] Meira, Gibson Rocha, et al. "Analysis of chloride threshold from laboratory and field experiments in marine atmosphere zone." *Construction and Building Materials* 55, 289-298, 2014.

[17] Thomas, M. D. A., and J. D. Matthews. "Performance of pfa concrete in a marine environment 10-year results." *Cement and Concrete Composites* 26.1, 5-20, 2004.

[18] Thomas, Michael DA, and Phil B. Bamforth. "Modelling chloride diffusion in concrete: Effect of fly ash and slag." *Cement and concrete research* 29.4, 487-495, (1999).

[19] Nanukuttan, Sreejith V., et al. "The performance of concrete exposed to marine environments: predictive modelling and use of laboratory/on site test methods." *Construction and Building Materials* 93 (831-840), 2015.

[20] Poupard, O., et al. "Corrosion damage diagnosis of a reinforced concrete beam after 40 years natural exposure in marine environment." *Cement and concrete research* 36.3, 504-520, 2006.

[21] Otieno, M., H. Beushausen, and M. Alexander. "Chloride-induced corrosion of steel in cracked concretePart I: Experimental studies under accelerated and natural marine environments." *Cement and Concrete Research* 79, 373-385, 2016.

[22] Shekarchi, Mohammad, Alireza Rafiee, and Hamed Layssi. "Long-term chloride diffusion in silica fume concrete in harsh marine climates." *Cement and Concrete Composites* 31.10, 769-775, 2009.

[23] Chalee, W., C. A. Jaturapitakkul, and P. Chindaprasirt. "Predicting the chloride penetration of fly ash concrete in seawater." *Marine structures* 22.3, 341-35, 2009.

[24] Ma, Haiyan, et al. "Durability of concrete subjected to dry-wet cycles in various types of salt lake brines." *Construction and Building Materials* 193, 286-294, 2018.

[25] Hussain, Raja Rizwan. "Underwater half-cell corrosion potential bench mark measurements of corroding steel in concrete influenced by a variety of material science and environmental engineering variables." *Measurement* 44.1, 274-280, 2011.

[26] Pour-Ghaz, M., O. Burkan Isgor, and P. Ghods. "The effect of temperature on the corrosion of steel in concrete. Part 1: Simulated polarization resistance tests and model development." *Corrosion Science* 51.2, 415-425, (2009).

[27] Cheng, Y. F., and J. L. Luo. "Electronic structure and pitting susceptibility of passive film on carbon steel." *Electrochimica Acta* 44.17, 2947-2957, (1999).

[28] Ma, Yafei, et al. "Influence of corrosion-induced cracking on structural behavior of reinforced concrete arch ribs." *Engineering Structures* 117, 184-194, 2016.

[29] Mundra, Shishir, et al. "Chloride-induced corrosion of steel rebars in simulated pore solutions of alkali-activated concretes." *Cement and Concrete Research* 100, 385-397, 2017.

[30] Bellal, Youcef, Fatiha Benghanem, and Saida Keraghel. "A new corrosion inhibitor for steel rebar in concrete: Synthesis, electrochemical and theoretical studies." *Journal of Molecular Structure* 1225 1292, 2021.

[31] P. Zhang, et al., "Effects of magnesia expansive agents on the self-healing performance of microcracks in strain-hardening cement-based composites (SHCC)," *Materials Today Communications*, vol. 25, p. 101421, 2020.

[32] X.W. Yuan, et al., "Natural passivation behavior and its influence on chloride-induced corrosion resistance of stainless steel in simulated concrete pore solution," *Journal of Materials Research and Technology*, vol. 9, no. 6, pp. 12378-12390, 2020.

[33] J.X. Peng, et al., "Influence of cracks on chloride diffusivity in concrete: a five-phase mesoscale model approach," *Construction & Building Materials*, vol. 197, pp. 587-596, 2019.

[34] N.K. Prasad, et al., "On the novel approach of sacrificial cathodic protection of mild steel in simulated concrete pore solution and concrete mortar by high phosphorus pig iron anodes," *Journal of Materials Research and Technology*, vol. 14, pp. 582-608, 2021.

[35] N. Li, et al., "Microstructural changes in alkali-activated slag mortars induced by accelerated carbonation," *Cement & Concrete Research*, vol. 100, pp. 214-226, 2017.

[36] Song, Dan, et al. "Improved corrosion resistance in simulated concrete pore solution of surface nanocrystallized rebar fabricated by wire-brushing." *Corrosion science* 82, 437-441, 2014.

[37] Harilal, Manu, et al. "A new ternary composite steel rebar coating for enhanced corrosion resistance in chloride environment." *Construction and Building Materials* 320 126, 2022.

[38] Rooby, Divya Rachel, et al. "Enhanced corrosion protection of reinforcement steel with nanomaterial incorporated fly ash based cementitious coating." *Construction and Building Materials* 275 122130, 2021.

[39] Shi, Jinjie, et al. "Improved corrosion resistance of a new 6% Cr steel in simulated concrete pore solution contaminated by chlorides." *Corrosion Science* 174, 108851, 2020.

[40] Wang, Pan-jun, et al. "Influence of grain refinement on the corrosion behavior of metallic materials: A review." *International Journal of Minerals, Metallurgy and Materials* 28 1112-1126, 2021.

[41] Mangaiyarkarasi, G., and S. Muralidharan. "Electrochemical protection of steel in concrete to enhance the service life of concrete structures." *Procedia Engineering* 86, 615-622,2014.

[42] A.A. Adewumi, et al., "Corrosion behavior of carbon steel and corrosion resistant steel under elevated temperature and chloride concentration in simulated concrete pore solution," *European Journal of Environmental and Civil Engineering*, vol. 25, no. 3, pp. 452-467, 2018.

[43] Z.Y. Zhou, et al., "Corrosion behavior and mechanism of FeCrNi medium entropy alloy prepared by powder metallurgy," *Journal of Alloys and Compounds*, vol. 867, p. 159094, 2021.

[44] J.K. Singh, et al., "The nature of rusts and corrosion characteristics of low alloy and plain carbon steels in three kinds of concrete pore solution with salinity and different pH," *Corrosion Science*, vol. 56, pp. 129-142, 2012.

[45] C. Chen, et al., "Corrosion behavior of low alloy corrosion resistant steel in simulated concrete environment," *Materials Research & Innovation*, vol. 18, no. sup4, pp. 285-289, 2014.

[46] L. Zhang, et al., "Initial-corrosion condition behavior of the Cr and Al alloy steel bars in coral concrete for marine construction," *Cement & Concrete Composites*, vol. 120, p. 104051, 2021.

[47] Kumar, Satendra, et al. "Corrosion resistance behavior of CrCu alloyed thermo-mechanically treated reinforced bars in 3.5% NaCl solution." *Protection of Metals and Physical Chemistry of Surfaces* 55, 554-565,2019.

[48] Liu, Ming, et al. "Corrosion behavior and durability of low-alloy steel rebars in marine environment." *Journal of Materials Engineering and Performance* 25, 4967-4979, 2016.

[49] Ye, Hailong, et al. "Performance of reinforced concrete beams corroded under sustained service loads: A comparative study of two accelerated corrosion techniques." *Construction and Building Materials* 162 286-297, 2018.

[50] Wang, Xiao-Hui, et al. "Shear behaviour of RC beams with corrosion damaged partial length." *Materials and structures* 45, 351-379, 2012.

[51] Yun-hong, C. H. E. N. G., S. U. N. Xiao-hui, and Z. H. A. N. G. Jing-yu. "Hydration kinetics of cementiron tailing powder composite cementitious materials and pore structure of hardened paste." *Construction and Building Materials* 370, 130673, 2023.

[52] H.Y. Wu, et al., "Grey relational analysis of static tensile properties of structural steel subjected to urban industrial atmospheric corrosion and accelerated corrosion," *Construction & Building Materials*, vol. 315, p. 125706, 2022.

[53] M. Jing, et al., "Effects of mill scale and steel type on passivation and accelerated corrosion behavior of reinforcing steels in concrete," *Journal of Materials in Civil Engineering*, vol. 32, p. 04020029, 2020.

[54] X.P. Xian, et al., "Ambient pressure carbonation curing of reinforced concrete for CO2 utilization and corrosion resistance," *Journal of CO2 Utilization*, vol. 56, p. 101861, 2022.

[55] W.P. Feng, et al., "Methods of accelerating chloride-induced corrosion in steel-reinforced concrete: a comparative review," *Construction & Building Materials*, vol. 289, p. 123165, 2021.

[56] Q. Li, et al., "Study of wiring method on accelerated corrosion of steel bars in concrete," *Construction & Building Materials*, vol. 269, p. 121286, 2021

[57] G. Duffo, et al., "Application of gamma-ray radiography and gravimetric measurements after accelerated corrosion tests of steel embedded in mortar," *Cement & Concrete Research*, vol. 74, pp. 1-9, 2015.

[58] S.X. Hong, et al., "Determination of impressed current efficiency during accelerated corrosion of reinforcement," *Cement & Concrete Composites*, vol. 108, p. 103536, 2020.

[59] E. Vandecruys, et al., "Challenges in assessing corrosion damage in reinforced concrete beams by vibration-based monitoring: literature analysis and experimental study," *Structural Health Monitoring*, 2023.

[60] Zheng, Yue, et al. "Experimental study and numerical model of the seismic behavior of reinforced concrete beams in an artificial corrosion environment." *Journal of Building Engineering* 46 103705, 2022.

[61] Zafar, Faiza, et al. "Mild steel corrosion behavior in a coastal megacity relevant to China Pakistan economic corridor." *Npj Materials Degradation* 7.1 37,2023.

[62] Engelund, Svend, Louise Mohr, and Carola Edvardsen. General guidelines for durability design and redesign: duracrete, probabilistic performance based durability design of concrete structures. *CUR*, 2000.

[63] Huang, Le, et al. "Local bond performance of rebar embedded in steel-polypropylene hybrid fiber reinforced concrete under monotonic and cyclic loading." *Construction and Building Materials* 103 77-92, 2016.

[64] Li, Chun Qing, and J. J. Zheng. "Propagation of reinforcement corrosion in concrete and its effects on structural deterioration." *Magazine of Concrete Research* 57.5 261-271,2005.

[65] Namdev, Vidur, and Gaurav Jain. "Experimental study of corrosion inhibition of RCC element using glass FRP mats." Journal of Physics: *Conference Series*. Vol. 2484. No. 1. IOP Publishing, 2023.

[66] S. Haridas and A. Raj, "Retrofitting and strengthening of Rcc beams: A critical review," AIP *Conference Proceedings*, vol. 2856, p. 040017, 2023.

[67] A. Michel, et al., "Propagation of steel corrosion in concrete: Experimental and numerical investigations," *Cement & Concrete Composites*, vol. 70, pp. 171-182, 2016.

[68] K.P. Balan, "Chapter Nine-Corrosion," in *Metallurgical Failure Analysis*, pp. 155-178, 2018.

[69] S.T. Banu, et al., "Structural retrofitting of corroded fly ash based concrete beams with fibres to improve bending characteristics," *Australian Journal of Structural Engineering*, vol. 20, pp. 198-203, 2019.

[70] G.G. Triantafyllou, et al., "Corroded RC beams patch repaired and strengthened in flexure with fiber-reinforced polymer laminates," *Composites Part B: Engineering*, vol. 112, pp. 125-136, 2017.

[71] V. Talakokula, et al., "Diagnosis of carbonation induced corrosion initiation and progression in reinforced concrete structures using piezo-impedance transducers," *Sensors and Actuators A: Physical*, vol. 242, pp. 79-91, 2016.

[72] S.K. Verma, et al., "Evaluating effect of chloride attack and concrete cover on the probability of corrosion," *Frontiers of Structural and Civil Engineering*, vol. 7, pp. 379-390, 2013.

[73] K. Heiza, et al., "State-of-the Art Review: Strengthening of Reinforced Concrete StructuresDifferent Strengthening Techniques," in *Proceedings of the International Conference on Nano-Technology in Construction, Cairo, Egypt, March 1, 2014*, pp. 1-24.

[74] Y.H. Mugahed Amran, et al., "Properties and applications of FRP in strengthening RC structures: A review," *Structures*, vol. 16, pp. 208-238, 2018.

[75] C. Pellegrino, et al., "FRP strengthening of steel and steel-concrete composite structures: An analytical approach," Materials & *Structures: Materials & Construction*, vol. 42, pp. 353-363, 2009.

[76] S.E. Gunaslan and A. Karasin, "Confining Concrete Columns with FRP Materials," *European Scientific Journal ESJ*, vol. 13, pp. 464-470, 2017.

[77] T. Sen and H.N. Jagannatha Reddy, "Strengthening of RC beams in flexure using natural jute fibre textile reinforced composite system and its comparative study with CFRP and GFRP strengthening systems," *International Journal of Sustainable Built Environment*, vol. 2, pp. 41-55, 2013.

[78] N. Attari, et al., "Flexural strengthening of concrete beams using CFRP, GFRP and hybrid FRP sheets," *Construction & Building Materials*, vol. 37, pp. 746-757, 2012.

[79] V. Matsagar, "Advances in Structural Engineering," in *Advances in Structural Engineering: Materials, V. Matsagar*, ed., vol. 3, Springer: New Delhi, India, 2015.

[80] S. Erdem, et al., "Investigation of Bond between Fibre Reinforced Polymer (FRP) Composites Rebar and Aramid Fibre-Reinforced Concrete," *International Journal of Composite Materials*, vol. 5, pp. 148-154, 2015.

[81] M.R. Garcez and S. Filho, "A Comparative Study of Reinforced Concrete Beams Strengthened with Glass, Carbon and Aramid Fibers," in *Proceedings of the 10DBMC International Conference on Durability of Building Materials and Components, Lyon, France, April 17-20*, 2005.

[82] M.A. Alam and K. Al Riyami, "Shear strengthening of reinforced concrete beam using natural fibre reinforced polymer laminates," *Construction & Building Materials*, vol. 162, pp. 683-696, 2018.

[83] I.E. Fakorede, "Mechanical Behaviour of Nigerian Long Bamboo Fibre-Reinforced Polymer Composite (Nlbfrpc)," *Journal of Multidisciplinary Engineering Science & Technology JMEST*, vol. 2, pp. 2654-2659, 2015.

[84] R.R. Karthik, et al., "Impact damage resistance of novel adhesively bonded natural fibre compositesteel hybrid laminates," *International Journal of Lightweight Materials and Manufacturing*, 2021.

[85] J.P. Torres, et al., "The mechanical properties of natural fibre composite laminates: A statistical study," *Composites Part A: Applied Science and Manufacturing*, vol. 98, pp. 99-104, 2017.

[86] A. Bashir, et al., "Analysis of Bamboo Fibre Reinforced Beam," *Journal of Steel Structures & Construction*, vol. 4, pp. 2-7, 2018.

[87] S.C. Chin, et al., "Strengthening of Reinforced Concrete Beams Using Bamboo Fiber/Epoxy Composite Plates in Flexure," *Key Engineering Materials*, vol. 821, pp. 465-471, 2019.

[88] S.C. Chin, et al., "External strengthening of reinforced concrete beam with opening by bamboo fiber reinforced composites," *Materials & Structures*, vol. 53, p. 141, 2020.

[89] T. Sen and H.N. Jagannatha Reddy, "A Numerical Study of Strengthening of RCC Beam Using Natural Bamboo Fibre," *International Journal of Computer Theory and Engineering*, vol. 3, p. 707, 2011.

[90] I. Cervantes, et al., "Flexural retrofitting of reinforced concrete structures using green natural fiber reinforced polymer plates," in *Proceedings of the 2014 International Conference on Sustainable Infrastructure, Long Beach, CA, USA, , pp. 1051-1062, November 6-8*, 2014.

[91] N.A.K. Hafizah, et al., "Kenaf fiber reinforced polymer composites for strengthening RC beams," *Journal of Advanced Concrete Technology*, vol. 12, pp. 167-177, 2014.

[92] T. Jirawattanasomkul, et al., "Structural behavior of pre-damaged reinforced concrete beams strengthened with natural fiber reinforced polymer composites," *Composites Structures*, vol. 244, p. 112309, 2020.

[93] C. Nwankwo, et al., "NFRP strengthening of reinforced concrete beams," *IOP Conference Series: Materials Science and Engineering*, vol. 640, p. 012074, 2019.

[94] H. Mohd Noh, et al., "Structural Effects of Reinforced Concrete Beam Due to Corrosion," in *E3S Web of Conferences*, vol. 34, 2018.

[95] Y. Zhao and W. Jin, "Steel Corrosion in Concrete," in *Steel Corrosion-Induced Concrete Cracking, Elsevier: Oxfordshire, UK,* pp. 19-29, 2016.

[96] M.H.F. Medeiros, et al., "Corrosion potential: Influence of moisture, water-cement ratio, chloride content and concrete cover," *Revista IBRACON de Estruturas e Materiais*, vol. 10, pp. 864-885, 2017.

[97] S. Huda, et al., "Ultra-light-weight composites from bamboo strips and polypropylene web with exceptional flexural properties," *Composites Part B: Engineering*, vol. 43, pp. 1658-1664, 2012.

[98] S. Karthik, et al., "Strength properties of bamboo and steel reinforced concrete containing manufactured sand and mineral admixtures," *Journal of King Saud University - Engineering Sciences*, vol. 29, pp. 400-406, 2017.

[99] B. Mondal, et al., "Tensile characterisation of bamboo strips for potential use in reinforced concrete members: Experimental and numerical study," *Materials & Structures*, vol. 53, p. 128, 2020.

[100] M.A. Al-Huri, et al., "Performance of corroded RC beams strengthened in flexure using UHPC: Effect of configuration and thickness of the UHPC layers," *Engineering Structures*, vol. 292, p. 116519, 2023.

[101] Jedrzejko, M. J., et al. "Strengthening of RC beams in shear with novel near-surface mounted (NSM) U-shaped fiber-reinforced polymer (FRP) composites." *Engineering Structures* 292 116479, 2023.

[102] Yu, Piyong, Pedro Silva, and Antonio Nanni. "Flexural strengthening of RC beams using GFRP grid bonded with sprayed polyurea." *Engineering Structures* 292 116516, 2023.

[103] Dangwal, Shubham, and Heaven Singh. "Seismic performance of corroded non-seismically and seismically detailed RC beam-column joints rehabilitated with High Strength Fiber Reinforced Concrete." *Engineering Structures* 291 116481, 2023.

[104] Jacobs, Robert R., and Christopher S. Williams. "Evaluation of flexural strengthening methods for beams with simulated deterioration using spike-anchored FRP externally bonded sheets and near-surface-mounted strips." *Composite Structures* 305 116463, 2023.

[105] Bhanugoban, Maheshwaran, Hiran D. Yapa, and Samir Dirar. "Efficient shear retrofitting of reinforced concrete beams using prestressed deep embedded bars." *Engineering Structures* 246 113053, 2021.

[106] A. Hassan, et al., "Retrofitting of shear-damaged RC T-beams using U-shaped SHCC jacket," *Engineering Structures*, vol. 245, p. 112892, 2021.

[107] A. Karmegam, et al., "Retrofitting RC beams using high-early strength alkali-activated concrete," *Case Studies in Construction Materials*, vol. 17, p. e01194, 2022.

[108] N. Moshiri, et al., "Experimental tests and numerical simulations on the mechanical response of RC slabs externally strengthened by passive and pre-stressed FRP strips," *Engineering Structures*, vol. 292, p. 116559, 2023.

[109] W. Abdullah, "Shear strengthening of normal steel reinforced concrete beams using post-tensioned metal straps fully wrapped around the beams," *Advances in Structural Engineering*, vol. 26, no. 9, pp. 1636-1646, 2023.

[110] Y.A. Zaki, et al., "Crack Detection and Classification of Repaired Concrete Beams by Acoustic Emission Monitoring," *Ultrasonics*, p. 107068, 2023.

[111] W. Zhang, et al., "Experimental investigation on steel bracing members with bolted gusset plate connections," *Journal of Building Engineering*, p. 107133, 2023.

[112] J. Cao, et al., "A simplified analysis method for long-span suspension bridges within the deck overlay retrofitting process from asphalt to UHPC," *Engineering Structures*, vol. 289, p. 116122, 2023.

[113] A.K. Azad, et al., "Residual strength of corrosion-damaged reinforced concrete beams," *ACI Materials Journal*, vol. 104, pp. 40-47, 2007.

[114] M. Lachemi, et al., "The effect of corrosion on shear behavior of reinforced self-consolidating concrete beams," *Engineering Structures*, vol. 79, pp. 1-12, 2014.

[115] G. Campione, et al., "Shear and flexural strength prediction of corroded R.C. beams," *Construction & Building Materials*, vol. 149, pp. 395-405, 2017.

[116] C. Fang, et al., "Bond behavior of corroded reinforcing steel bars in concrete," *Cement & Concrete Research*, vol. 36, pp. 1931-1938, 2006.

[117] Y. Zhao, et al., "Characteristics of pitting corrosion in an existing reinforced concrete beam exposed to marine environment," *Construction & Building Materials*, vol. 234, p. 117392, 2020.

[118] C. Fu, et al., "Corrosion characteristics of a 4-year naturally corroded reinforced concrete beam with load-induced transverse cracks," *Corrosion Science*, vol. 117, pp. 11-23, 2017.

[119] K. Hjkov, et al., "Prediction of reinforcement corrosion due to chloride ingress and its effects on serviceability," *Engineering Structures*, vol. 174, pp. 768-777, 2018.

[120] H. Ye, et al., "Chloride ingress profiles and binding capacity of mortar in cyclic drying-wetting salt fog environments," *Construction & Building Materials*, vol. 127, pp. 733-742, 2016.

[121] L. Chung, et al., "Flexural behavior of concrete slabs with corroded bars," *Cement & Concrete Composites*, vol. 30, pp. 184-193, 2008.

[122] W. Zhu, et al., "Effect of corrosion of reinforcement on the mechanical behavior of highly corroded RC beams," *Engineering Structures*, vol. 56, pp. 544-554, 2013.

[123] W. Dong, et al., "Residual load capacity of corroded reinforced concrete beam undergoing bond failure," *Engineering Structures*, vol. 127, pp. 159-171, 2016.

[124] B.H. Oh, et al., "Critical corrosion amount to cause cracking of reinforced concrete structures," *ACI Materials Journal*, vol. 106, pp. 333-339, 2009.

[125] S.J. Han, et al., "Degradation of flexural strength in reinforced concrete members caused by steel corrosion," *Construction & Building Materials*, vol. 54, pp. 572-583, 2014.

[126] Z. Cui and A. Alipour, "Concrete cover cracking and service life prediction of reinforced concrete structures in corrosive environments," *Construction & Building Materials*, vol. 159, pp. 652-671, 2018.

[127] E. Gudonis, et al., "FRP reinforcement for concrete structures: state-of-the-art review of application and design," *Engineering Structures & Technology*, vol. 5, pp. 147-158, 2014.

[128] M. Garcez, et al., "Structural performance of RC beams poststrengthened with carbon, aramid, and glass FRP systems," *Journal of Composites for Construction*, vol. 12, pp. 522-530, 2008.

[129] J.G. Dai, et al., "Experimental investigation of the influence of moisture on the bond behavior of FRP to concrete interfaces," *Journal of Composites for Construction*, vol. 14, pp. 834-844, 2010.

[130] M. Elghazy, et al., "Post-repair flexural performance of corrosion-damaged beams rehabilitated with fabric-reinforced cementitious matrix (FRCM)," *Construction & Building Materials*, vol. 166, pp. 732-744, 2018.

[131] J.H. Gonzalez-Libreros, et al., "Behavior of RC beams strengthened in shear with FRP and FRCM composites," *Engineering Structures*, vol. 150, pp. 830-842, 2017.

[132] L. Ombres and S. Verre, "Structural behavior of fabric reinforced cementitious matrix (FRCM) strengthened concrete columns under eccentric loading," *Composites Part B: Engineering*, vol. 75, pp. 235-249, 2015.

[133] E. Bernat-Maso, et al., "Experimental assessment of textile reinforced sprayed mortar strengthening system for brickwork wallettes," *Construction & Building Materials*, vol. 50, pp. 226-236, 2014.

[134] H. Toutanji, et al., "Flexural behavior of reinforced concrete beams externally strengthened with CFRP sheets bonded with an inorganic matrix," *Engineering Structures*, vol. 28, pp. 557-566, 2006.

[135] B. Hu, et al., "Experimental and theoretical investigation on the hybrid CFRP-ECC flexural strengthening of RC beams with corroded longitudinal reinforcement," *Engineering Structures*, vol. 200, p. 109717, 2019.

[136] C. Wu and V.C. Li, "CFRP-ECC hybrid for strengthening of the concrete structures," *Composites Structures*, vol. 178, pp. 372-382, 2017.

[137] K. Yu, et al., "A strain-hardening cementitious composites with the tensile capacity up to 8%," *Construction & Building Materials*, vol. 137, pp. 410-419, 2017.

[138] H. Li, et al., "Tensile and flexural properties of ultra high toughness cemontious composite," *Journal of Wuhan University of Technology - Science Edition*, vol. 24, pp. 677-683, 2009.

[139] V.C. Li, et al., "Tensile strain-hardening behavior or polyvinyl alcohol engineered cementitious composite (PVA-ECC)," *ACI Materials Journal*, vol. 98, pp. 483-492, 2001.

[140] M. ahmaran and V.C. Li, "Durability of mechanically loaded engineered cementitious composites under highly alkaline environments," *Cement & Concrete Composites*, vol. 30, pp. 72-81, 2008.

[141] M. ahmaran, V.C. Li, and C. Andrade, "Corrosion resistance performance of steel-reinforced engineered cementitious composite beams," *ACI Materials Journal*, vol. 105, pp. 243-250, 2008.

[142] Y.Z. Zheng, et al., "Flexural behavior of reinforced concrete beams strengthened with a composite reinforcement layer: BFRP grid and ECC," *Construction & Building Materials*, vol. 115, pp. 424-437, 2016.

[143] X. Yang, et al., "Flexural strengthening of RC beams with CFRP grid-reinforced ECC matrix," *Composites Structures*, vol. 189, pp. 9-26, 2018.

[144] N. Al Nuaimi, et al., "Durability of Reinforced Concrete Beams Externally Strengthened with CFRP Laminates under Harsh Climatic Conditions," *Journal of Composites for Construction*, vol. 25, no. 2, 2021.

[145] P. Joyklad, et al., "Flexural Response of JFRP and BFRP Strengthened RC Beams," *International Journal of Engineering and Technology*, vol. 11, no. 3, 2019.

[146] Z. Peng, et al., "Improvement of basalt fiber dispersion and its effect on mechanical characteristics of oil well cement," *Journal of Building Engineering*, p. 107244, 2023.

[147] J. He, et al., "Flexural performance and damage evaluation on basalt fiber reinforced polymer (BFRP) sheet reinforced concrete," *Construction & Building Materials*, vol. 395, p. 132321, 2023.

[148] J. He, et al., "Investigation on bonding behavior of basalt fiber reinforced polymer (BFRP) sheet reinforced concrete beam," *Journal of Building Engineering*, p. 106963, 2023.

[149] M.A. Adam, et al., "Experimental and analytical study of high performance concrete beams reinforced with Basalt FRP bars," *Structures*, vol. 55, pp. 510-530, 2023.

[150] J. Shi, et al., "Bond behavior between basalt fiberreinforced polymer sheet and concrete substrate under the coupled effects of freeze-thaw cycling and sustained load," *Journal of Composites for Construction*, vol. 17, no. 4, pp. 530-542, 2013.

[151] A. Ali, et al., "A Comparative Study on Corrosion Rate of Carbon Steel in NaCl Solution with Continuous and Discontinuous Weight Loss Methods," 2022.

[152] O. Oparaodu, et al., "Comparison of Percentage Weight Loss and Corrosion Rate Trends in Different Metal Coupons from two Soil Environments," 2014.

[153] H. Kitagawa, et al., "Cathodic Current of Steel Structures with Seawater Resistant Stainless Steel and Estimation of Weight Loss of Sacrificial Anode," 2010.

[154] R. Souza, et al., "Technical note Weight loss investigation of alternating voltage corrosion of 301, 304, and 316 stainless steels in boiling NaCI solution," 1995.

[155] T. Gjerse, et al., "Weight Optimization of Steel Monopile Foundations for Offshore Windfarms, 2015.

[156] A. Adday, et al., "Flexural behavior of RC beams contains rubberized pieces and strengthened with CFRP sheets," 2023.

[157] A. Al zubi, "Flexural Strengthening of Reinforced Concrete Beams with Variable Compressive Strength Using Near-Surface Mounted Carbon-Fiber-Reinforced Polymer Strips [NSM-CFRP]," 2022.

[158] Dawood and A. Asadi, "Flexural Behavior of Reinforced Recycled Aggregate Concrete Beams Strengthened by CFRP," 2022.

[159] A. Abbas, et al., "Flexural Strengthening of Prestressed Girders with Partially Damaged Strands Using Enhancement of Carbon Fiber Laminates by End Sheet Anchorages," 2022.

[160] A. Al fahdawi, et al., "Simulation Behavior of Flexure in Reinforced Concrete Beams Strengthened with Carbon Fiber Reinforced Polymer (CFRP)," 2015.

[161] A. Kadhim and M. Ozakca, "Flexural performance of RC beams externally strengthened with a single-layer of basalt fiber reinforced polymer sheets," 2022.

[162] D. Do-dai, et al., "Efficacy of CFRP/BFRP laminates in flexurally strengthening of concrete beams with corroded reinforcement," 2022.

[163] K. Chhorn, et al., "Flexural Strengthening of Reinforced Concrete Beam Bonded with Built-in T Type BFRP Plate," 2022.

[164] D. Diab, "An anchorage technique for flexural strengthening of RC beams using NSM BFRP bars," 2022.

[165] A. Hakiki and M. Mujiman, "Flexural Behavior of Glulam-Concrete Composite Beams Reinforced Using CFRP Sheets," 2020.

[166] S. Sbahieh, et al., "A comparative life cycle assessment of fiber-reinforced polymers as a sustainable reinforcement option in concrete beams," 2023.

[167] A. Subhani, "Development of Basalt Fibre Reinforced Polymer (BFRP) Rebar Infused with Geopolymer Binder," 2023.

[168] P. Bigenwald, "Experimental and Numerical Investigations of BFRP-Reinforced Normal and High Strength Concrete Beams," 2023.

[169] Y. Niu, et al., "Failure Study of BFRP Joints with Two Epoxy Adhesives under Hygrothermal Coupling," 2023.

[170] R. Fegade, et al., "A review on basalt fiber reinforced polymeric composite materials," 2022.

[171] V. Fegade, et al., "A review on basalt fiber reinforced polymeric composite materials," *AIP Conference Proceedings*, vol. 2393, no. 1, 2022.

[172] Y. Wang and J. Wu, "Flexural Behavior of Corroded Concrete Beams Strengthened with Carbon Fiber-Reinforced Polymer," *Materials*, vol. 16, no. 12, pp. 4355, 2023.

[173] S. Yehia, et al., "Strength of Hybrid Steel-BFRP Reinforced Concrete Beams with Openings in the D-Region Strengthened Internally and Externally," *Buildings*, vol. 13, no. 10, pp. 2522, 2023.

[174] B. Hu and H.-B. Wang, "Performance evaluation and FRP strengthening of concrete-filled steel tubular columns subjected to vehicle impact," *Advances in Structural Engineering*, vol. 27, no. 8, pp. 1377-1396, 2024.

[175] L.S. Chen, et al., "Experimental-numerical study on axial compression performance of square concrete columns confined by new-type BFRP," *Physica Scripta*, vol. 99, no. 6, p. 065042, 2024.

[176] M. Khadim and A. Abdulridha, "Enhancing the flexural performance of lightweight concrete slabs with CFRP Sheets: an experimental analysis," *Frattura ed Integrit Strutturale*, vol. 18, no. 69, pp. 181-191, 2024.

[177] S. Yehia, et al., "Short-Term Efficiency of Using Sustainable BFRP Bars in Post-Tensioning Systems for One-Way RC Slab," *JES. Journal of Engineering Sciences*, vol. 51, no. 5, pp. 318-344, 2023.

[178] G.C. Okpokwasili and K.O. Oparaodu, "Comparison of percentage weight loss and corrosion rate trends in different metal coupons from two soil environments," International *Journal of Environmental Bioremediation & Biodegradation*, vol. 2, no. 5, pp. 243-249, 2014.

[179] S. Lim, et al., "Investigation of the spatial variability of steel weight loss and corrosion cracking: A novel X-ray technique," 2016.

[180] O.K. Idiapho, et al., "Evaluation of the Impact of Corrosion Attack in Carbon Steel C-1040 Marine Piping System in Two Media," 2023.

[181] N.U.R.D.I.N. Ali, et al., "A Comparative Study on Corrosion Rate of Carbon Steel in NaCl Solution with Continuous and Discontinuous Weight Loss Methods," *Key Engineering Materials*, vol. 930, pp. 35-41, 2022.

[182] I. Hocaoglu and I.B. Topcu, "Effect of DC Current and NaCl Ratio on Accelerated Corrosion at Different Diameter of Steels," *BSEU Journal of Engineering Research and Technology*, vol. 1, no. 1, pp. 18-23, 2020.

[183] M. Dixit and A.K. Gupta, "Assessment of corrosion in rebars by impressed current technique," in Advances in Geotechnics and Structural Engineering: *Select Proceedings of TRACE 2020, Springer Singapore*, 2021.

[184] S.X. Hong, et al., "Determination of impressed current efficiency during accelerated corrosion of reinforcement," *Cement & Concrete Composites*, vol. 108, p. 103536, 2020.

[185] H. Liu, et al., "Effect of stray current on corrosion behavior of Mg alloy sacrificial anode in buried pipeline," *Engineering Failure Analysis*, vol. 143, p. 106852, 2023.

[186] S. Tastani, "Bond of corroded reinforcement in strain resilient cementitious composites," *Corrosion Reviews*, vol. 41, no. 2, pp. 201-212, 2023.

[187] M.A. Al-Osta, et al., "Strategies for strengthening of corroded reinforced concrete beams using CFRP laminates and UHPC jacketing," *Structural Concrete*, vol. 24, no. 1, pp. 1546-1571, 2023.

[188] P.K. Silwal, et al., "Numerical Investigation on Strengthening of Steel Beams for Corrosion Damage or Web Openings Using Carbon Fiber Reinforced Polymer Sheets," *Buildings*, vol. 14, no. 4, p. 1069, 2024.

[189] Y. Han, et al., "Study on Flexural Behavior of Corroded I-Shaped Steel Beams Strengthened with Hybrid CFRP/GFRP Sheets," *Materials*, vol. 16, no. 14, p. 5080, 2023.

[190] M.A. Al-Osta, et al., "Strategies for strengthening of corroded reinforced concrete beams using CFRP laminates and UHPC jacketing," *Structural Concrete*, vol. 24, no. 1, pp. 1546-1571, 2023.

[191] M. Yang, et al., "Bond behavior between CFRP and corroded steel plate associations with surface treatments," Composites Part B: *Engineering*, vol. 246, p. 110280, 2022.

[192] T. Do-Dai, et al., "Efficacy of CFRP/BFRP laminates in flexurally strengthening of concrete beams with corroded reinforcement," *Journal of Building Engineering*, vol. 53, p. 104606, 2022.

[193] A.S. Aween and S.H. Mohmmad, "Investigating the Flexural Performance of Basalt Fiber Reinforced Polymer (BFRP) Bars at Elevated Temperatures," *British Journal of Multidisciplinary and Advanced Studies*, vol. 4, no. 3, pp. 14-20, 2023.

[194] N. Zavatta, et al., "Effect of thermal ageing on the mechanical strength of carbon fiber reinforced epoxy composites," *Polymers*, vol. 13, no. 12, p. 2006, 2021.

[195] G. Sun, et al., "On the effects of temperature on tensile behavior of carbon fiber reinforced epoxy laminates," *Thin-Walled Structures*, vol. 164, p. 107769, 2021.

[196] K. Abdulla, et al., "Numerical investigation of FRCM-strengthened corroded RC beams under cathodic protection," *Materials*, vol. 15, no. 15, p. 5334, 2022.

[197] B. Guo, et al., "Impressed current cathodic protection of chloride-contaminated RC structures with cracking: A numerical study," *Journal of Building Engineering*, vol. 44, p. 102943, 2021.

[198] D.W. Whitmore and T. Becker, "Cathodic corrosion protection system with rebar mounting assembly," *U.S. Patent No. 10*,745,811, 2020.

[199] G. Qiao, et al., "Numerical simulation to optimize impressed current cathodic protection systems for rc structures," *Journal of Materials in Civil Engineering*, vol. 29, no. 6, p. 04017005, 2017.

[200] G. Qiao, et al., "Numerical simulation of the impressed current cathodic protection system for a reinforced concrete structure," in *2015 Fifth International Conference on Instrumentation and Measurement, Computer, Communication and Control (IMCCC), IEEE*, 2015.

[201] S.K. Sharma, et al., "Retrofitting existing buildings to improve energy performance," *Sustainability*, vol. 14, no. 2, p. 666, 2022.

[202] G.M. Mauro, et al., "A multi-step approach to assess the lifecycle economic impact of seismic risk on optimal energy retrofit," *Sustainability*, vol. 9, no. 6, p. 989, 2017.

[203] Y. Tian, et al., "A CostBenefit Analysis Framework for City-Scale Seismic Retrofitting Scheme of Buildings," *Buildings*, vol. 13, no. 2, p. 477, 2023.

[204] F.A. Mohamad, et al., "Cost-benefit Analysis of Seismic Retrofitting Strategies for Residential Buildings in Surabaya, Indonesia," *Disaster Advances*, vol. 15, no. 9, pp. 16-23, 2022.

[205] K. Larsen, "Corrosion Effects on the Durability of Reinforced Concrete Structures," *Materials Performance*, November, 2015.

[206] K. Tang, "Corrosion of steel fibre reinforced concrete (SFRC) subjected to simulated stray direct (DC) interference," *Materials Today Communications*, vol. 20, p. 100564, 2019.

[207] C. Apostolopoulos and K. Koulouris, "Corrosion effects on durability of RC structures," *Metals*, vol. 11, no. 11, p. 1812, 2021.

[208] M. Sompura, et al., "Nonlinear Finite Element Analysis of Corroded Reinforced Concrete Beams," in *ASPS Conference Proceedings*, vol. 1, no. 5, pp. 1377-1381, 2022.

[209] Z. Ye, et al., "Potential change of failure modes and time-dependent behavior of RC beams under a marine atmospheric environment," *Structure and Infrastructure Engineering*, pp. 1-13, 2023.

[210] W.W. Li, et al., "Steel corrosion induced shear performance deterioration of RC beams: Experimental investigation and numerical simulation," *Case Studies in Construction Materials*, vol. 20, p. e03266, 2024.

[211] N.C. Luyen, et al., "Experimental and analytical investigations on flexural performance of corroded RC beams using RBSM-based corrosion model," *Tp ch Khoa hc v Cng ngh-i hc Nng*, pp. 35-40, 2024.

[212] M. Assad, et al., "Flexural strengthening of reinforced concrete beams with CFRP laminates and spike anchors," *Composites Part C: Open Access*, vol. 13, p. 100443, 2024.

[213] N. Meja, et al., "Flexural and shear strengthening of RC beams reinforced with externally bonded CFRP laminates postfire exposure by experimental and analytical investigations," *Engineering Structures*, vol. 308, p. 117995, 2024.

[214] Z. Zhang, et al., "Flexural behavior of the corroded RC beams strengthened with BFRP grid-reinforced ECC," *Structures*, vol. 58, p. 105541, 2023.

[215] S. Shoaib, et al., "Behavior of Shear-Critical Recycled Aggregate Concrete Beams Containing BFRP Reinforcement," *Buildings*, vol. 13, no. 11, p. 2785, 2023.

[216] T.A. Nguyen, et al., "Enhanced bond strength prediction in corroded reinforced concrete using optimized ML models," *Structures*, vol. 63, p. 106461, 2024.

[217] S. Sathe and S. Patil, "Corrosion effects on bond strength in reinforced concrete with fly ash," *Journal of Adhesion Science and Technology*, pp. 1-29, 2024.